Nanomaterials Development for CO_2 Geo-Storage in Shallow Reservoirs

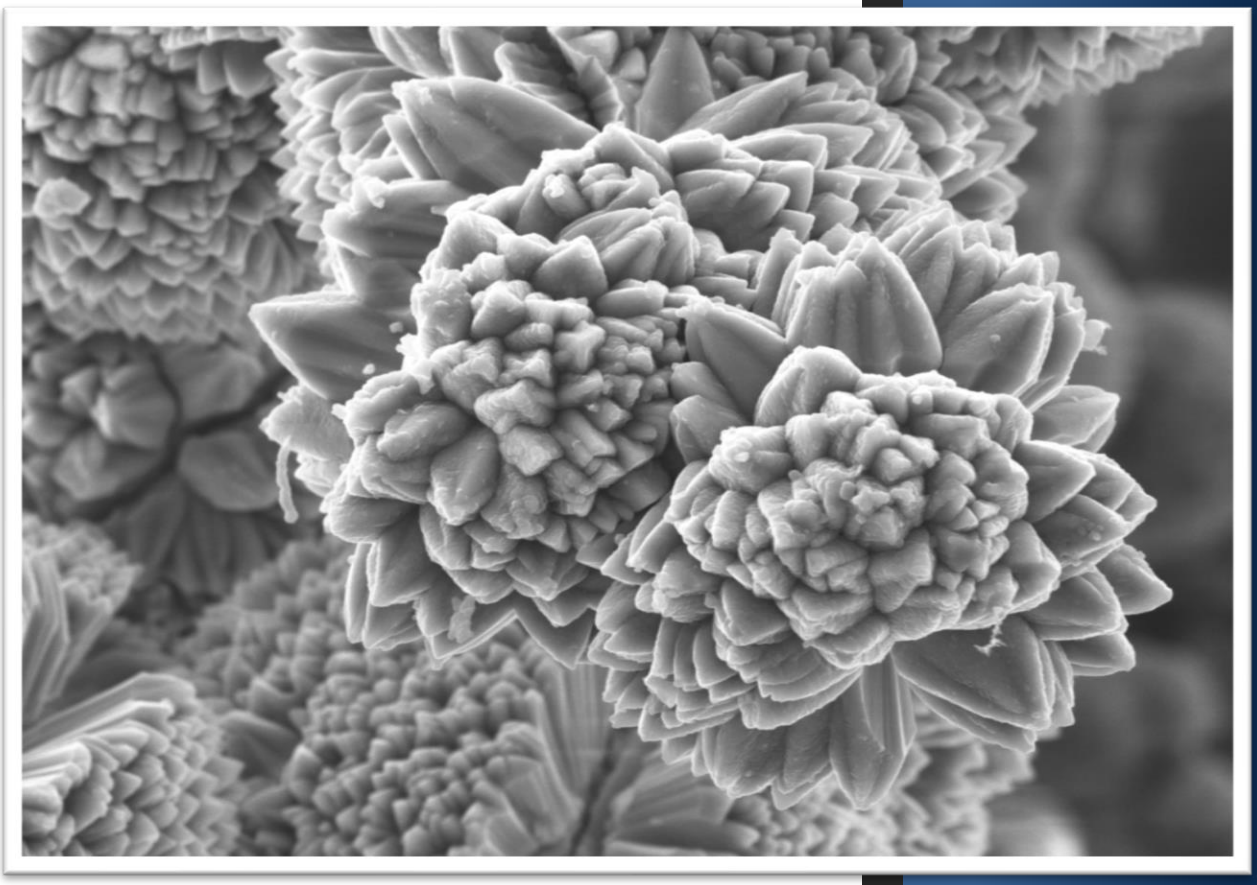

Elizabeth Cristina Rodríguez Acevedo

Universidad Nacional de Colombia
Universidad de Granada
2019


LIBERTAD Y ORDEN
INTER · AULAS · ACADEMIÆ · QUÆRE · VERUM


UNIVERSITAS · GRANATENSIS
PLUS ULTRA
1531

Nanomaterials Development for CO_2 Geo-Storage in shallow reservoirs

Elizabeth Cristina Rodríguez Acevedo
M.Sc., Chemical Engineer

Thesis submitted as a requirement for obtaining a Ph.D. degree means an academic cooperation agreement. It is associated with the programs:
Ph.D. in Engineering – Energy Systems
Ph.D. in Chemistry

Supervisors:
Farid Bernardo Cortés Correa, Ph.D., M.Sc., Ch. Eng.
Francisco Carrasco Marin Ph.D., Chemist

Research groups:
Surface Phenomena “Michael-Polanyi”
Universidad Nacional de Colombia
Facultad de Minas, Departamento de Procesos y Energía
Medellin, Colombia

Carbon Materials
University of Granada
Faculty of Science, Inorganic Chemistry Department
Granada, Spain

2019


LIBERTAD Y ORDEN
INTER · AULAS · ACADEMIÆ · QUÆRE · VERUM


UNIVERSITAS · GRANATENSIS
PLUS ULTRA
1531

Farid Bernardo Cortés Correa and Francisco Carrasco Marín as supervisors, and Elizabeth C. Rodriguez Acevedo as Ph.D. candidate

GUARANTEE

By signing this doctoral thesis, that the doctoral candidate has done the work, and the rights of other authors have been respected, and their results or publications have been cited when these have been used.

Granada, November ___, 2019

Farid B. Cortés Correa, Ph.D.
Full Professor
Universidad Nacional de Colombia

Francisco Carrasco Marín, Ph.D.
Full Professor
University of Granada

Elizabeth C. Rodriguez Acevedo, Ph.D (c)
Universidad Nacional de Colombia


LIBERTAD Y ORDEN
INTER · AULAS · ACADEMIÆ · QUÆRE · VERUM


UNIVERSITAS · GRANATENSIS
PLUS ULTRA
1531

Dedicatory

To my mother

My motivation, my best friend

My Angel

“The most beautiful thing we can experience is the mysterious. It is the source of all true art and science. He to whom the emotion is a stranger, who can no longer pause to wonder and stand wrapped in awe, is as good as dead; his eyes are closed.”

Albert Einstein

Acknowledgments

I want to express my sincere thanks to my Directors, Professors Farid Cortés Correa and Francisco Carrasco Marín, their knowledge, vast experience, trust, unconditional support, and friendship allowed me to grow professionally and personally. I am convinced that without them, it would have been impossible to carry out this work.

My sincere acknowledge to the members of the research groups in surface phenomena “Michael Polanyi” (Universidad Nacional de Colombia), Carbon Materials (University of Granada-Spain) and Bio-Sourced Materials-Institut Jean Lamour (Université de Lorraine-France), especially to Professors Camilo Franco Ariza, Jaime Gallego, Agustín Cardona Molina, Agustín Pérez-Cadenas, Francisco Maldonado-Hódar, Carlos Moreno, Antonio Rodríguez, Isidora Bautista, María Ángeles, Vanessa Fierro and Alain Celzard, their experience, friendship, and invaluable help were key to the development of this research.

And a special thanks to all my friends at Surface Phenomena-Michael Polanyi research group, especially to Karol, Yira, Ma. Angélica, Daniela, Johana R., Johana V., Saray, Cristina, Eliana, Mayra, Lady, Mónica, Daniel L, Daniel M., Juan David, Esteban, Óscar, Cristian, Luis, José, Steven, Santiago, Maribel, Alejandro, Leonardo and all of you, for your friendship, learning, and constant support; we are a great family, and I am very proud to be part of this great team.

Also, acknowledge to my adventure friends in Spain and France, especially to my best friends Jésica Castelo, Adriana Moral and Sonia Segovia; to Aurora Puerta, Safae, Luisa and Sergio (and their beautiful Amelia), Cesar and Jimena (and her mother Angeles), Angela, Nada, Eliza, Zélie, Alex, Oussama, Jose, Hakim, Hesham, Sebastien, Giuseppe, Blagoj, Radouan, Balázs, Mari Carmen, Antonio De La Torre, and Philippe Gadonneix for your academic and spiritual support, adventures, smiles, and friendship.

Special and endless thanks to my family and Leonardo (and his family), which have always believed in me, have supported me and encouraged me always to be my best version. To my mother for her patience and dedication throughout this adventure, for making me a passionate person for knowledge and for her inexhaustible love.

Special acknowledge to Departamento Administrativo de Ciencia, Tecnología e Innovación-COLCIENCIAS for financing the doctoral studies through the call 647-2014. Also, acknowledge to Agencia Nacional de Hidrocarburos-ANH, Fondo Nacional de Financiamiento para la Ciencia, la Tecnología y la Innovación “Francisco José de Caldas”, COLCIENCIAS and Universidad Nacional de Colombia for the support provided in the agreement 272-2017. Also, thanks to ERASMUS+ program (agreement F NANCY43) and ENLAZAMUNDOS-SAPIENCIA program for economical support for international internships.

"A good scientist values criticism almost higher than friendship: no, in science, criticism is the height and measure of friendship."

Francis Crick


LIBERTAD Y ORDEN
INTER · AULAS · ACADEMIÆ · QUÆRE · VERUM


UNIVERSITAS · GRANATENSIS
PLUS ULTRA
· 1531 ·

Abstract

The implementation of carbon capture and storage process (CCS) has been proposed as an effective method to reduce anthropogenic CO_2 emissions from industry. However, its implementation has been unsuccessful to date, mainly due to the technical issues and high costs associated with two main stages: 1) CO_2 separation from flue gas and 2) CO_2 injection in deep geological deposits, more than 300 m. At these conditions, CO_2 is in supercritical conditions, and CO_2 capture and storage are mainly due to the inter-particle volume filling. This study proposes, for the first time, an enhanced CCS process (e-CCS), in which the stage of CO_2 separation is removed, and the flue gas is injected directly in shallow reservoirs located at less than 300 m deep. In e-CCS, the adsorptive phenomena control gaseous CO_2 capture and storage in situ. For this, it is necessary to add a surface modifying agent to the porous medium to improve the selective adsorption capacity to CO_2. Besides, the modifying agent should not affect the naturally porous structure of the deposit to avoid operational problems. In this way, nanotechnology, for the first time for a CCS process, could be used as modifying media due to their characteristics can be customized, obtaining specific chemical-physical properties for the selective adsorption process. Also, the nanometric size allows its application in geological deposits. In this work, different nanostructures were synthesized and characterized. After that, Ottawa sandstone and real oilfield sandstone were impregnated with nanofluids, which are composed of deionized water and dispersed nanoparticles. The CO_2 adsorption performance of nanomaterials was evaluated at different conditions of temperature (0, 25, and 50 ° C) and pressure (3×10^{-3} MPa to 3.0 MPa) to mimic the reservoir conditions. For the best nanomaterials, the adsorption process at reservoir condition was also modeled and evaluated at different mixing and pressure conditions, through the Ideal Adsorbed Solution Theory-IAST, using experimental information obtained. Each stage was carried out under conditions similar to the real operation in case of a possible application. The obtained results for each material are promising and competitive with those reported in the literature, obtaining increments of more than 60000% at 20% of nanomaterials mass fraction.

Keywords: Nanomaterials, carbon dioxide-CO_2, adsorption, carbon capture and storage process-CCS, shallow reservoirs

Resumen

El proceso de captura y almacenamiento de carbono (CCS por sus siglas en inglés) ha sido propuesto como un método efectivo para la reducción de las emisiones de CO_2 provenientes de la industria, pero su implementación a nivel industrial no ha sido exitosa debido a consideraciones técnico-económicas asociadas a dos etapas principales: 1) Separación inicial del CO_2 de los gases de combustión y 2) Inyección del CO_2 en depósitos geológicos profundos, más de 300 m, en donde el CO_2. A estas condiciones el CO_2 se encuentra en condiciones supercríticas y su almacenamiento se debe principalmente al llenado de la estructura porosa del yacimiento. Este trabajo propone por primera vez en el mundo, un proceso mejorado de captura y almacenamiento de carbono, e-CCS, en el cual la etapa inicial de captura/separación de CO_2 es suprimida y los gases de combustión son inyectados directamente al yacimiento superficial (<300 m). En este caso, el proceso de selectiva adsorción controla la captura in-situ de CO_2 gaseoso y su almacenamiento. Para esto, es indispensable modificar la superficie de yacimiento con el fin de incrementar la capacidad de adsorción y la selectividad del CO_2. Adicional a esto, el agente modificante no debe obstruir la estructura porosa natural del yacimiento con el fin de evitar problemas operacionales. En este sentido, la nanotecnología, por primera vez en el mundo, podría ser usada como agente modificador de la superficie del yacimiento, debido a ventajas relacionadas con la síntesis a medida, obteniendo materiales con características fisicoquímicas específicas al proceso de adsorción selectiva; Además, su tamaño nanométrico permite su uso sin obstrucción del medio poroso del yacimiento. En este trabajo fueron sintetizadas y caracterizadas diversas nanoestructuras. Luego, arenisca tipo Ottawa y arenisca de yacimientos reales de crudo, fueron impregnadas con nanofluidos compuestos por nanomateriales dispersos en agua desionizada. El desempeño de estos sistemas en el proceso de adsorción fue evaluado a diferentes condiciones de temperatura (0, 25 y 50 ° C) y presión (3×10^{-3} MPa a 3.0 MPa), tratando de simular las condiciones de un yacimiento. Para los mejores nanomateriales el sistema fue modelado y simulado a diferentes condiciones de presión y concentraciones de CO_2-N_2, por medio de la Teoría de la Solución Ideal Adsorbida (IAST por sus siglas en inglés), usando datos experimentales obtenidos y el software libre PyIAST. Los resultados obtenidos son prometedores y competitivos en comparación con los reportado en la literatura, además en la aplicación se obtienen incrementos de más de 60000% en la capacidad de adsorción de CO_2 con concentraciones de 20% en masa de nanomaterial.

Palabras clave: Nanomateriales, dióxido de carbono-CO_2, adsorción, proceso de captura y almacenamiento de carbono-CCS, yacimientos someros


LIBERTAD
Y
ORDEN
INTER · AULAS · ACADEMIÆ · QUÆRE · VERUM


UNIVERSITAS · GRANATENSIS
PLUS
ULTRA
1531

Table of Contents

List of figures

Pág.

List of tables

Pág.


LIBERTAD
Y
ORDEN
INTER · AULAS · ACADEMIÆ · QUÆRE · VERUM


UNIVERSITAS · GRANATENSIS
PLUS
ULTRA
· 1531 ·

1. Introduction

Global warming is one of the most significant problems facing humanity and threatening life on the planet. In recent decades, climate changes have generated negative consequences such as loss of sea ice, accelerated rise in sea level, the extinction of species, natural disasters, drought, population displacements, among others [1]. These changes are being caused by human activities, mainly through the release of greenhouse gas emissions [1-5]. It is estimated that a temperature increase of 3 °C represents a population risk, and could be related to heatwave exposure (7909 millions of people-MP), water stress (3920 MP), risk to power production (742 MP), Crop yield change (1817 MP) and habitat degradation (1357 MP) [6].

Although carbon dioxide, CO_2, does not have a significant heating capacity (methane has a value of 21 times greater), many daily emissions increase its responsibility [7-11]. The CO_2 anthropogenic emissions from fossil fuel combustion and industrial processes contributed to about 78% of the total greenhouse gas emissions [12-14], and CO_2 emissions have increased by 46% since pre-industrial times [7, 15]. In the 1950s, the average pre-industrial global CO_2 concentration was approximately 280 ppm, which to date has increased by 46%, which is related to the average global temperature rise pattern at 0.93 °C [7] (Figure 1. 1).

Primary material industries such as the chemical, petrochemical, iron, steel, cement, and others consume more than two-thirds of world energy consumptions of the industrial sector and contribute to the highest CO_2 emissions worldwide [16, 17]. The advantage of CO_2 industrial emissions is that they are fixed sources so that they can be controlled in-situ.

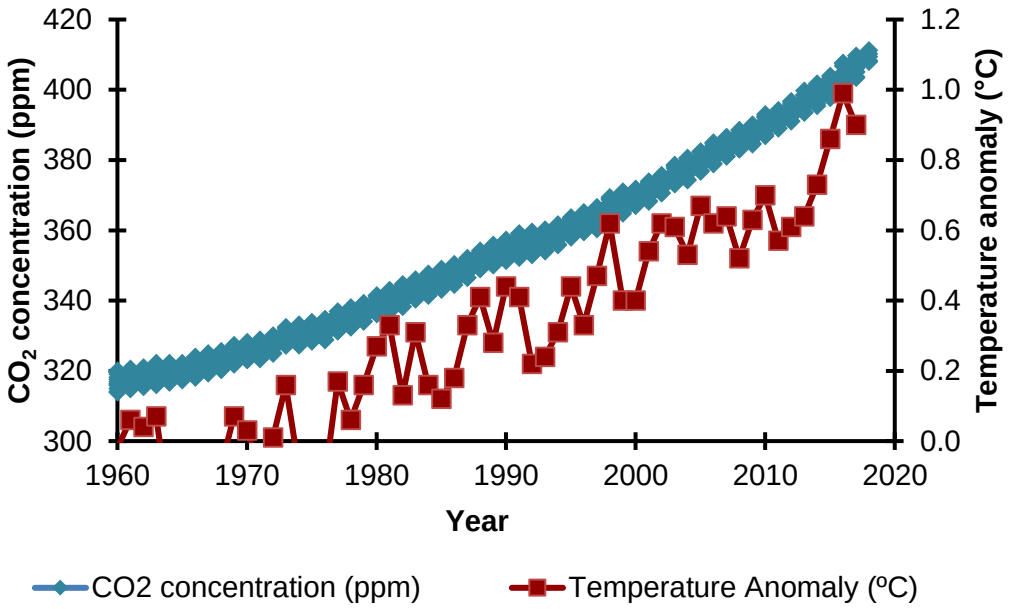

Figure 1. 1. Relation between CO_2 concentration and global temperature increases. Adapted from *Nasa, EPA, and NOAA [7, 15]*

In 2009, the Nature Geoscience Journal published a special issue on the management of CO_2 emissions [18], emphasizing that the only alternative to balance climate change is zero CO_2 emissions [18], which is impossible considering the base of development in our society. The method most frequently used at industrial levels for CO_2 capture is absorption. However, this method has significant limitations related to solvent regeneration, the composition of flue gas, CO_2 concentration, corrosion, high-energy consumption, among others [10, 11, 17, 19]. Other technologies are cryogenic distillation, membranes, absorption by ionic liquids, and adsorption by porous solids. The current methods used to capture CO_2 do not represent a solution that will stabilize long-term industrial CO_2 emissions. Also, these methods are not enough, and CO_2 emissions continue to increase [7, 16, 20]. For this reason, it is necessary to broaden the portfolio of methods to reduce CO_2 emissions significantly in the years to come.

The Intergovernmental Panel on Climate Change (IPCC) promotes the Carbon Capture and Storage process (CCS), which allows the geological storage of CO_2 emitted by the industry for the long term. The CCS process could decrease CO_2 emissions by approximately 22% in 2035 [21, 22]. The CCS process has three main stages: 1) capture

and separation of the CO_2 from flue gas, 2) transport of the CO_2 to the storage site, and 3) injection of CO_2 into the deep geological storage site, 300 to 4000 m, an average of 800 m^2 [19-21]. Figure 1. 2 presents a scheme of the conventional CCS process. In this case, the volume occupation is the main reason to capture and storage of CO_2, due to the inter-particle volume filling.

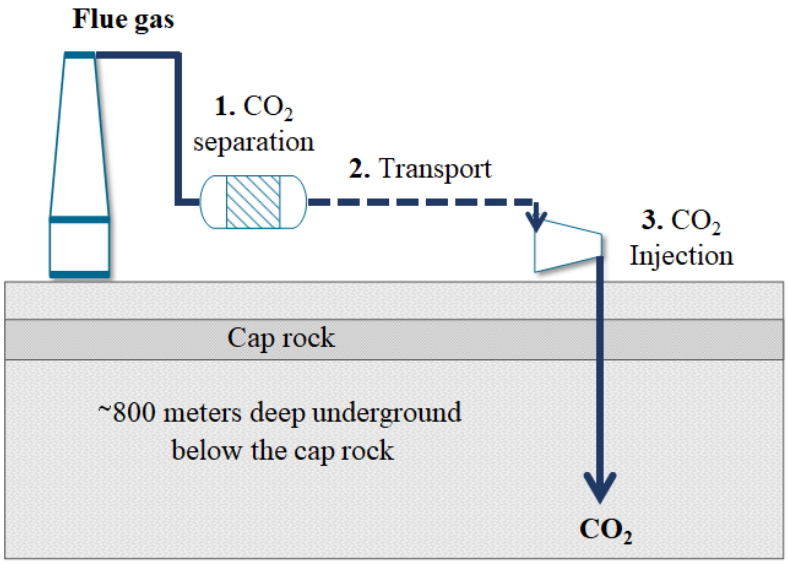

Figure 1. 2. Conventional Carbon Capture and Storage Process, CCS [23]

However, its in-situ industrial implementation has been unsuccessful, mainly due to the technical and economic costs associated with the separation and storage stages. In general, the cost of CO_2 capture is 70–80% of the total CCS costs [24-26]. For this reason, the current research focuses mainly on increasing the CO_2/flue gas separation capacity in order to decrease energy consumption, or on the use of waste energy, among others.

This study proposes an alternative to minimize the technical and economic costs for the viability of the CCS process. Figure 1. 3 presents, for the first time, the configuration of an enhanced CCS process (e-CCS), in which the stage of CO_2 capture/separation is removed, and the flue gas is injected directly into shallow deposits, at depths less than 300 m. In this case, CO_2 remains in the gaseous state into the reservoir, and the in-situ adsorption process controls the capture and storage [23]. The density of CO_2 is very different in gaseous or supercritical conditions, which affects the amount of CO_2 stored in the e-CCS

process. Also, the adsorption affinity between CO_2 and sandstone reservoir is low. For this, it is necessary to add a modifying agent to the surface of the porous medium in order to improve the adsorption capacity and the CO_2 selectivity, since the adsorption (capture/storage) process is done underground. Besides, the modifying agent should not affect the naturally porous structure of the deposit to avoid operational problems.

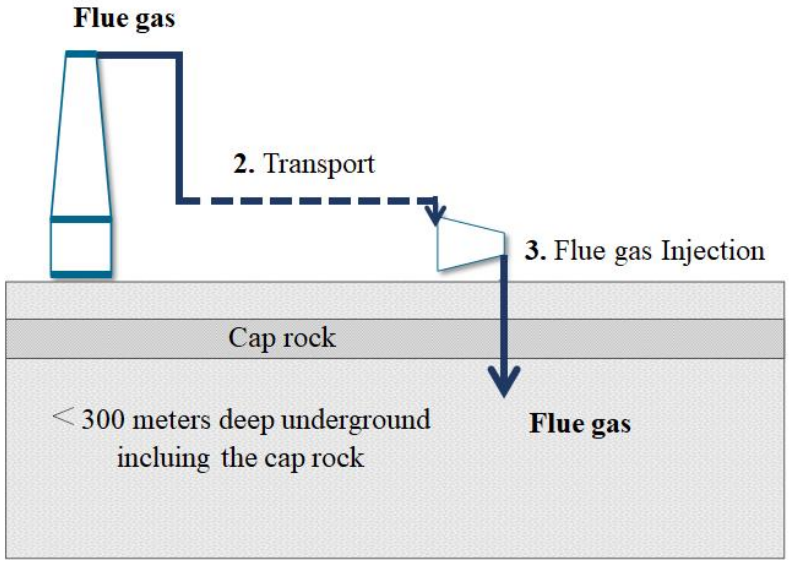

Figure 1. 3. Enhanced Carbon Capture and Storage Process, e-CCS [23]

It is estimated that 50% of the CCS projects at a small scale, use sandstone deposits for storage because they have technical advantages and high availability [21]. The oil and gas deposits are composed mostly of sandstone, which has a natural storage structure, with porous structure, upper and lateral seals that allow long-term storage.

Nanostructured materials or nanotechnology is a vast and active research area. Nanoscale materials, less than 100 nm, have different properties compared to the same material on a larger scale. From synthesis, the characteristics of nanoparticles can be adjusted according to their application, such as size, structure, molecular affinity, high surface area-volume ratio, high surface activity, dispersion capacity, optical and electronic properties, among others [27]. At the reservoir level, different nanoparticles have been used to solve different problems, mainly associated with oil and gas fields, where physicochemical properties of reservoirs have been modified [28, 29]. The obtained results demonstrate its efficacy without the obstruction of porous structure [28-32]. The nanoparticles have been used for

the alteration of reservoir wettability, adsorption and catalysis of heavy crude compounds (asphaltenes), stabilization of fines in reservoirs, among others [28-32].

Based on the above, the nanospheres will be an option for the modification of the reservoir surface in an e-CCS process. The nanoparticles have never been used for the modification of porous media in the conventional CCS process. An application of nanomaterial for the conventional CCS process is reported; in this case, a nanofluid is used to improve CO_2 transport in the saline aquifers [33]. The desirable conditions of a nanomaterial for e-CCS are high surface area, high nitrogen content, high CO_2 selectivity, spherical structure, nanometric size, nanofluid stability, and stability at geological conditions.

Carbon materials show good results both in terms of adsorption capacity and selectivity of CO_2 adsorption [11, 34-37]; Wang and collaborators have analyzed various types of materials. They suggest that carbon materials are one of the best adsorbents due to low cost, high surface area, porous structure design, surface functionalization, and easy regeneration [11]. Many carbon nanostructures have been evaluated for CO_2 adsorption, as nanofibers, nanosheets and nanotubes, which despite the good results in the CO_2 adsorption process nanotubes (adsorption capacity between 0.26 to 4.15 mmol/g at atmospheric conditions) [11, 35, 38-42], but they are not suitable for application in reservoirs due to the structure and dimensions that could affect the naturally porous structure of reservoir. In the last five years, research on carbon nanospheres has made it possible to precisely control particle size, surface area, pore size, chemical composition, and dispersion [11], but studies on its performance in CO_2 adsorption at atmospheric and high pressure are limited. For applications at high pressure, a high surface area is essential, but the CO_2 molecule has an acid character, whereby a high nitrogen content in adsorbent could enhance the adsorption capacity and selectivity. In literature, there are some methods to increase the nitrogen content like impregnation with amines, but this is an additional stage, increasing the cost of material; Also, the amines could obstruct the microporous structure of nanomaterial, decreasing the adsorption capacity [11, 43]. Therefore, it is desirable to incorporate the nitrogenous groups from the synthesis process of nanomaterial.

The metal-organic frameworks-MOF, which are constructed by using transition metal ions as core and organic ligands, have been evaluated in the process of adsorption of CO_2 [11,

44, 45]. In this case, the research focuses on the development of new structures, different metal ions, and ligands, functionalization, hybrid materials, among others [11, 45, 46]. The main disadvantage of MOF is the stability at humidity conditions, which occur at reservoir conditions; also, size and shape may not be desirable for reservoir applications. On the other hand, MOF has a high surface area, which is desirable at high-pressure processes (P> 2 MPa), and porous structure would allow high selectivity in the CO_2 capture process [11].

Another type of relevant material is molecular sieves, where CO_2 is permitted to pass through the porous structure than other gas components, resulting in the selective elimination of CO_2 from flue-gas.[39, 47-50]. CO_2 adsorption capacity is competitive, but the shape and size may not be suitable for reservoir level applications.

Hence, the main objective of this study is “to develop carbon nanomaterials for CO_2 selective adsorption to enhance the carbon capture and geo-storage process in shallow reservoirs”. In this work, different nanostructures were synthesized and characterized. The nanoparticles were synthesized under methods that did not require extreme operating conditions, the least amount of stages, considering economic and available carbon precursors. After that, Ottawa sandstone and real oilfield sandstone were impregnated with nanofluids, which are composed of deionized water and dispersed nanoparticles. The impregnation was carried out under conditions similar to the real operation in case of a possible application. The nanomaterial's performance to adsorb CO_2 was evaluated at different conditions of temperature (0, 25, and 50 °C) and pressure (3×10^{-3} MPa to 3.0 MPa) in order to characterize the process and to mimic the reservoir conditions. For the best nanomaterials, the adsorption process at reservoir conditions was modeled and evaluated at different mixing (N_2/CO_2) and pressure conditions, through the Ideal Adsorbed Solution Theory-IAST, using information obtained experimentally.

This document is divided into five main chapters, that include: **1)** State of the art about nanoparticles for proposed enhanced CCS process, e-CCS, **2)** Synthesis, surface modifications and characterization of different carbon nanospheres for selective CO_2 adsorption process, **3)** Nitrogen-rich nanospheres for selective CO_2 adsorption focused on e-CCS, **4)** Carbonized Mg/Ni MOF-74 for selective CO_2 adsorption focused on e-CCS, and

5) Carbon molecular nanosize synthesized from cane molasses for selective CO_2 adsorption focused on e-CCS.

References

[1] T. L. Root, J. T. Price, K. R. Hall, S. H. Schneider, C. Rosenzweig, and J. A. Pounds, "Fingerprints of global warming on wild animals and plants," *Nature,* vol. 421, p. 57, 2003.

[2] L. D. Harvey, *Global warming*: Routledge, 2018.

[3] H. Baer and M. Singer, *Global warming and the political ecology of health: Emerging crises and systemic solutions*: Routledge, 2016.

[4] D. A. Lashof and D. R. Ahuja, "Relative contributions of greenhouse gas emissions to global warming," *Nature,* vol. 344, p. 529, 1990.

[5] T. R. Anderson, E. Hawkins, and P. D. Jones, "CO2, the greenhouse effect and global warming: from the pioneering work of Arrhenius and Callendar to today's Earth System Models," *Endeavour,* vol. 40, pp. 178-187, 2016.

[6] J. Tollefson. (2019, 2019). *The hard truths of climate change — by the numbers*. Available: https://www.nature.com/immersive/d41586-019-02711-4/index.html

[7] NASA. (2019, March 30). *Global Climate Change. Vital Signs of the Planet*. Available: https://climate.nasa.gov/vital-signs/carbon-dioxide/

[8] R. J. Norby and Y. Luo, "Evaluating ecosystem responses to rising atmospheric CO2 and global warming in a multi-factor world," *New Phytologist,* vol. 162, pp. 281-293, 2004.

[9] M. M. Halmann, *Chemical Fixation of Carbon DioxideMethods for Recycling CO2 into Useful Products*: CRC press, 2018.

[10] P. M. Cox, R. A. Betts, C. D. Jones, S. A. Spall, and I. J. Totterdell, "erratum: Acceleration of global warming due to carbon-cycle feedbacks in a coupled climate model," *Nature,* vol. 408, p. 750, 2000.

[11] J. Wang, L. Huang, R. Yang, Z. Zhang, J. Wu, Y. Gao*, et al.*, "Recent advances in solid sorbents for CO 2 capture and new development trends," *Energy & Environmental Science,* vol. 7, pp. 3478-3518, 2014.

[12] E. P. A. US-EPA. (2019). *Global Greenhouse Gas Emissions Data*. Available: https://www.epa.gov/ghgemissions/global-greenhouse-gas-emissions-data

[13] O. Edenhofer, R. Pichs-Madruga, Y. Sokona, E. Farahani, S. Kadner, K. Seyboth*, et al.*, "IPCC, 2014: Summary for Policymakers, In: Climate Change 2014, Mitigation of Climate Change," in *Contribution of Working Group III to the Fifth Assessment Report of the Intergovernmental Panel on Climate Change*, ed, 2014.

[14] Y. Tan, W. Nookuea, H. Li, E. Thorin, and J. Yan, "Property impacts on Carbon Capture and Storage (CCS) processes: A review," *Energy Conversion and Management,* vol. 118, pp. 204-222, 2016.

[15] N. G. C. Change, "Vital Signs of the Planet," *Earth Science Communications Team at NASA's Jet Propulsion Laboratory. Accessed June,* vol. 30, 2018.

[16] J. Conti, P. Holtberg, J. Diefenderfer, A. LaRose, J. T. Turnure, and L. Westfall, "International energy outlook 2016 with projections to 2040," USDOE Energy Information Administration (EIA), Washington, DC (United States …2016.

[17] B. Metz, O. Davidson, and H. De Coninck, *Carbon dioxide capture and storage: special report of the intergovernmental panel on climate change*: Cambridge University Press, 2005.

[18] N. G. L. (2009) Saved by Sequestration? *Nature Geoscience*. 809.

[19] M. Bui, C. S. Adjiman, A. Bardow, E. J. Anthony, A. Boston, S. Brown*, et al.*, "Carbon capture and storage (CCS): the way forward," *Energy & Environmental Science,* vol. 11, pp. 1062-1176, 2018.

[20] W. Knorr, "Is the airborne fraction of anthropogenic CO2 emissions increasing?," *Geophysical Research Letters,* vol. 36, 2009.

[21] P. Cook, R. Causebrook, J. Gale, K. Michel, and M. Watson, "What have we learned from small-scale injection projects?," *Energy Procedia,* vol. 63, pp. 6129-6140, 2014.

[22] I. IEA, "World energy outlook 2011," *Int Energy Agency,* vol. 666, 2011.

[23] E. Rodriguez Acevedo, F. B. Cortés, C. A. Franco, F. Carrasco-Marín, A. F. Pérez-Cadenas, V. Fierro*, et al.*, "An Enhanced Carbon Capture and Storage Process (e-CCS) Applied to Shallow Reservoirs Using Nanofluids Based on Nitrogen-Rich Carbon Nanospheres," *Materials,* vol. 12, p. 2088, 2019.

[24] H. Balat and C. Öz, "Technical and Economic Aspects of Carbon Capture an Storage—A Review," *Energy Exploration & Exploitation,* vol. 25, pp. 357-392, 2007.

[25] C. Gough, *Carbon capture and its storage: an integrated assessment*: Routledge, 2016.

[26] C. Gough, "State of the art in carbon dioxide capture and storage in the UK: An experts' review," *International Journal of Greenhouse Gas Control,* vol. 2, pp. 155-168, 2008.

[27] E. P.-C. Bailon-García, Agustín F.; Rodriguez Acevedo, Elizabeth; Carrasco-Marín, Francisco, "Nanoparticle Fabrication Methods," in *Formation Damage in Oil and Gas Reservoirs. Nanotechnology Applications for its Inhibition/Remediation*, C. A. a. C. C. Franco, Farid B, Ed., 1 ed: Nova Science Publishers, 2018, pp. 69-150.

[28] C. A. C. C. Franco, Farid B, *Formation Damage in Oil and Gas Reservoirs. Nanotechnology Applications for its Inhibition/Remediation*: Nova Science Publishers, 2018.

[29] C. A. Franco, R. Zabala, and F. B. Cortés, "Nanotechnology applied to the enhancement of oil and gas productivity and recovery of Colombian fields," *Journal of Petroleum Science and Engineering,* vol. 157, pp. 39-55, 2017.

[30] C. A. Franco, N. N. Nassar, M. A. Ruiz, P. Pereira-Almao, and F. B. Cortés, "Nanoparticles for inhibition of asphaltenes damage: adsorption study and displacement test on porous media," *Energy & Fuels,* vol. 27, pp. 2899-2907, 2013.

[31] I. Moncayo-Riascos, C. A. Franco, and F. B. Cortés, "Dynamic Molecular Modeling and Experimental Approach of Fluorocarbon Surfactant-Functionalized SiO2 Nanoparticles for Gas-Wettability Alteration on Sandstones," *Journal of Chemical & Engineering Data,* 2019.

[32] Y. Hurtado, C. Beltrán, R. D. Zabala, S. H. Lopera, C. A. Franco, N. N. Nassar*, et al.*, "Effects of Surface Acidity and Polarity of SiO2 Nanoparticles on the Foam Stabilization Applied to Natural Gas Flooding in Tight Gas-Condensate Reservoirs," *Energy & fuels,* vol. 32, pp. 5824-5833, 2018.

[33] D. Yang, S. Wang, and Y. Zhang, "Analysis of CO2 migration during nanofluid-based supercritical CO2 geological storage in saline aquifers," *Aerosol Air Qual. Res,* vol. 14, pp. 1411-1417, 2014.

[34] J. Silvestre-Albero and F. R. Reinoso, "Nuevos materiales de carbón para la captura de CO2," *Boletín del Grupo Español del Carbón,* pp. 2-6, 2012.

[35] Y. Ma, Z. Wang, X. Xu, and J. Wang, "Review on porous nanomaterials for adsorption and photocatalytic conversion of CO2," *Chinese Journal of Catalysis,* vol. 38, pp. 1956-1969, 2017.

[36] X.-q. Zhang, W.-c. Li, and A.-h. Lu, "Designed porous carbon materials for efficient CO2 adsorption and separation," *New Carbon Materials,* vol. 30, pp. 481-501, 2015.

[37] T. J. Bandosz, M. Seredych, E. Rodríguez-Castellón, Y. Cheng, L. L. Daemen, and A. J. Ramírez-Cuesta, "Evidence for CO2 reactive adsorption on nanoporous S-and N-doped carbon at ambient conditions," *Carbon,* vol. 96, pp. 856-863, 2016.

[38] G. P. Lithoxoos, A. Labropoulos, L. D. Peristeras, N. Kanellopoulos, J. Samios, and I. G. Economou, "Adsorption of N2, CH4, CO and CO2 gases in single walled carbon nanotubes: A combined experimental and Monte Carlo molecular simulation study," *The Journal of Supercritical Fluids,* vol. 55, pp. 510-523, 2010.

[39] M. Bikshapathi, A. Sharma, A. Sharma, and N. Verma, "Preparation of carbon molecular sieves from carbon micro and nanofibers for sequestration of CO2," *Chemical Engineering Research and Design,* vol. 89, pp. 1737-1746, 2011.

[40] S. Chowdhury and R. Balasubramanian, "Highly efficient, rapid and selective CO2 capture by thermally treated graphene nanosheets," *Journal of CO2 Utilization,* vol. 13, pp. 50-60, 2016.

[41] A. Alonso, J. Moral-Vico, A. A. Markeb, M. Busquets-Fité, D. Komilis, V. Puntes*, et al.*, "Critical review of existing nanomaterial adsorbents to capture carbon dioxide and methane," *Science of the total environment,* vol. 595, pp. 51-62, 2017.

[42] D. J. Babu, M. Bruns, R. Schneider, D. Gerthsen, and J. r. J. Schneider, "Understanding the influence of N-doping on the CO2 adsorption characteristics in carbon nanomaterials," *The Journal of Physical Chemistry C,* vol. 121, pp. 616-626, 2017.

[43] M. Plaza, C. Pevida, A. Arenillas, F. Rubiera, and J. Pis, "CO2 capture by adsorption with nitrogen enriched carbons," *Fuel,* vol. 86, pp. 2204-2212, 2007.

[44] X. Wu, Z. Bao, B. Yuan, J. Wang, Y. Sun, H. Luo*, et al.*, "Microwave synthesis and characterization of MOF-74 (M= Ni, Mg) for gas separation," *Microporous and Mesoporous Materials,* vol. 180, pp. 114-122, 2013.

[45] Y. Lin, C. Kong, Q. Zhang, and L. Chen, "Metal-organic frameworks for carbon dioxide capture and methane storage," *Advanced Energy Materials,* vol. 7, p. 1601296, 2017.

[46] J. An and N. L. Rosi, "Tuning MOF CO2 adsorption properties via cation exchange," *Journal of the American Chemical Society,* vol. 132, pp. 5578-5579, 2010.

[47] R. V. Siriwardane, M.-S. Shen, E. P. Fisher, and J. A. Poston, "Adsorption of CO2 on molecular sieves and activated carbon," *Energy & Fuels,* vol. 15, pp. 279-284, 2001.

[48] C. W. Jones and W. J. Koros, "Carbon molecular sieve gas separation membranes-I. Preparation and characterization based on polyimide precursors," *Carbon,* vol. 32, pp. 1419-1425, 1994.

[49] A. Wahby, J. M. Ramos-Fernández, M. Martínez-Escandell, A. Sepúlveda-Escribano, J. Silvestre-Albero, and F. Rodríguez-Reinoso, "High-surface-area carbon molecular sieves for selective CO2 adsorption," *ChemSusChem,* vol. 3, pp. 974-981, 2010.

[50] X. Xu, C. Song, J. M. Andresen, B. G. Miller, and A. W. Scaroni, "Novel polyethylenimine-modified mesoporous molecular sieve of MCM-41 type as high-capacity adsorbent for CO2 capture," *Energy & Fuels,* vol. 16, pp. 1463-1469, 2002.


LIBERTAD
Y
ORDEN
INTER · AULAS · ACADEMIÆ · QUÆRE · VERUM


UNIVERSITAS · GRANATENSIS
PLUS
ULTRA
1531

2. State of the art: Nanomaterials for e-CCS process

Global warming is mainly associated with anthropogenic carbon dioxide-CO_2 emissions (20%), steam (50%), clouds (25%), and other gases (5%) [1]. However, CO_2 concentration is indirectly related to the participation of steam and clouds. CO_2 concentration increases air temperature, which increases steam concentration and clouds formation [1]. Therefore, the CO_2 emissions are considered one of the main factors that affect the global warming [1-6]; As mentioned before, CO_2 does not have a significant heating capacity (methane has a heating power 21 times greater), but many daily emissions increase its responsibility [1-6].

The industry sector accounted for 37% of total global final energy use in 2017 [7]. Primary materials industries such as the chemical, petrochemical, iron, steel, cement, paper, cellulose, minerals, and metals industries emit the highest CO_2 emissions worldwide, close to 8.8 Gt in 2019 [1, 5, 7, 8]. The basic compounds are used as the main method to control CO_2 emission due to the acidic character of the CO_2 molecule. Some amines commonly used at the industrial level are monoethanolamine-MEA, diethanolamine-DEA, and methyl diethanolamine-MDEA, among others. However, this method has significant limitations related to solvent regeneration, temperature, flue-gas composition, CO_2 concentration, corrosion, high-energy consumption, among others [9-12]. Other technologies for CO_2 separation are cryogenic distillation, membranes, absorption by ionic liquids, adsorption by porous solids, among others. Academic and industrial sectors have widely accepted the adsorption method; many studies have been developed in this area [6, 10, 13-15]. Between 2011 and 2014, more than 2000 articles on solid adsorbents for CO_2 capture were published [10].

Emission reduction is an urgent objective worldwide, but it is also difficult to reach. Currently, CO_2 concentration continues increasing despite efforts to reduce it [1, 16], and there is no sign of a decrease in global CO_2 emissions. In 2009, The Nature Geoscience Journal published a special edition about the management of CO_2 emissions. There, the zero CO_2 emissions were proposed as the only alternative to equilibrate climate change [9]; but this alternative is a difficult objective due to economic development and living standards of actual society.

The carbon capture and storage process (CCS) is a promising alternative for CO_2 capture from industrial emissions. The CCS process might decrease CO_2 emissions by approximately 22% in 2035 [17]. As mentioned before, this process commonly has three main stages: 1) CO_2 capture and separation from flue gas, 2) CO_2 transport to the storage site, and 3) CO_2 injection into deep geological storage sites, between 300 to 4000 m (800 m on average) [18, 19]. In this case, CO_2 is in supercritical conditions in those geological conditions, and the capture and storage process is mainly due to the inter-particle volume filling. In general, the cost of on-site CO_2 capture is 70–80% of the total CCS costs [20-22].

Scientists around the world agree with the CCS process is one of the most promising ways to solve the problems associated with CO_2 emissions. Many CCS projects have been evaluated worldwide, mainly in the United States. Latin America does not have CCS projects either in planning or execution [19]. It is estimated that 50% of projects are developed in sandstone deposits[19]. These deposits do not have a high affinity to CO_2, but geological configuration, porosity, and full availability allow advantages for the CCS process. The oil and gas deposits are mostly sandstones, which, having naturally stored hydrocarbons. These spaces have an ideal structure for CO_2 storage, from the porous structure and the upper and lateral seals that allow long term storage. The CCS process has been evaluated in enhanced oil recovery processes (22%), enhanced recovery of methane gas from coal beds (24%), deep saline aquifers (40%), depleted oil and gas fields (9%), and basalt deposits (5%) [19].

In view of the preceding, the current research is mainly focused on improving CO_2 separation, national political regulations, reduction in costs, injection and storage simulation, evaluation of geological reservoirs as storage, among others [12, 19, 23-26].

Nevertheless, there are multiple obstacles to CCS implementation, including the absence of a clear business case for CCS investment and the absence of strong economic incentives to support the high additional capital and operating costs of the entire CCS process.

Whereby, given the previous, this work proposes an alternative to the CCS process to minimize the technical and economic costs. The enhanced CCS process (e-CCS), proposes to remove the stage of CO_2 capture/separation and inject directly the flue gas into shallow deposits, at depths less than 300 m. In this case, CO_2 is in a gaseous state, and the selective adsorption process is carried out underground, and molecular interactions control to capture and storage processes. However, it is necessary to add a modifying agent to the surface of the porous medium in order to improve the selective CO_2 adsorption. Besides, the modifying agent should not affect the naturally porous structure of the deposit to avoid operational problems. For this reason, nanotechnology could be an alternative to improve the molecular interactions of porous media in e-CCS.

Nanostructured materials constitute a vast and active field of research in various areas, due to their intrinsic characteristics that can be adjusted depending on the foreseen application, such as porosity, structure, molecular affinity, high surface-area-to-volume ratio, high surface activity, dispersion capacity, and optical and electronic properties, among others. [27]. Nanoparticles have been used to increase the recovery of oil and gas by modifying the physicochemical properties of the reservoirs [28, 29], and to modify reservoirs' wettability, asphaltenes adsorption, catalysis and stabilization of fines in reservoirs, among others [23, 27-34]. The obtained results demonstrate their effectiveness in achieving this objective without the obstruction of the porous media. In this way, nanospheres can be an option for the modification of the surface in shallow reservoirs for the e-CCS process. Although nanoparticles have been evaluated for the conventional CCS process in the form of a nanofluid used to improve CO_2 transport in saline aquifers [25], they have not been used for rock modification and improvement of the CO_2 storage capacity, such as in the case of the proposed e-CCS process, to the best of our knowledge.

The advantage of CO_2 industrial emissions is that they are fixed sources so that they can be controlled in-situ. Typical flue gas from coal-fired boilers may contain 12–14 vol% CO_2,

8–10 vol% H_2O, 3–5 vol% O_2, and 72–77% N_2 [35-37]. However, this mixture affects the selective adsorption performance. Many experimental investigations have been developed in this area [38-42]. The gas purification allows separating gases with exergy potential, separating gaseous hydrocarbons in the petroleum industry, capturing radioactive noble gases from used nuclear fuel reprocessing off-gas, among others. Also, CO_2 capture over N_2, H_2O, O_2 allows the CO_2 separation for final disposal, as is the case with CCS and e-CCS. Porous Materials, molecular sieves, membranes, metal-organic frameworks, among others, are used to improve the CO_2 selective. Also, materials have been modified with nitrogen compounds to increase the molecular interaction with CO_2 and to improve the selectivity [38-42]. The Ideal adsorbed solution theory (IAST) allows predicting multi-component adsorption isotherms from only the pure-component adsorption isotherms at the same temperature [43].

The design of suitable materials for CO_2 capture is one of the most important challenges in environmental chemistry [6]. A suitable material must have specific characteristics for the CO_2 capture and separation, such as [10, 26, 44]:

- High adsorption capacity
- Stability
- Hydrophobicity
- CO_2 selectivity
- High adsorption kinetics
- Adequate regeneration.
- Low cost.

As mention before, the e-CCS application requires specific material characteristics such as spherical structure, nanometric size, nanofluid stability, and stability at geological conditions [28, 29]. Also, high nitrogen content allows molecular interactions with CO_2 [45-47].

Many adsorbents for CO_2 capture have been reported, such as carbon materials, metal-organic frameworks, zeolites, alkali metal carbonates, among others. [10, 44, 47, 48], but nanometric materials have not been widely investigated, including spherical structures, which are the best option to use at geological conditions [49]. Many carbon nanostructures

have been evaluated for CO_2 capture, among them nanofibers, nanosheets, and nanotubes, leading to adsorption capacities ranging from 0.26 to 4.15 $mmol.g^{-1}$ under atmospheric and high-pressure conditions [10, 13, 38, 49-52]. However, these materials can not applied to reservoirs due to their structure and dimensions that might affect the nature of the reservoir's porous structure.

Carbon materials show good results both in terms of adsorption capacity and selectivity towards preferential adsorption of CO_2 [44]; Wang and collaborators have analyzed various materials and suggest that carbon materials are one of the best supports, due to low costs, high surface area, modifiable pore structure, surface functionalization and easy regeneration [10, 26, 39, 44]. The last scientific studies have been focused on modifications for increasing the surface area, adjustment of the porous structure and surface modification normally with functional groups containing nitrogen, oxygen, metal oxides, among others [10, 25, 41, 53].

Studies about physical adsorption are mainly based on the Van der Waals interactions. Son adsorbents are carbon, zeolite, MOF, silica, polymer, and clay. In this case, the adsorption is mainly attributed to the high specific surface area and pore size. The CO_2 selectivity requires a well-developed microporous structure; Pore dimensions should be close to 0.35-0.4 nm [10, 44]. In any case, the selectivity based only on specific pore structure and pore size is not considerable compared to the selectivity that can occur by the chemistry of the material [10, 44]. Surface modification with amines, alkali metal carbonates, immobilized ionic liquids, among others, promote chemical bonding, which can benefit sorption from a kinetic point of view, of thermal stability, resistance to moisture, selectivity, durability, among others aspects [10]. It is also important to mention that the success of surface modification depends on the modification method and pore size [10, 45].

The methods for loading amines that offer high capture capacity are impregnation, post-synthesis grafting, and direct condensation. Efficiency depends on the support and application conditions [10]. One of the disadvantages is the possibility of leaching of the amines, limiting their long-term performance [10]. It should be noted that in the geological storage process, this would not be a problem, since the process does not involve regeneration, but loading method must immobilize the amine on a material surface. The

modification with polyethylamine-PEI and tetraethylenepentamine-PETA benefit CO_2 adsorption, where CO_2 adsorption capacities increased 6 and 8 mmol/g (silica supports), from gases with a CO_2 mass fraction of 10% at 75 °C and atmospheric pressure [10, 54].

However, treatment with amines can obstruct the microporosity, thereby decreasing its adsorption capacity; also, the surface modification process increases the final cost of nanomaterial [10, 45]. Also, in some cases, samples containing grafted primary and tertiary monoamines, the material could be deactivated in the presence of oxygen-containing gases [47]. Thus, it is desirable to incorporate nitrogen groups during material synthesis. Hence, amine or amino acid functional groups are grafted on the surface of the support during the synthesis process instead of physically dispersed in the pores after synthesizing the support material [55].

Metal-organic frameworks-MOF have structures that may not be suitable for application in the reservoir, but their evaluation is important due to the high capacity of CO_2 capture [10]. MOF is constructed employing transition metal ions and organic ligands, have been evaluated in the CO_2 adsorption process [10, 14, 56]. In this case, the investigations are focused on the development of new structures, a different configuration of metal ions and ligands, functionalization, hybrid materials, among others [10]. The metal ion directly influences the molecular interactions with CO_2, and organic ligand allows defining the porosity magnitude and specific surface area, which generates more interaction sites with CO_2. A disadvantage of MOFs is the performance in aqueous media due to the competition of H_2O with CO_2 for active adsorption sites [10].

In high-pressure processes (P> 20 bar), the CO_2 adsorption capacity is critically dependent on the surface area of the adsorbent [10, 26, 57, 58]. Whereby MOF has a high adsorption capacity in high-pressure processes; MOF has reached adsorbed amounts of up to 250% by weight at pressures of 55 bar [59]. However, the proper design of carbon materials allows obtaining adsorbents capable of competing and even surpassing the best MOFs [27, 44]. Meng and Park [61] reported a capacity of CO_2 capture of 248% by weight at a pressure of 30 bar, using graphene nanoplates [59], this is due to greater access to microporous volume and therefore so much more adsorption area [26, 57, 58].

2.1. Partial conclusions

The CCS process is a promising method for the stabilization of CO_2 emissions from the industry. However, despite the great efforts to massify it, its costs are appreciable. For this reason, the e-CCS process could be an alternative to the conventional process, in which the adsorption process modifies the physical principle of capture. Here the interactions of gaseous CO_2 with the porous medium take on particular relevance. Therefore, research to improve this process is of vital importance. In this case, the possibility of using nanoparticles as surface modifiers were evaluated, although there is development in the area of nanotechnology applied to CO_2 capture, many of these materials do not meet the requirements to be injected into geological deposits. Therefore, this thesis becomes relevant by focusing on the synthesis of nanomaterials with desirable physicochemical characteristics for the e-CCS process.

2.2. References

[1] NASA. (2019, March 30). *Global Climate Change. Vital Signs of the Planet*. Available: https://climate.nasa.gov/vital-signs/carbon-dioxide/

[2] N. G. C. Change, "Vital Signs of the Planet," *Earth Science Communications Team at NASA's Jet Propulsion Laboratory. Accessed June,* vol. 30, 2018.

[3] J. Tollefson. (2019, 2019). *The hard truths of climate change — by the numbers*. Available: https://www.nature.com/immersive/d41586-019-02711-4/index.html

[4] T. R. Anderson, E. Hawkins, and P. D. Jones, "CO2, the greenhouse effect and global warming: from the pioneering work of Arrhenius and Callendar to today's Earth System Models," *Endeavour,* vol. 40, pp. 178-187, 2016.

[5] R. J. Norby and Y. Luo, "Evaluating ecosystem responses to rising atmospheric CO2 and global warming in a multi-factor world," *New Phytologist,* vol. 162, pp. 281-293, 2004.

[6] D. A. Lashof and D. R. Ahuja, "Relative contributions of greenhouse gas emissions to global warming," *Nature,* vol. 344, p. 529, 1990.

[7] A. Fernandez Pales, P. Levi, and T. Vass, "Tracking Industry - IEA Report 2019," Internacional Energy Agency, IEA, https://www.iea.org/reports/tracking-industry-2019May, 2019 2019.

[8] M. M. Halmann, *Chemical Fixation of Carbon DioxideMethods for Recycling CO2 into Useful Products*: CRC press, 2018.

[9] P. M. Cox, R. A. Betts, C. D. Jones, S. A. Spall, and I. J. Totterdell, "erratum: Acceleration of global warming due to carbon-cycle feedbacks in a coupled climate model," *Nature,* vol. 408, p. 750, 2000.

[10] J. Wang, L. Huang, R. Yang, Z. Zhang, J. Wu, Y. Gao*, et al.*, "Recent advances in solid sorbents for CO 2 capture and new development trends," *Energy & Environmental Science,* vol. 7, pp. 3478-3518, 2014.

[11] B. Metz, O. Davidson, and H. De Coninck, *Carbon dioxide capture and storage: special report of the intergovernmental panel on climate change*: Cambridge University Press, 2005.

[12] M. Bui, C. S. Adjiman, A. Bardow, E. J. Anthony, A. Boston, S. Brown*, et al.*, "Carbon capture and storage (CCS): the way forward," *Energy & Environmental Science,* vol. 11, pp. 1062-1176, 2018.

[13] Y. Ma, Z. Wang, X. Xu, and J. Wang, "Review on porous nanomaterials for adsorption and photocatalytic conversion of CO2," *Chinese Journal of Catalysis,* vol. 38, pp. 1956-1969, 2017.

[14] X. Wu, Z. Bao, B. Yuan, J. Wang, Y. Sun, H. Luo*, et al.*, "Microwave synthesis and characterization of MOF-74 (M= Ni, Mg) for gas separation," *Microporous and Mesoporous Materials,* vol. 180, pp. 114-122, 2013.

[15] A. Chen, S. Li, Y. Yu, L. Liu, Y. Li, Y. Wang*, et al.*, "Self-catalyzed strategy to form hollow carbon nanospheres for CO2 capture," *Materials Letters,* vol. 185, pp. 63-66, 2016.

[16] H. R. a. R. Simmon. (2011, July 24). *The Carbon Cycle*. Available: https://earthobservatory.nasa.gov/features/CarbonCycle/page1.php

[17] I. IEA, "World energy outlook 2011," *Int Energy Agency,* vol. 666, 2011.

[18] !!! INVALID CITATION !!! [10-12].

[19] P. Cook, R. Causebrook, J. Gale, K. Michel, and M. Watson, "What have we learned from small-scale injection projects?," *Energy Procedia,* vol. 63, pp. 6129-6140, 2014.

[20] H. Balat and C. Öz, "Technical and Economic Aspects of Carbon Capture an Storage—A Review," *Energy Exploration & Exploitation,* vol. 25, pp. 357-392, 2007.

[21] C. Gough, *Carbon capture and its storage: an integrated assessment*: Routledge, 2016.

[22] C. Gough, "State of the art in carbon dioxide capture and storage in the UK: An experts' review," *International Journal of Greenhouse Gas Control,* vol. 2, pp. 155-168, 2008.

[23] E. Rodriguez Acevedo, F. B. Cortés, C. A. Franco, F. Carrasco-Marín, A. F. Pérez-Cadenas, V. Fierro*, et al.*, "An Enhanced Carbon Capture and Storage Process (e-CCS) Applied to Shallow Reservoirs Using Nanofluids Based on Nitrogen-Rich Carbon Nanospheres," *Materials,* vol. 12, p. 2088, 2019.

[24] N. Álvarez-Gutiérrez, M. Gil, F. Rubiera, and C. Pevida, "Adsorption performance indicators for the CO2/CH4 separation: Application to biomass-based activated carbons," *Fuel Processing Technology,* vol. 142, pp. 361-369, 2016.

[25] D. Yang, S. Wang, and Y. Zhang, "Analysis of CO2 migration during nanofluid-based supercritical CO2 geological storage in saline aquifers," *Aerosol Air Qual. Res,* vol. 14, pp. 1411-1417, 2014.

[26] M. E. Casco, M. Martínez-Escandell, J. Silvestre-Albero, and F. Rodríguez-Reinoso, "Effect of the porous structure in carbon materials for CO2 capture at atmospheric and high-pressure," *Carbon,* vol. 67, pp. 230-235, 2014.

[27] E. P.-C. Bailon-García, Agustín F.; Rodriguez Acevedo, Elizabeth; Carrasco-Marín, Francisco, "Nanoparticle Fabrication Methods," in *Formation Damage in Oil and Gas Reservoirs. Nanotechnology Applications for its Inhibition/Remediation*, C. A. a. C. C. Franco, Farid B, Ed., 1 ed: Nova Science Publishers, 2018, pp. 69-150.

[28] C. A. C. C. Franco, Farid B, *Formation Damage in Oil and Gas Reservoirs. Nanotechnology Applications for its Inhibition/Remediation*: Nova Science Publishers, 2018.

[29] C. A. Franco, R. Zabala, and F. B. Cortés, "Nanotechnology applied to the enhancement of oil and gas productivity and recovery of Colombian fields," *Journal of Petroleum Science and Engineering,* vol. 157, pp. 39-55, 2017.

[30] I. Moncayo-Riascos, C. A. Franco, and F. B. Cortés, "Dynamic Molecular Modeling and Experimental Approach of Fluorocarbon Surfactant-Functionalized SiO2

Nanoparticles for Gas-Wettability Alteration on Sandstones," *Journal of Chemical & Engineering Data,* 2019.

[31] Y. Hurtado, C. Beltrán, R. D. Zabala, S. H. Lopera, C. A. Franco, N. N. Nassar*, et al.*, "Effects of Surface Acidity and Polarity of SiO2 Nanoparticles on the Foam Stabilization Applied to Natural Gas Flooding in Tight Gas-Condensate Reservoirs," *Energy & fuels,* vol. 32, pp. 5824-5833, 2018.

[32] L. Cardona, D. Arias-Madrid, F. Cortés, S. Lopera, and C. Franco, "Heavy oil upgrading and enhanced recovery in a steam injection process assisted by NiO-and PdO-Functionalized SiO2 nanoparticulated catalysts," *Catalysts,* vol. 8, p. 132, 2018.

[33] M. Franco-Aguirre, R. D. Zabala, S. H. Lopera, C. A. Franco, and F. B. Cortés, "Interaction of anionic surfactant-nanoparticles for gas-Wettability alteration of sandstone in tight gas-condensate reservoirs," *Journal of Natural Gas Science and Engineering,* vol. 51, pp. 53-64, 2018.

[34] C. A. Franco, N. N. Nassar, M. A. Ruiz, P. Pereira-Almao, and F. B. Cortés, "Nanoparticles for inhibition of asphaltenes damage: adsorption study and displacement test on porous media," *Energy & Fuels,* vol. 27, pp. 2899-2907, 2013.

[35] S.-P. Kang and H. Lee, "Recovery of CO2 from flue gas using gas hydrate: thermodynamic verification through phase equilibrium measurements," *Environmental science & technology,* vol. 34, pp. 4397-4400, 2000.

[36] H. Yang, Z. Xu, M. Fan, R. Gupta, R. B. Slimane, A. E. Bland*, et al.*, "Progress in carbon dioxide separation and capture: A review," *Journal of environmental sciences,* vol. 20, pp. 14-27, 2008.

[37] X. Xu, C. Song, J. M. Andresen, B. G. Miller, and A. W. Scaroni, "Novel polyethylenimine-modified mesoporous molecular sieve of MCM-41 type as high-capacity adsorbent for CO2 capture," *Energy & Fuels,* vol. 16, pp. 1463-1469, 2002.

[38] S. Chowdhury and R. Balasubramanian, "Highly efficient, rapid and selective CO2 capture by thermally treated graphene nanosheets," *Journal of CO2 Utilization,* vol. 13, pp. 50-60, 2016.

[39] A. Wahby, J. M. Ramos-Fernández, M. Martínez-Escandell, A. Sepúlveda-Escribano, J. Silvestre-Albero, and F. Rodríguez-Reinoso, "High-surface-area carbon molecular sieves for selective CO2 adsorption," *ChemSusChem,* vol. 3, pp. 974-981, 2010.

[40] H. S. Choi and M. P. Suh, "Highly selective CO2 capture in flexible 3D coordination polymer networks," *Angewandte Chemie International Edition,* vol. 48, pp. 6865-6869, 2009.

[41] V. Chandra, S. U. Yu, S. H. Kim, Y. S. Yoon, D. Y. Kim, A. H. Kwon*, et al.*, "Highly selective CO2 capture on N-doped carbon produced by chemical activation of polypyrrole functionalized graphene sheets," *Chemical communications,* vol. 48, pp. 735-737, 2012.

[42] H. B. Park, J. Kamcev, L. M. Robeson, M. Elimelech, and B. D. Freeman, "Maximizing the right stuff: The trade-off between membrane permeability and selectivity," *Science,* vol. 356, p. eaab0530, 2017.

[43] C. M. Simon, B. Smit, and M. Haranczyk, "pyIAST: Ideal adsorbed solution theory (IAST) Python package," *Computer Physics Communications,* vol. 200, pp. 364-380, 2016.

[44] J. Silvestre-Albero and F. R. Reinoso, "Nuevos materiales de carbón para la captura de CO2," *Boletín del Grupo Español del Carbón,* pp. 2-6, 2012.

[45] M. Plaza, C. Pevida, A. Arenillas, F. Rubiera, and J. Pis, "CO2 capture by adsorption with nitrogen enriched carbons," *Fuel,* vol. 86, pp. 2204-2212, 2007.

[46] J. Wei, D. Zhou, Z. Sun, Y. Deng, Y. Xia, and D. Zhao, "A controllable synthesis of rich nitrogen-doped ordered mesoporous carbon for CO2 capture and supercapacitors," *Advanced Functional Materials,* vol. 23, pp. 2322-2328, 2013.

[47] T. J. Bandosz, M. Seredych, E. Rodríguez-Castellón, Y. Cheng, L. L. Daemen, and A. J. Ramírez-Cuesta, "Evidence for CO2 reactive adsorption on nanoporous S-and N-doped carbon at ambient conditions," *Carbon,* vol. 96, pp. 856-863, 2016.

[48] X.-q. Zhang, W.-c. Li, and A.-h. Lu, "Designed porous carbon materials for efficient CO2 adsorption and separation," *New Carbon Materials,* vol. 30, pp. 481-501, 2015.

[49] A. Alonso, J. Moral-Vico, A. A. Markeb, M. Busquets-Fité, D. Komilis, V. Puntes*, et al.*, "Critical review of existing nanomaterial adsorbents to capture carbon dioxide and methane," *Science of the total environment,* vol. 595, pp. 51-62, 2017.

[50] G. P. Lithoxoos, A. Labropoulos, L. D. Peristeras, N. Kanellopoulos, J. Samios, and I. G. Economou, "Adsorption of N2, CH4, CO and CO2 gases in single walled carbon nanotubes: A combined experimental and Monte Carlo molecular simulation study," *The Journal of Supercritical Fluids,* vol. 55, pp. 510-523, 2010.

[51] M. Bikshapathi, A. Sharma, A. Sharma, and N. Verma, "Preparation of carbon molecular sieves from carbon micro and nanofibers for sequestration of CO2," *Chemical Engineering Research and Design,* vol. 89, pp. 1737-1746, 2011.

[52] D. J. Babu, M. Bruns, R. Schneider, D. Gerthsen, and J. r. J. Schneider, "Understanding the influence of N-doping on the CO2 adsorption characteristics in carbon nanomaterials," *The Journal of Physical Chemistry C,* vol. 121, pp. 616-626, 2017.

[53] B. Chen, Z. Yang, G. Ma, D. Kong, W. Xiong, J. Wang*, et al.*, "Heteroatom-doped porous carbons with enhanced carbon dioxide uptake and excellent methylene blue adsorption capacities," *Microporous and Mesoporous Materials,* vol. 257, pp. 1-8, 2018.

[54] W.-J. Son, J.-S. Choi, and W.-S. Ahn, "Adsorptive removal of carbon dioxide using polyethyleneimine-loaded mesoporous silica materials," *Microporous and Mesoporous Materials,* vol. 113, pp. 31-40, 2008.

[55] Y.-R. Dong, N. Nishiyama, Y. Egashira, and K. Ueyama, "Basic Amid Acid-Assisted Synthesis of Resorcinol− Formaldehyde Polymer and Carbon Nanospheres," *Industrial & engineering chemistry research,* vol. 47, pp. 4712-4716, 2008.

[56] J. An and N. L. Rosi, "Tuning MOF CO2 adsorption properties via cation exchange," *Journal of the American Chemical Society,* vol. 132, pp. 5578-5579, 2010.

[57] S. Cavenati, C. A. Grande, and A. E. Rodrigues, "Adsorption equilibrium of methane, carbon dioxide, and nitrogen on zeolite 13X at high pressures," *Journal of Chemical & Engineering Data,* vol. 49, pp. 1095-1101, 2004.

[58] S. Himeno, T. Komatsu, and S. Fujita, "High-pressure adsorption equilibria of methane and carbon dioxide on several activated carbons," *Journal of Chemical & Engineering Data,* vol. 50, pp. 369-376, 2005.

[59] L.-Y. Meng and S.-J. Park, "Effect of exfoliation temperature on carbon dioxide capture of graphene nanoplates," *Journal of colloid and interface science,* vol. 386, pp. 285-290, 2012.


LIBERTAD Y ORDEN
INTER · AULAS · ACADEMIÆ · QUÆRE · VERUM


UNIVERSITAS · GRANATENSIS
PLUS ULTRA
1531

3. Synthesis and characterization of carbon nanostructures for CO_2 adsorption

As mentioned in the previous chapter, carbon materials show good results regarding adsorption capacity and selectivity of CO_2, due to high surface area, modifiable pore structure, surface functionalization, and easy regeneration, also can be synthesized at low cost [1-7].

The physical interactions are the main cause of CO_2 adsorption on carbon materials [1, 8]. The last scientific studies have been focused on modifications for increasing surface area, adjustment of the porous structure, synthesis of carbon-based hybrid composites, and surface modification with functional groups containing nitrogen, oxygen, metal oxides, among others [5-7, 9-13].

This chapter has, like the main objective, develop carbon nanospheres for the selective CO_2 capture at e-CCS conditions. Specific chemical-physical properties are required, such as nanometric particle size, high surface area, spherical structure, high affinity, synthesis reproducibility, among others. Also, materials should be industrially scalable. For this purpose, a commercially available triblock copolymer called Pluronic F127 was employed as a soft template, to obtain porous nanoparticles [14]. The operation conditions were varied, such as reagent concentration, stirring, the molar ratio between water and carbon precursor. In some materials, chemical/physical surface modifications were carried out to optimize the physicochemical properties and, therefore, their performance in an adsorption process. Finally, the best nanomaterial and sandstone impregnated was evaluated in the

CO_2 adsorption process at atmospheric and high-pressure conditions (shallow reservoir conditions). The details are presented below.

3.1. Materials and Methods

3.1.1. Materials and Reagents

For the synthesis and surface modification processes, the following reagents were used: Formaldehyde (37%), resorcinol (≥ 99%), Pluronic-F127 (> 99%), melamine (> 99%), N-Buthylamine (> 99%), 2-Hyddroxypyridine (> 99%), 3-Aminophenol (> 99%), ammonia (32%), urea (> 99%), acetone (99.9%), and deionized water.

For carbonization was used N_2 (high purity, grade 5.0). Clean Ottawa sandstone was used as porous media.

3.1.2. Synthesis of Nanomaterials

Carbon nanospheres were synthesized, varying some operating conditions. Subsequently, the best nanomaterial was superficially modified through 1) nitrogen compounds (solvothermal reaction) or 2) physical activation using CO_2 at high temperatures. The methods are presented below.

3.1.2.1. Synthesis method

The general procedure was adapted from Fang et. Al [14], changing carbon precursor and some operating conditions in order to obtain nanometric size and high surface area. The original method uses phenolic resol as a carbon source, but the material yield is less than 10%. For this reason, resorcinol was used as a carbon precursor. The Pluronic F127 was employed as a soft template, to obtain porous nanoparticles. The pluronic concentration, stirring, and molar ratio water/resorcinol (W/R) were varied (Table 3. 1) to obtain particles with the smallest possible size and the highest CO_2 adsorption capacity.

Initially, a solution of resorcinol/formaldehyde (R/F) (molar ratio 1:2), Pluronic F127, and deionized water are stirring at 25 ºC for 18 hours. The solution is carried out to a hydrothermal reactor for 24 hours at 130 ºC. The obtained polymer is cleaned with acetone

for 3 days to remove the water inside the porous structure. After that, the material is carbonized in N_2 at 700 ºC for 4 hours. Table 3. 1 presents the variables evaluated.

Table 3. 1. Synthesis conditions and variables

Variable	Values	Samples	Other conditions
Pluronic F127 concentration (mol.L^{-1})	10^{-5} 10^{-10}	EOP-5 EOP-10	R/F: 1:2 W/R: 450:1 Rpm: 200
Stirring (rpm)	200 5000	EOP-200 EOP-5000	R/F: 1:2 W/R: 450:1 Pluronic: 10^{-5} mol L^{-1}
Molar ratio of Water/Resorcinol	250:1 450:1 1350:1 2250:1	EOP-250 EOP-450 EOP-1350 EOP-2250	R/F: 1:2 Rpm: 200 Pluronic: 10^{-5} mol L^{-1}

In this synthesis process, spherical R/F-F127 monomicelles are formed from the hydrogen-bond interaction between pluronic F127 and R/F under low-concentration conditions (to avoid the excessive cross-linking between micelles). During the hydrothermal process at high temperature (130 °C), the monomicelles can be promoted assemble. Because the cross-linking process occurs actively at the high temperature and the crystal growth is isotropic, a spherical morphology is obtained. The lower the concentration of reagents, the fewer monomicelles are assembled in the reachable domain, resulting in a smaller diameter of the carbon spheres [14].

3.1.2.2. Superficial modification with nitrogen compounds

The best material (EOP-2250) was modifying with different nitrogen compounds such as melamine, N-Buthylamine, 2-Hyddroxypyridine, 3-Aminophenol, ammonia, and urea.

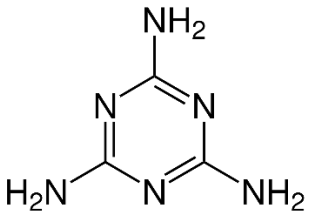

Melamine

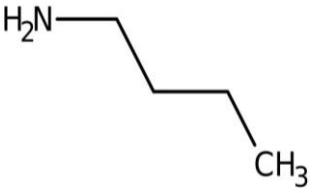

n-butylamine

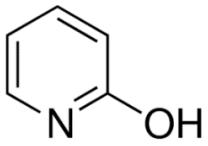

2-hydroxy pyridine

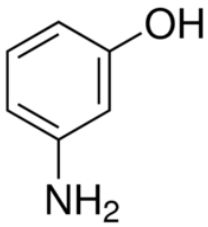

3-Aminophenol

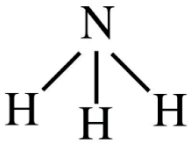

Ammonia

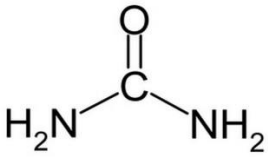

Urea

For amines and ammonia, a solvothermal procedure was carried out at 180 °C for 24 h. This process was used to anchor the nitrogen compound to the surface. This process is important due to the functionalized material would be transported in an aqueous medium through the reservoir, which removes nitrogen compounds from the surface if it is not anchored. The reaction was carried out with 200 mg of nanoparticles and a nitrogen mass fraction of 20%, keeping the same molar ratio of nitrogen to set the nitrogen concentration, independent of reagent's weight.

For modification with urea, a mass ratio of urea/carbon material of 2:1 is mixed (after sifting and drying each material under a dynamic vacuum for 24 hours). After mixing, the solid is taken to a tubular oven under an air atmosphere for 4 hours at 450 °C.

3.1.2.2. Impregnation of sandstone

The sandstone was impregnated to decorate the rock surface with the best nanoparticles to improve the surface area and molecular interactions. Ottawa sandstone (SS) was impregnated with EOP-2250 at mass fractions 5, 10, and 20% by immersion and soaking [15]. Initially, a nanofluid composed of nanoparticles and deionized water was sonicated at 40 °C for 4 h. Subsequently, the SS was introduced in the nanofluid at 60 °C for 24 h without stirring. This method mimics the reservoir conditions in which the porous medium might be impregnated.

3.1.3. Characterization of the Nanomaterials

The following procedures allowed characterizing the physicochemical characteristics of the materials, essential for a good understanding of the results. For the e-CCS application, nanoparticles must have a nanometer size, a spherical shape, a high surface area, and high nitrogen content.

3.1.3.1. Size and Structure of Nanomaterials

Scanning electron microscopy (SEM) was used to obtain the dry particle size, size distribution, and morphology of carbon materials. The observations were carried out using a JSM-7100 emission electron microscope (JEOL, Nieuw-Vennep, The Netherlands), a GEMINI-LEO1530 VP FE-SEM emission electron microscope (Carl Zeiss, Cambridge, UK).

Dynamic light scattering (DLS) was carried out using a NanoPlus-3 zeta/nanoparticle analyzer (Micromeritics, Norcross, USA) at 25 °C. A glass cell (capacity of 0.9 mL) was used to obtain the mean particle size of nanoparticles dispersed in a fluid, which hydrate and interact with each other. The mean particle size was calculated from the diffusional properties of the particle, indicating the size of the hydrated and solvated particle. For this purpose, a nanoparticle solution, 10 mg L^{-1}, was dispersed in water or ethanol and sonicated for 6 h before analysis. Particles suspended in a liquid have a Brownian motion due to the random collisions with solvent molecules. This motion causes the particles to diffuse through the medium. The diffusion coefficient, D, is inversely proportional to the particle size or hydrodynamic diameter, d, according to the Stokes-Einstein equation:

$$D = \frac{k_B T}{3\pi \eta d} \quad \textbf{(3.1)}$$

where k_B is Boltzmann's constant, T is the absolute temperature, and η is the viscosity.

3.1.3.2. Textural parameters

Materials were characterized by N_2 and CO_2 adsorption at −196 °C and 0 °C, respectively, using 3-Flex manometric adsorption equipment (Micromeritics, Norcross, USA). The total adsorbed volume ($V_{0.95}$) is taken as the physisorbed volume of N_2 at a relative pressure

P/P_0 = 0.95. The Brunauer–Emmett–Teller (BET) model was applied to obtain the BET area (A_{BET}). Micropore volume (V_{mic}), average pore size (L_0), and CO_2 adsorption energy ($E_{ads–CO2}$) were obtained by application of the Dubinin–Radushkevich equation. The mesopore volume (V_{meso}) was obtained through the Barrett–Joyner–Halenda (BJH) model.

3.1.3.3. Chemical composition of nanomaterials and sandstone

The chemical characterization was carried out by carbon, hydrogen, oxygen, and nitrogen (CHON) analysis for nanomaterials, and by Fourier transform infrared spectroscopy (FTIR) for sandstone. An IRAffinity-1S FTIR spectrometer (Shimadzu, Columbia, USA) was operated at room temperature using potassium bromide in a KBr-to-material ratio of 30:1 (% w/w). The impregnation percentages of nanoparticles on sandstone were corroborated by thermogravimetric analysis (TGA) (TA Instruments, New Castle, USA). For this, the sample was burned under an air atmosphere at 10 °C min^{-1} up to 800 °C.

3.1.3.4. Dispersion of Nanoparticles in Solution

The electrophoretic light scattering (ELS) technique was used to evaluate the surface charge of the particles and their dispersion stability at 25 °C in a NanoPlus-3 zeta/nanoparticle analyzer (Micromeritics, Norcross, USA). In this test, several nanoparticle suspensions were prepared at 10 mg L^{-1}, with a pH adjusted between 2 to 12 by adding solutions of 0.1 mol L^{-1} HCl or 0.01 mol L^{-1} NaOH and then subjected to analysis. The zeta potential was calculated using the Smoluchowski equation, derived from the calculation of the Doppler effect.

$$\zeta = \eta U / \varepsilon \quad \textbf{(3.2)}$$

$$U = \frac{V}{E} \quad \textbf{(3.3)}$$

$$\Delta\nu = 2V\, n \sin\left(\frac{\theta}{2}\right) / \lambda \quad \textbf{(3.4)}$$

where ζ is the zeta potential, η is the viscosity of the fluid (water), U is the electrophoretic mobility, ε is the permittivity, V represents the speed of movement of the particles, E is the electric field, $\Delta\nu$ is the Doppler effect, n is the index of refraction, θ is the angle of detection, and λ is the wavelength of the incident light.

3.1.4. Adsorption Tests at High Pressure

At high pressure, the CO_2 adsorption capacity was evaluated under pure CO_2 in a manometric device (up to 3.0 MPa) for EOP-2250.

The High-Pressure Volume Analyzer, HPVAII-200 (Micromeritics, Norcross, USA) was operated at 0 °C, 25 °C, and 50 °C and at pressures from 3×10^{-3} up to 3.0 MPa. In order to have enough total surface area for adsorption and to minimize measurement errors, the amount of each material inside the sample holder was around 0.5 g for nanoparticles and 14 g for sandstone. The contribution of the empty sample holder was systematically measured and subtracted to all data to improve accuracy. The isosteric heat of adsorption, Q_{ST}, was calculated using the isosteric method through Microactive software (from Micromeritics, Norcross, USA). For this, three adsorption isotherms (at 0, 25, and 50 °C) were used to calculate utilizing Clausius–Clapeyron equation [16]:

$$-\frac{Q_{ST}}{R} = \frac{\partial \ln(P)}{\partial(1/T)} \quad \textbf{(3.5)}$$

where R is the universal gas constant (8.314 J mol^{-1} K^{-1}), P is the absolute pressure, and T is the temperature.

The excess adsorbed CO_2 amount (N_{exc}, $g_{CO2}.g_{adsorbent}^{-1}$) is equal to the absolute adsorbed CO_2 amount ($N_{ads,}$ $g_{CO2}.g_{adsorbent}^{-1}$) minus the product of gas density in the bulk phase by the volume of the adsorbed phase. The values provided by the HPVA device were obtained on an excess basis, and therefore, the absolute amounts had to be determined as follows [17]:

$$N_{ads} = N_{exc}\left(1 + \frac{P + M_{CO2}}{Z\,\rho_{liq}\,RT}\right) \quad \textbf{(3.6)}$$

where M_{CO2} is the molecular weight of CO_2 (44.013 g mol^{-1}), Z is the compressibility factor at the considered pressure and temperature, and ρ_{liq} is the density of liquid CO_2 (1032×10^3 g m^{-3}).

The isotherms were fitted with two conventional models (Langmuir and Freundlich), and a model takes into account multilayer adsorption (Sips model) at high pressure. Table 3. 2 presents the equations for each model [5, 10, 18]. K_L, K_F, and K_S represent adsorption

equilibrium constants for the Langmuir, Freundlich, and Sips models, respectively, and the *n* parameter indicates the heterogeneity of the system. The heterogeneity may originate from the solid structure, from the solid energy properties, or the adsorbate [10]. The *n* is usually higher than unity, and when they are the unit, the model assumes the Langmuir equation [10].

Table 3. 2. Models for adsorption isotherms

Model	Equations	Parameters
Langmuir	$\boldsymbol{N_{ads} = \frac{N_m * K_L * P}{1 + K_L * P}}$ **(3.7)**	N_{ads} (mmol/g) is the adsorbed amount, N_m (mmol/g) monolayer adsorption capacity, P (kPa) is the equilibrium pressure, and K_L (1/kPa) is the Langmuir adsorption equilibrium constant
Freundlich	$\boldsymbol{N_{ads} = K_F * P^{(1/n)}}$ **(3.8)**	N_{ads} (mmol/g) is the adsorbed amount, P (kPa) is the equilibrium pressure, K_F and n are the Freundlich adsorption equilibrium constants
Sips	$N_{ads} = N_m \frac{(K_S P)^{1/n}}{1 + (K_S P)^{1/n}}$ **(3.9)**	N_{ads} (mmol g^{-1}) is the adsorbed amount, N_m (mmol g^{-1}) is the adsorption capacity at equilibrium, *P* (kPa) is the equilibrium pressure, and K_S and *n* are the Sips adsorption equilibrium constants, related to the affinity and the heterogeneity of the system, respectively.

3.2. Results and Discussion

The results are divided into two main sections: a) materials characteristics (nanoparticles and sandstone) and b) study of adsorption under different operation conditions (T, P).

3.2.1. Materials Characteristics

The morphology of the carbon materials obtained from variation of synthesis conditions, are presented in Figure 3. 1, Figure 3. 2 and Figure 3. 3.

SEM images for different pluronic concentrations, where the lower Pluronic concentration (10^{-10} mol.L^{-1}) allowed to decrease the particle size but did not become nanometric (Figure 3. 1-b), and the size is more heterogeneous than material obtaining at a highest pluronic concentration (10^{-5} mol.L^{-1}, Figure 3. 1-a). The low pluronic concentration avoids the excessive cross-linking between micelles.

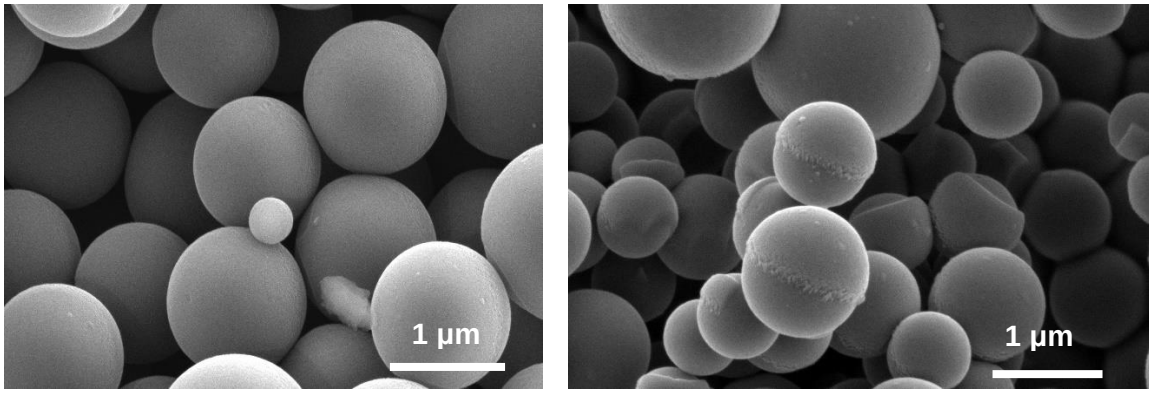

(a) **(b)**

Figure 3. 1. SEM images at 5 kV of carbon nanospheres varying Pluronic F127 at (**a**) 10^{-5} mol.L^{-1} and (**b**) 10^{-10} mol.L^{-1}. Constant parameters: R/F: 1:2, W/R: 450:1, Rpm: 200

With more considerable agitation, a smaller aggregation of micelles was expected and, therefore, a smaller size. The Figures 3. 2-a,b do not present a significant change between them, and also failed to generate nanometric sizes.

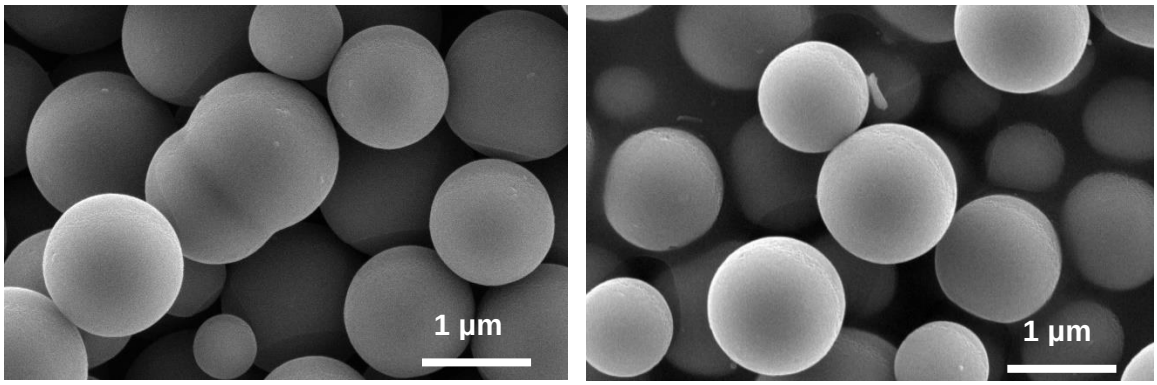

(a) **(b)**

Figure 3. 2. SEM images at 5 kV of carbon nanospheres varying stirring at (**a**) 200 rpm, (**b**) 5000 rpm. Constant parameters: R/F: 1:2, W/R: 450:1, Pluronic: 10^{-5} mol L^{-1}

The most significant effect is observed by varying of W/R concentration (Figure 3. 3). For low concentrations of R/F, the monomicelles are not close in the solution, so they are less likely to bind, resulting in a smaller diameter of the carbon spheres (Figure 3. 3-d). The smallest possible particle size was only possible for EOP-1350 and EOP-2250.

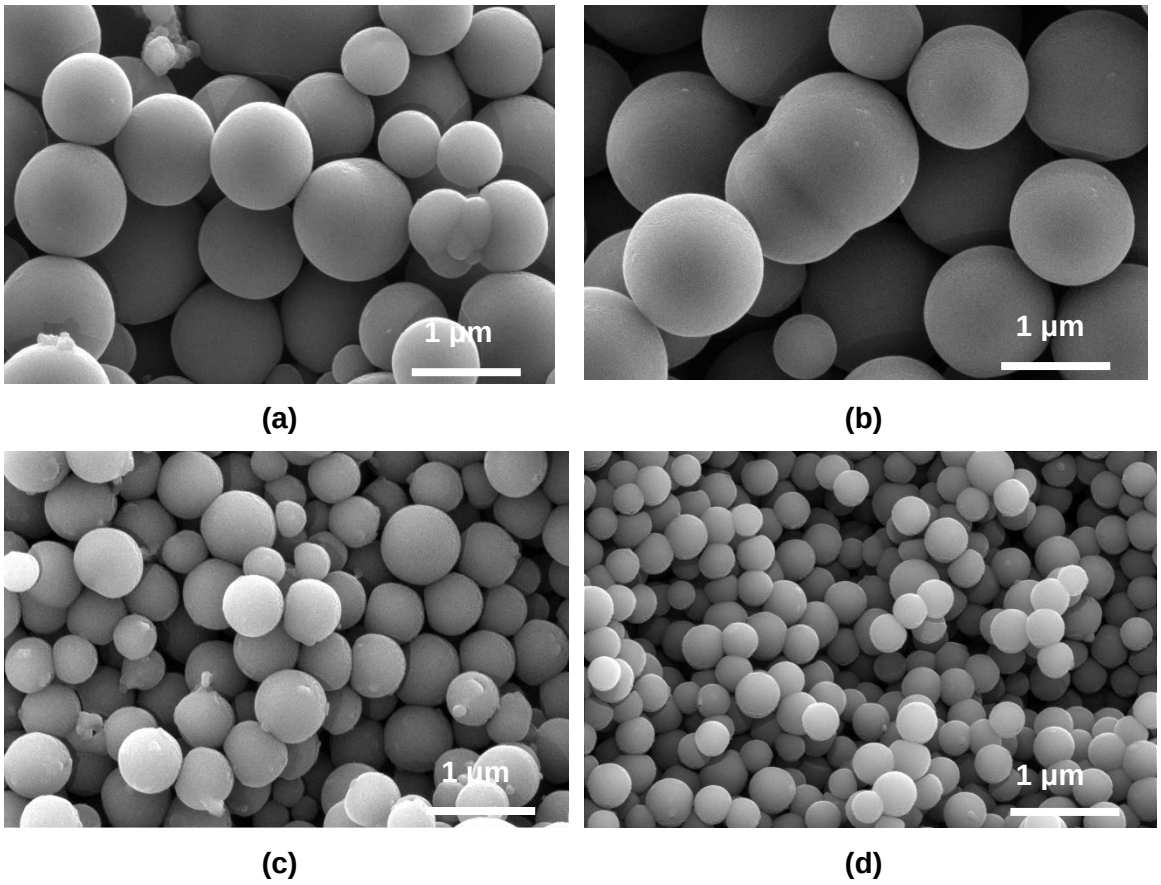

Figure 3. 3. SEM images at 5 kV of carbon nanospheres varying molar ratio of W/R at (**a**) 250:1, (**b**) 450:1, (**c**) 1350:1 and (**d**) 2250:1. Constant parameters: R/F: 1:2, Rpm: 200, Pluronic: 10^{-5} mol L^{-1}

The hydrodynamic diameter value was only possible for EOP-1350 and EOP-2250. Other materials exceeded the detection limit of the equipment (10 µm), which indicates large particles and possibly aggregation by hydrophobic characteristics. For the e-CCS process,

these materials might, thus, induce technical problems, due to the possible obstruction of the naturally porous structure of the rock.

Table 3. 3. Mean particle size of nanomaterials in suspension.

Material	d_p 50 (nm) in water (pH 5.8)	d_p 50 (nm) in ethanol (pH 7)
EOP-1350	3655	2954
EOP-2250	952	765

Figure 3.4 presents the zeta potential. A pH higher than 6 could be the best and feasible condition for impregnation at reservoir conditions (water as aqueous media). The zeta potential was farther from zero, and there are fewer aggregates in the system, which benefits the greater distribution of the nanomaterial in the porous medium.

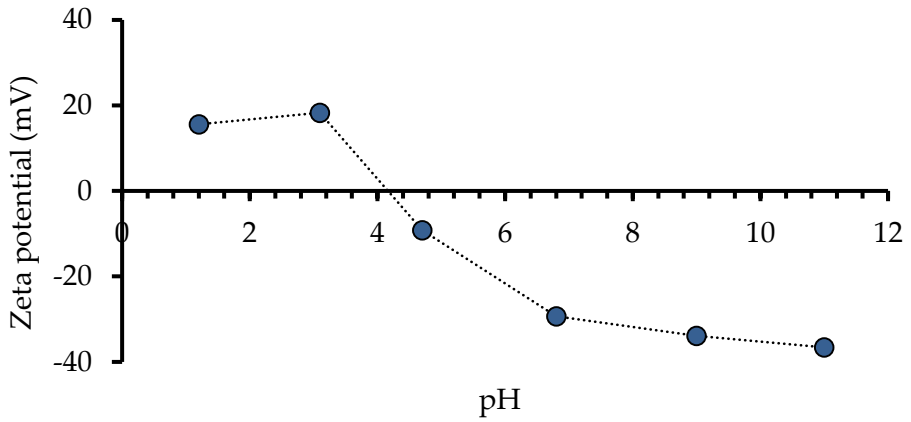

Figure 3. 4. Zeta potential for EOP-2250

The EOP-2250 is the best materials due to its particle size and behavior in an aqueous medium. For this reason, the following characterization analysis was carried out for this nanomaterial. The synthesis yield of EOP-2250 is 61%.

For textural parameters were evaluated for EOP-2250 and sandstone impregnated with a mass fraction of 5, 10, and 20% of EOP-2250 (Table 3. 4, Figure 3. 5 and Figure 3. 6). The textural parameters of the impregnated sandstones were indeed improved as the

percentage of nanoparticles on their surface increased. The EOP-2250 material is mainly microporous (> 93%). The sandstone presented an A_{BET} of 0.4 m^2 g^{-1}, and its CO_2 adsorption capacity could not be measured using conventional methods (< 0.0013 mmol g^{-1} at 0 °C and atmospheric pressure). From FTIR, sandstone is mainly composed of silica, which has an acidic character as the CO_2 molecule. Consequently, if the specific area of the sandstone is low, its CO_2 adsorption capacity is even lower than that which might be expected for this specific area.

Table 3. 4. Parameters obtained from adsorption isotherms (N_2 at −196 °C and CO_2 at 0 °C) for EOP-2250 and sandstone impregnated with mass fractions of 5, 10, and 20 % of EOP-2250.

	A_{BET} ($m^2.g^{-1}$)	V_{mic-N2} ($cm^3.g^{-1}$)	$V_{0,95}$ ($cm^3.g^{-1}$)	V_{meso} ($cm^3.g^{-1}$)	$V_{micro-CO2}$ ($cm^3.g^{-1}$)	L_{0-CO2} (nm)	$E_{ads-CO2}$ ($kJ.mol^{-1}$)
EOP-2250	645,6	0,243	0,261	0,018	0,251	0,56	30,7
SS-5	2,54	0,007	0,009	0,002	0,008	0,54	31,2
S-10	6,53	0,017	0,021	0,004	0,018	0,51	32,7
S-20	11,76	0,033	0,040	0,007	0,033	0,49	33,2

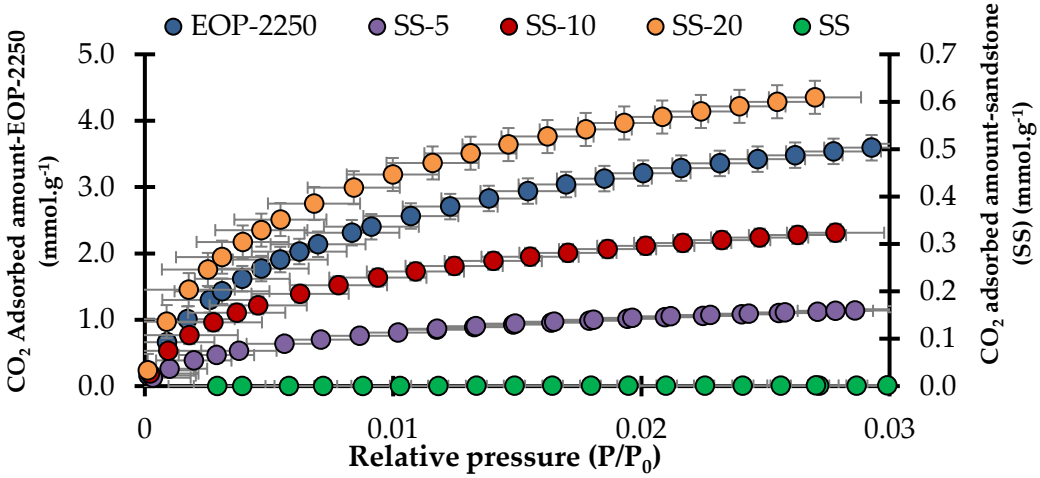

Figure 3. 5. Adsorption isotherms of CO_2 at atmospheric pressure and 0 °C for EOP-2250 and sandstone impregnated with a mass fraction of 5, 10, and 20 % EOP-2250.

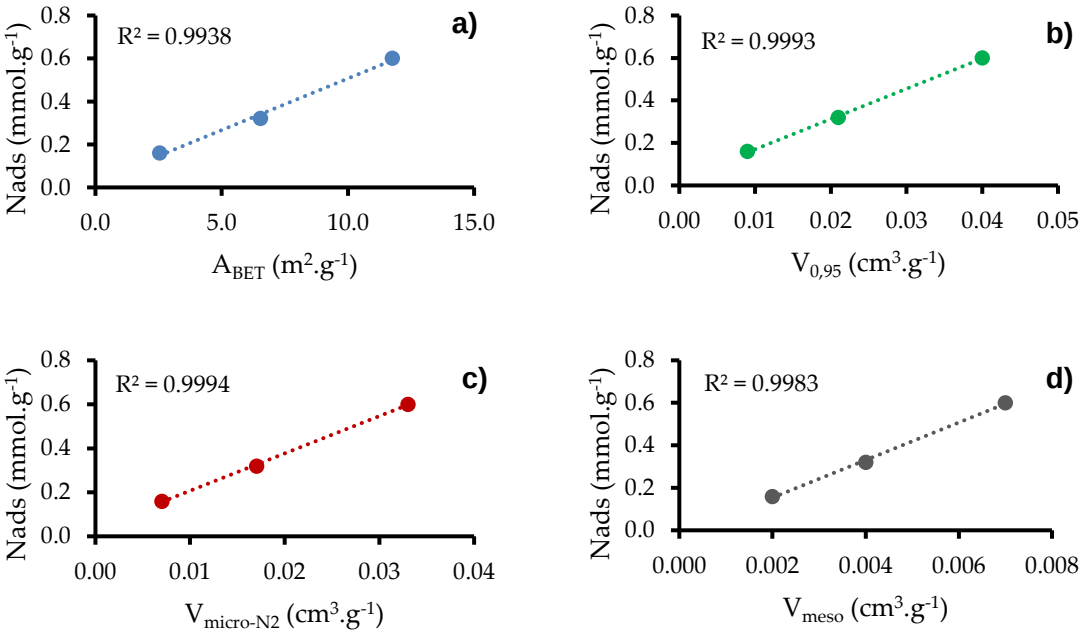

Figure 3. 6. Relationship between CO_2 adsorption capacity (N_{ads}) and: (**a**) Superficial area (A_{BET}), (**b**) Total adsorbed volume ($V_{0.95}$), taken as the of N_2 at a relative pressure P/P_0 = 0.95, (**c**) Micropore volume ($V_{mic\text{-}N2}$), and (**d**) mesopore volume (V_{meso}). EOP-2250 and sandstone impregnated with a mass fraction of 5, 10, and 20 % EOP-2250 at 0 °C (CO_2 adsorption) and -196 °C (N_2 adsorption) and atmospheric pressure.

The possible synergistic behavior between EOP-2250 and sandstone was evaluated using the theoretical and experimental values of the CO_2 adsorption capacity (Table 3. 5). The difference between theoretical and experimental values corresponds to the experimental error given the inaccuracy in the measurement of the insufficient CO_2 adsorption capacity of the sandstone. The differences could also be related to the segregation of nanoparticles during the impregnation process, and the nanoparticles may not be homogeneously distributed on the surface of the sandstone.

The system has no appreciable synergistic effect. From the thermogravimetric analysis, a variation between 6 and 12 % is observed concerning the amount of impregnation desired. The real percentages are 4.7, 11.2, and 18.2%.

Table 3. 5. CO_2 adsorption capacity at atmospheric pressure, 0°C, and mass fractions of 5, 10, and 20 %. Theoretical and experimental values.

	5%	**10%**	**20%**
Theoretical N_{ads} (mmol g^{-1})	0.18	0.36	0.72
Real theoretical N_{ads} (mmol g^{-1})	0.17	0.40	0.66
Experimental N_{ads} (mmol g^{-1})	0.16	0.32	0.60
Relative difference (%)	5.9	20.0	9.1

The increase of sandstone adsorption capacity is 12208 % (at 5% of EOP-2250), 24515 % (at 10% of EOP-2250) and 46054 % (at 20% of EOP-2250).

In order to increase the CO_2 adsorption capacity of EOP-2250, physical modifications (an increase of area through an activation with CO_2) and chemical modifications (an increase of nitrogen content) were made. Table 3. 6 presents the textural parameter after chemical-physical surface modification. EOP-2250 presents an A_{BET} of 645.6 $m^2.g^{-1}$, which decreases considerably with the modification with nitrogen compounds. In some cases, it was impossible to measure it. In physical activation with CO_2, EOP-2250 increases A_{BET} at 755 $m^2.g^{-1}$ (17%).

Table 3. 6. Parameters obtained from adsorption isotherms (N_2 at −196 °C and CO_2 at 0 °C) for EOP-2250 superficially modified with amines, ammonia, urea, and CO_2 activation

Modification	A_{BET} $m^2.g^{-1}$	V_{mic-N2} $cm^3.g^{-1}$	$V_{0,95}$ $cm^3.g^{-1}$	V_{meso} $cm^3.g^{-1}$	$V_{mic-CO2}$ $cm^3.g^{-1}$	L_{0-CO2} nm	$E_{ads-CO2}$ $kJ.mol^{-1}$	$N_{ads-CO2}$ $mmol.g^{-1}$
EOP-2250	645.6	0.243	0.261	0.018	0.271	0.56	30.7	3.6
Act. CO_2	755	0.288	0.296	0.008	0.374	0.96	22.7	4.0
n-butylamine	7.1	-	0.012	0.012	0.060	0.80	24.9	0.8
2-Hydroxypyridine	-	-	-	-	0.190	1.01	22.0	2.4
Melamine	-	-	-	-	0.205	0.88	23.7	2.6
Aminophenol	3	-	-	-	0.167	0.81	24.8	2.2
Ammonia	-	-	-	-	0.13	0.92	24.5	2.7
Urea	6.3	-	-	-	0.191	0.67	27.6	2.6

The elemental analysis is presented in Table 3. 7. Some N-rich carbon materials, reported in the literature, have nitrogen content close to those obtained in this work [1]. The oxygen content was measured independently from carbon, hydrogen, and nitrogen content.

Table 3. 7. Parameters obtained from adsorption isotherms (N_2 at −196 °C and CO_2 at 0 °C) for EOP-2250 superficially modified with amines, ammonia, urea, and CO_2 activation

Material	N	C	H	O
	Mass fraction (%)			
EOP-2250	0.04	93.4	1.8	6.0
Act. CO_2	0.03	91.7	1.7	7.9
n-butylamine	0.8	91.6	1.6	9.5
2-Hydroxypyridine	1.5	85.5	2.1	10.2
Melamine	7.3	84.2	2.2	11.1
Aminophenol	1.4	87.2	2.0	10.9
Ammonia	0.6	93.1	1.7	9.8
Urea	10.2	78.7	2.1	9.4

Figure 3. 7 presents the N_{ads} increase or decrease related to nitrogen contents and physical parameters such as surface area (A_{BET}) and micropore volume ($V_{mic\text{-}CO2}$) from CO_2 isotherm at 0 °C.

The modification with nitrogen compounds increases the nitrogen content considerably. However, A_{BET} and $V_{mic\text{-}CO2}$ decrease to almost 100 % (A_{BET}) and 78 % ($V_{mic\text{-}CO2}$), this effect could be generated by the obstruction of the mainly microporous structure of nanomaterial, similar cases are presented in the literature [7]. However, the adsorption capacity does not decrease in the same proportion (Figure 3. 7-a-c). The nitrogen content enhances the N_{ads}, although N_{ads} of the original material is higher (without modification with nitrogen compounds) due to capacity-related porous volume [19].

In the case of the material activated with CO_2, a N_{ads} increases can be observed, due to the increase of surface area and micropore volume. This material presents the best N_{ads} despite not having a considerable concentration of nitrogen.

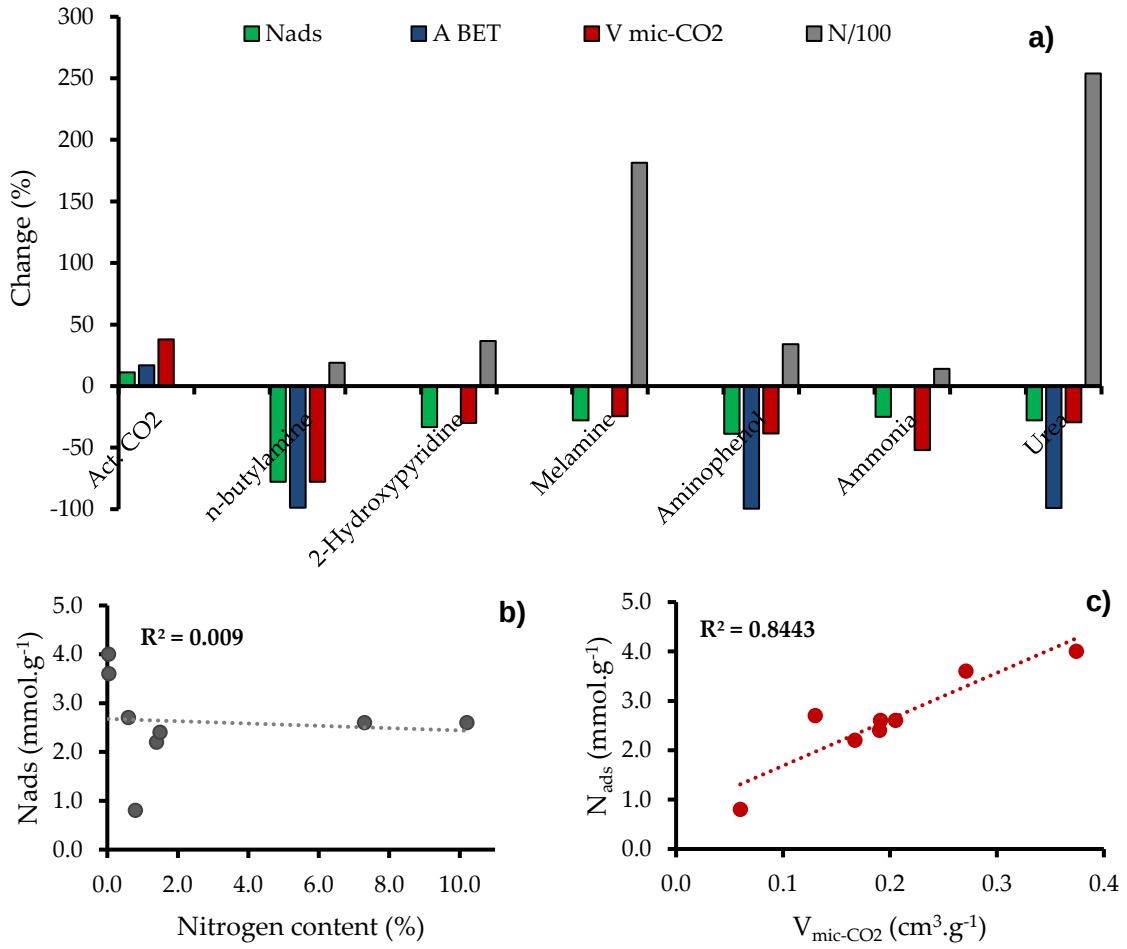

Figure 3. 7. Relationship between CO_2 adsorption capacity (N_{ads}) and: (**a**) Superficial area (A_{BET}) and Micropore volume ($V_{mic\text{-}N2}$), (**b**) Total adsorbed volume ($V_{0.95}$), taken as the of N_2 at a relative pressure P/P_0 = 0.95, (**c**), and (**d**) mesopore volume (V_{meso}). EOP-2250 and sandstone impregnated with a mass fraction of 5, 10, and 20 % EOP-2250 at 0 °C (CO_2 adsorption) and -196 °C (N_2 adsorption) and atmospheric pressure.

In order to improve the material and the N_{ads}, something important could be to develop highly microporous nanomaterials that incorporate nitrogen into the synthesis process, in order to enhance the two previous effects, but avoiding: 1) obstructing the porous structure of the material and 2) costs associated with subsequent stages of surface modification.

3.2.2. High-Pressure Adsorption Tests

The e-CCS process requires to evaluate the behavior of the materials at high pressure (0-3 MPa) and a temperature of a reservoir (50°C). Figure 3. 8 presents the CO_2 adsorption capacity for EOP-2250 (a) 0 °C, (b) 25 °C and (c) 50 °C. If Nads (at 0 °C) is compared with N_{ads} (at high and atmospheric pressure), an increase of 49 % is obtained. This increase is due to the pressure effect in the porous structure of nanomaterial. This is indicating a physisorption adsorption mechanism meanly.

At 50 °C, as it was expected, the adsorption capacity decreases 19.4 %, due to the exothermic character of adsorption. The difference between absolute amount and the excess amount represents 8.2 % (at 0 °C), 6.3 % (at 25 °C) and 5.8 % (at 50 °C). This difference is lower with the increment of temperature. The adsorption capacity obtained is competitive, compared with another reported for nanomaterials in literature at similar conditions [20-22].

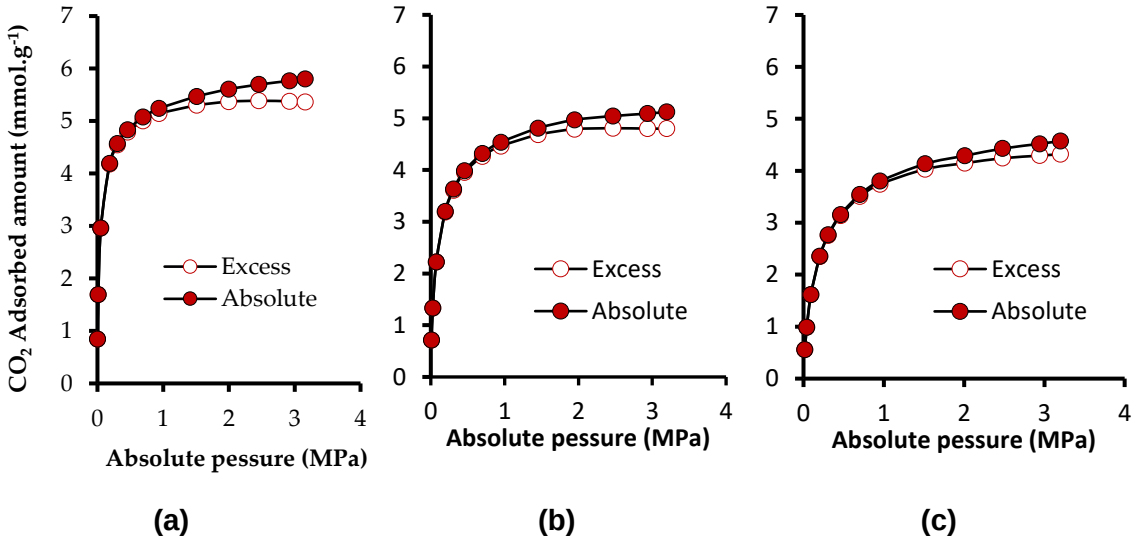

Figure 3. 8. Adsorption isotherms of CO_2 at high pressure (3×10^{-3} up to 3.0 MPa) of EOP-2250 at (**a**) 0 °C, (**b**) 25 °C, and (**c**) 50 °C

Figure 3. 9 presents the fit of the Langmuir, Freundlich, and Sips models to the CO_2 adsorption isotherms at high pressure and 0, 25, and 50°C for EOP-2250. As expected, the Sips model leads to perfect fits: $R^2 > 0.999$. For the other models, $R^2 > 98$ % (Langmuir) and 92 % (Freundlich).

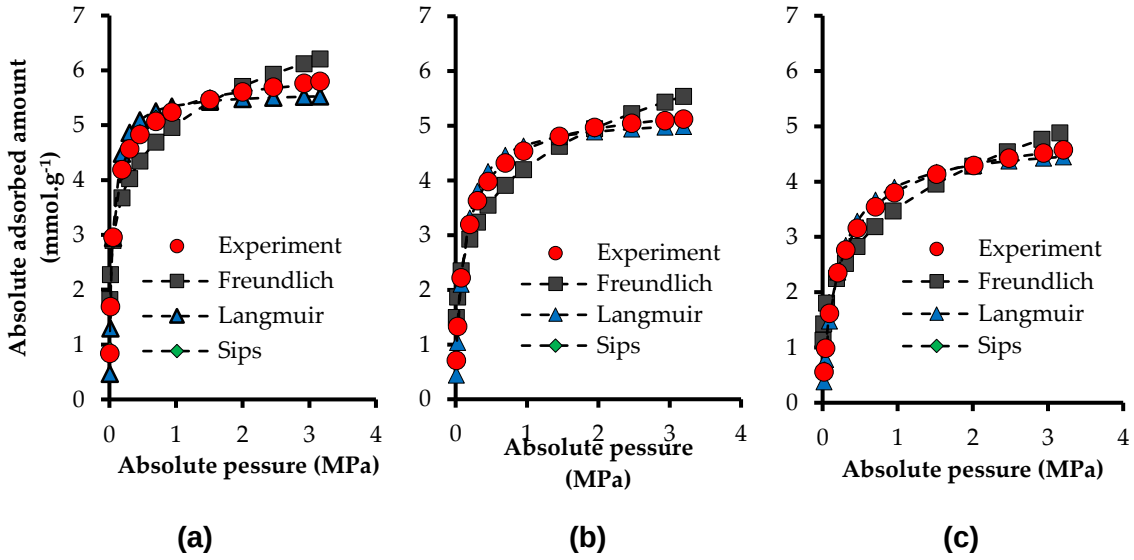

Figure 3. 9. Adsorption models fit CO_2 isotherms for EOP-2250 at high pressure and (**a**) 0 °C, (**b**) 25 °C, (**c**) 50 °C

Figure 3.10 presents the isosteric heat of adsorption (Q_{st}) of EOP-2250, as a function of N_{ads} expressed in mmol per gram of total adsorbent material. The values of Q_{st} varied from 28 to 32 kJ mol^{-1}, which indicates a strong interaction in the adsorption system (high affinity). The interactions with the porous carbon structure could be increased by nitrogen-containing groups that are present onto the carbon surface. Nitrogen groups can indeed promote interactions between CO_2 and the substrate. The values of Q_{st} compare favorably with those reported in the literature for different materials doped or not with nitrogen (20–25 kJ mol^{-1}, on average) [9, 12, 23, 24].

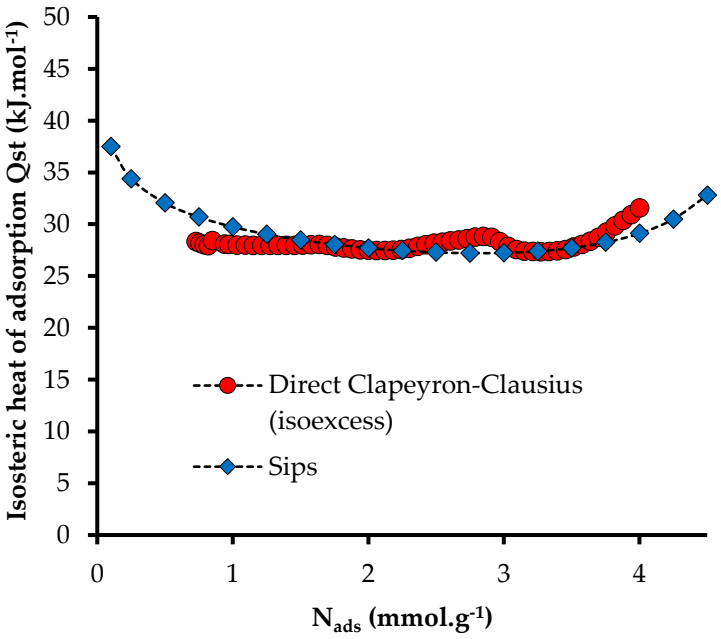

Figure 3. 10. Isosteric heat of adsorption of EOP-2250

If the synergistic effects are omitted (which were not previously appreciated), the maximum N_{ads} increase at reservoir conditions (3 MPa and 50 °C) would be 16610 % (5 % EOP-2250), 33220 % (10 % EOP-2250) and 66441 % (20 % EOP-2250).

3.3. Partial conclusions

Carbon nanospheres allowed increasing the adsorption capacity in an e-CCS process. This increase was possible thanks to the higher surface area and to the favorable chemical composition, which promoted the capture and storage of CO_2. At reservoir conditions (50 °C and 3 MPa), the increase is 66441 % at a mass fraction of 20 % of EOP-2250 (Equals to 0.87 $mmol.g^{-1}$).

In this case, although the nitrogen content benefits N_{ads}, the surface modification method can affect access to the pore structure, which causes a decrease in adsorbed capacity. Carbon nanospheres could be synthesized by other processes, to obtain higher porous

volume and high nitrogen content in the same synthesis stage. This evaluation could improve the material's performance and reduce time and cost for possible future applications of the e-CCS process.

3.4. References

[1] J. Wang, L. Huang, R. Yang, Z. Zhang, J. Wu, Y. Gao*, et al.*, "Recent advances in solid sorbents for CO 2 capture and new development trends," *Energy & Environmental Science,* vol. 7, pp. 3478-3518, 2014.

[2] J. Silvestre-Albero and F. R. Reinoso, "Nuevos materiales de carbón para la captura de CO2," *Boletín del Grupo Español del Carbón,* pp. 2-6, 2012.

[3] E. P.-C. Bailon-García, Agustín F.; Rodriguez Acevedo, Elizabeth; Carrasco-Marín, Francisco, "Nanoparticle Fabrication Methods," in *Formation Damage in Oil and Gas Reservoirs. Nanotechnology Applications for its Inhibition/Remediation*, C. A. a. C. C. Franco, Farid B, Ed., 1 ed: Nova Science Publishers, 2018, pp. 69-150.

[4] T. J. Bandosz, M. Seredych, E. Rodríguez-Castellón, Y. Cheng, L. L. Daemen, and A. J. Ramírez-Cuesta, "Evidence for CO2 reactive adsorption on nanoporous S-and N-doped carbon at ambient conditions," *Carbon,* vol. 96, pp. 856-863, 2016.

[5] N. Tzabar and H. ter Brake, "Adsorption isotherms and Sips models of nitrogen, methane, ethane, and propane on commercial activated carbons and polyvinylidene chloride," *Adsorption,* vol. 22, pp. 901-914, 2016.

[6] G. P. Lithoxoos, A. Labropoulos, L. D. Peristeras, N. Kanellopoulos, J. Samios, and I. G. Economou, "Adsorption of N2, CH4, CO and CO2 gases in single walled carbon nanotubes: A combined experimental and Monte Carlo molecular simulation study," *The Journal of Supercritical Fluids,* vol. 55, pp. 510-523, 2010.

[7] M. Plaza, C. Pevida, A. Arenillas, F. Rubiera, and J. Pis, "CO2 capture by adsorption with nitrogen enriched carbons," *Fuel,* vol. 86, pp. 2204-2212, 2007.

[8] A. Arenillas, K. Smith, T. Drage, and C. Snape, "CO2 capture using some fly ash-derived carbon materials," *Fuel,* vol. 84, pp. 2204-2210, 2005.

[9] R. V. Siriwardane, M.-S. Shen, E. P. Fisher, and J. A. Poston, "Adsorption of CO2 on molecular sieves and activated carbon," *Energy & Fuels,* vol. 15, pp. 279-284, 2001.

[10] N. Álvarez-Gutiérrez, M. Gil, F. Rubiera, and C. Pevida, "Adsorption performance indicators for the CO2/CH4 separation: Application to biomass-based activated carbons," *Fuel Processing Technology,* vol. 142, pp. 361-369, 2016.

[11] M. Nandi, K. Okada, A. Dutta, A. Bhaumik, J. Maruyama, D. Derks*, et al.*, "Unprecedented CO 2 uptake over highly porous N-doped activated carbon monoliths prepared by physical activation," *Chemical Communications,* vol. 48, pp. 10283-10285, 2012.

[12] D. J. Babu, M. Bruns, R. Schneider, D. Gerthsen, and J. r. J. Schneider, "Understanding the influence of N-doping on the CO2 adsorption characteristics in carbon nanomaterials," *The Journal of Physical Chemistry C,* vol. 121, pp. 616-626, 2017.

[13] A. Chen, S. Li, Y. Yu, L. Liu, Y. Li, Y. Wang*, et al.*, "Self-catalyzed strategy to form hollow carbon nanospheres for CO2 capture," *Materials Letters,* vol. 185, pp. 63-66, 2016.

[14] Y. Fang, D. Gu, Y. Zou, Z. Wu, F. Li, R. Che*, et al.*, "A low-concentration hydrothermal synthesis of biocompatible ordered mesoporous carbon nanospheres with tunable and uniform size," *Angewandte Chemie International Edition,* vol. 49, pp. 7987-7991, 2010.

[15] M. Franco-Aguirre, R. D. Zabala, S. H. Lopera, C. A. Franco, and F. B. Cortés, "Interaction of anionic surfactant-nanoparticles for gas-Wettability alteration of sandstone in tight gas-condensate reservoirs," *Journal of Natural Gas Science and Engineering,* vol. 51, pp. 53-64, 2018.

[16] S. Schaefer, V. Fierro, M. Izquierdo, and A. Celzard, "Assessment of hydrogen storage in activated carbons produced from hydrothermally treated organic materials," *international journal of hydrogen energy,* vol. 41, pp. 12146-12156, 2016.

[17] S. Schaefer, V. Fierro, A. Szczurek, M. Izquierdo, and A. Celzard, "Physisorption, chemisorption and spill-over contributions to hydrogen storage," *international journal of hydrogen energy,* vol. 41, pp. 17442-17452, 2016.

[18] A. Abdeljaoued, N. Querejeta, I. Durán, N. Álvarez-Gutiérrez, C. Pevida, and M. Chahbani, "Preparation and Evaluation of a Coconut Shell-Based Activated Carbon for CO2/CH4 Separation," *Energies,* vol. 11, p. 1748, 2018.

[19] M. E. Casco, M. Martínez-Escandell, J. Silvestre-Albero, and F. Rodríguez-Reinoso, "Effect of the porous structure in carbon materials for CO2 capture at atmospheric and high-pressure," *Carbon,* vol. 67, pp. 230-235, 2014.

[20] A. Alonso, J. Moral-Vico, A. A. Markeb, M. Busquets-Fité, D. Komilis, V. Puntes*, et al.*, "Critical review of existing nanomaterial adsorbents to capture carbon dioxide and methane," *Science of the total environment,* vol. 595, pp. 51-62, 2017.

[21] S. Himeno, T. Tomita, K. Suzuki, and S. Yoshida, "Characterization and selectivity for methane and carbon dioxide adsorption on the all-silica DD3R zeolite," *Microporous and Mesoporous Materials,* vol. 98, pp. 62-69, 2007.

[22] Y. Ma, Z. Wang, X. Xu, and J. Wang, "Review on porous nanomaterials for adsorption and photocatalytic conversion of CO2," *Chinese Journal of Catalysis,* vol. 38, pp. 1956-1969, 2017.

[23] J. Dunne, R. Mariwala, M. Rao, S. Sircar, R. Gorte, and A. Myers, "Calorimetric heats of adsorption and adsorption isotherms. 1. O2, N2, Ar, CO2, CH4, C2H6, and SF6 on silicalite," *Langmuir,* vol. 12, pp. 5888-5895, 1996.

[24] S. Himeno, T. Komatsu, and S. Fujita, "High-pressure adsorption equilibria of methane and carbon dioxide on several activated carbons," *Journal of Chemical & Engineering Data,* vol. 50, pp. 369-376, 2005.


LIBERTAD Y ORDEN
INTER · AULAS · ACADEMIÆ · QUÆRE · VERUM


UNIVERSITAS · GRANATENSIS
PLUS ULTRA
1531

4. Nitrogen-rich carbon nanospheres applied to e-CCS process

As mentioned above, the solid adsorbents with loaded organic amines are intensively investigated. These materials usually require lower cost, lower pressure for gas recovery, and less energy for regeneration compared to aqueous amine [1, 2]. In the last year, amine-impregnated or amine-grafted porous materials for CO_2 capture have been investigated. The main researcher lines are focused on physicochemical properties of solid, supporting methods, type of amine, interactions between CO_2 and amine, among others [1-3].

The nitrogen increasing in the carbon structure using amines modifies not only the surface chemistry but also the physical structure, by considerably reducing of available surface area, which affects the adsorption capacity. Various investigations reported an increase of CO_2 capture when the pore size is larger [1, 4]. Which is challenging to consider in nanomaterials due to the mesoporous amount could be limited. Also, the impregnation process with amines is carried out at an additional stage, which generates time and costs that can block a possible escalation at the industrial level [1]. Therefore, it would be desirable to increase the nitrogen content at the same synthesis time.

For this purpose, this chapter presents the synthesis, characterization, and evaluation of nitrogen-rich carbon nanospheres that could be scalable at the industrial level. L-lysine and melamine were used as catalysts and nitrogen precursors in sol-gel and solvothermal reactions, respectively. The best material was impregnated on the sandstone surface using different mass ratios of nanoparticles, 0.01, 0.1, 1, 5, 10 and 20%, in order to validate the lowest possible percentage for a large-scale application. The CO_2 adsorption process, as well as its thermodynamic parameters, were evaluated under atmospheric and high-pressure conditions, mimic reservoir conditions. Also, the Ideal Adsorbed Solution Theory-

IAST was considered to model and simulate the process at mixing conditions for best-synthesized material.

This chapter was published at “Materials” journal, as part of the Special Issue “Element-Doped Functional Carbon-based Materials”. The paper was called “*An Enhanced Carbon Capture and Storage Process (e-CCS) Applied to Shallow Reservoirs Using Nanofluids Based on Nitrogen-Rich Carbon Nanospheres”*. Materials, 12(13), 2088. doi: 10.3390/ma12132088.

4.1. Materials and Methods

Two different carbon nanostructures were synthesized using either a sol-gel method or a solvothermal method. The synthesized nanostructures were labeled and synthesized as follows:

-***CN.LYS:*** Carbon nanospheres obtained from a sol-gel method, using resorcinol/formaldehyde as carbon precursor and L-lysine as a catalyst and nitrogen precursor.

-***CN.MEL:*** Carbon nanostructures obtained from a solvothermal method, using carbon tetrachloride as carbon precursor and melamine as a nitrogen precursor.

Both CN.LYS and CN.MEL were characterized in order to select the best material, considering the nanometer size, adsorption capacity, lower technical and economic cost, and method of synthesis.

Ottawa sandstone was used as a porous medium and was impregnated with the best nanomaterial at different percentages. The performances of the materials were evaluated by CO_2 adsorption at atmospheric pressure and 0 °C, and by varying pressure and temperature conditions. The detailed procedures are presented below.

4.1.1. Materials and Reagents

For the synthesis processes, the following reagents were used, all from Sigma–Aldrich, St. Louis, USA: carbon tetrachloride (≥ 99.9%), melamine (99%), formaldehyde (37%), resorcinol (≥ 99%), L-lysine (> 98%), sodium dodecylbenzene sulfonate (SDBS), and deionized water.

For cleaning, drying, and carbonization, the following chemicals were used, all from Sigma–Aldrich again except N_2: acetone (99.9%), ethanol (99.5%), hydrochloric acid (37%,), tert-butanol (≥ 99.5%), and N_2 (high purity, grade 5.0). Clean Ottawa sandstone and sandstone from a real reservoir were used as porous media. The real sandstone was obtained from a Colombian oil field, which allows evaluating the real rock that might be used to implement the e-CCS process in depleted oil fields.

4.1.2. Synthesis of Nanomaterials

4.1.2.1. CN.LYS Synthesis

The synthesis process was adapted from Yong–Rong et al. [5], changing the L-lysine concentration, the reaction time, and the resorcinol/water molar ratio. A solution (S1) of resorcinol/formaldehyde in a 1:2 molar ratio and deionized water was stirred at 25 °C for 1 h. In parallel, a solution (S2) of L-lysine and deionized water was stirred at 60 °C for 1 h. The molar ratio of resorcinol/L-lysine was 1:0.16. Subsequently, the solutions S1 and S2 were mixed at 60 °C for 1 h to obtain the solution S3. The latter was maintained at 25 °C for 20 h to benefit from the natural precipitation of the nanomaterial. Finally, the obtained polymer was dried at 120 °C for 12 h and carbonized under N_2 flowing at 60 mL min^{-1}, using a tubular furnace. The temperature was increased up to 800 °C at a rate of 1 °C min^{-1}, and the final temperature was held for 5 h. The employed molar ratios of resorcinol/water (for S1) were 1:2778 (without dilution), 1:5556 (dilution 1), and 1:11112 (dilution 2) for obtaining the CN.LYS1, CN.LYS2, and CN.LYS3 materials, respectively. Different molar ratios of resorcinol to water were used to reduce particle size.

4.1.2.2. CN.MEL Synthesis

The CN.MEL synthesis was adapted from Bai et al. [6] by dissolving 2 g of melamine in 120 mL of carbon tetrachloride. This solution was put in a stainless-steel autoclave (Techinstro,

Nagpur, India) with a capacity of 200 mL and introduced into an oven (Thermo Fisher Scientific, Massachusetts, USA) at 250 °C for 24 hours. The synthesis was carried out under auto-generated pressure. Subsequently, the carbonaceous material that formed was separated from the solution and was cleaned with acetone, ethanol, and finally 0.1 mol L^{-1} HCl. A mixture of nanospheres and fibers (formed by aggregation of nanospheres) was obtained (Gel.MEL1).

To obtain N-rich carbon spheres, the Gel.MEL1 was coated with a mixture of resorcinol and formaldehyde in a 1:2 molar ratio. Initially, the gel was stirred with sodium dodecylbenzene sulfonate (SDBS) at 25 °C for 18 h to promote the subsequent interaction with resorcinol/formaldehyde. After 18 h, the gel/SDBS was mixed with resorcinol/formaldehyde (in proportions of 0.37 g of nanoparticles per 1 g of resorcinol) and put in a stainless-steel autoclave at 130 °C for 24 h. In order to maintain its porous texture, the gel was dried by freeze-drying. First, the material was impregnated with *tert*-butanol for three days. Then, the impregnated material was frozen at −5 °C and lyophilized for two days until the *tert*-butanol was entirely removed (Gel.MEL2). Finally, the lyophilized gel was carbonized under N_2 flow (60 mL min^{-1}) in a tubular furnace (Thermo Fisher Scientific, Massachusetts, USA). The temperature was increased at a heating rate of 1 °C min^{-1} up to 700 °C, and the latter temperature was held for 6 h.

4.1.3. Impregnation of Sandstones

The sandstone was impregnated to decorate the rock surface with the nanoparticles and improve the surface area and molecular interactions. Ottawa sandstone (SS) was impregnated with CN.LYS2 at mass fractions of 0.01, 0.1, 1, 5, 10, and 20% by immersion and soaking [7]. Initially, a nanofluid composed of nanoparticles and deionized water was sonicated at 40 °C for 4 h. Subsequently, the SS was introduced in the nanofluid at 60 °C for either 6 h at 600 rpm or for 24 h without stirring.

The latter method better mimics the reservoir conditions in which the porous medium might be impregnated. Finally, the impregnated material was dried at 110 °C for 12 h. The same procedure was followed for impregnating the sandstone from a real reservoir (RS) but using only a mass fraction of 10 and 20% of CN.LYS2 to RS and 24 h of soaking.

4.1.4. Characterization of the Nanomaterials

The following procedures allowed characterizing the physicochemical characteristics of the materials, essential for a good understanding of the results. For the e-CCS application, nanoparticles must have a nanometer size, a spherical shape, a high surface area, and high nitrogen content.

4.1.4.1. Size and Structure of Nanomaterials

Different techniques were used to evaluate the particle size distribution: scanning electron microscopy (SEM) (manufacturer, city, country) was used to obtain the dry particle size, size distribution, and morphology of CN.MEL, whereas transmission electron microscopy (TEM) (manufacturer, city, country) was used to analyze the dry particle size, size distribution, and surface characteristics of CN.LYS. The CN.LYS showed a different porous structure after dilutions, which was observed by N_2 adsorption (at −196 °C). Further, TEM was used to characterize the structure after dilutions to analyze the causes of pore structure modification. Scanning electron microscopy analysis was also carried out to analyze the distribution of carbon nanoparticles on sandstone after impregnation. The observations were carried out by means of a JSM-7100 emission electron microscope (JEOL, Nieuw-Vennep, The Netherlands), a GEMINI-LEO1530 VP FE-SEM emission electron microscope (Carl Zeiss, Cambridge, UK), and a Tecnai F20 Super Twin TMP transmission electron microscope (FEI, Hillsboro, USA).

Dynamic light scattering (DLS) was carried out by means of a NanoPlus-3 zeta/nanoparticle analyzer (Micromeritics, Norcross, USA) at 25 °C in a glass cell (capacity of 0.9 mL), which was used to obtain the mean particle size of nanoparticles dispersed in a fluid, which hydrate and interact with each other. The mean particle size was calculated from the diffusional properties of the particle, indicating the size of the hydrated and solvated particle. For this purpose, a nanoparticle solution, 10 mg L^{-1}, was dispersed in water or ethanol and sonicated for 6 h before analysis. Particles suspended in a liquid have a Brownian motion due to the random collisions with solvent molecules. This motion causes the particles to diffuse through the medium. The diffusion coefficient, D, is inversely proportional to the particle size or hydrodynamic diameter, d, according to the Stokes–Einstein equation:

$$D = \frac{k_B T}{3\pi \eta d} \quad \textbf{(4.1)}$$

where, k_B is Boltzmann's constant, T is the absolute temperature, and η is the viscosity.

4.1.4.2. Porous Structure of Nanomaterials and Sandstone

All materials were characterized by N_2 and CO_2 adsorption at −196 °C and 0 °C, respectively, using 3-Flex manometric adsorption equipment (Micromeritics, Norcross, USA). The total adsorbed volume ($V_{0.95}$) was taken as the physisorbed volume of N_2 at a relative pressure P/P_0 = 0.95. The Brunauer–Emmett–Teller (BET) model was applied to obtain the BET area (A_{BET}). Micropore volume (V_{mic}), average pore size (L_0), and CO_2 adsorption energy ($E_{ads–CO2}$) were obtained by application of the Dubinin–Radushkevich equation. The mesopore volume (V_{meso}) was obtained through the Barrett–Joyner–Halenda (BJH) model.

4.1.4.3. Chemical Composition of Nanomaterials and Sandstone

The chemical characterization was carried out by carbon, hydrogen, oxygen, and nitrogen (CHON) analysis for nanomaterials, and by Fourier transform infrared spectroscopy (FTIR) for sandstone. An IRAffinity-1S FTIR spectrometer (Shimadzu, Columbia, USA) was operated at room temperature using potassium bromide in a KBr-to-material ratio of 30:1 (% w/w). The impregnation percentages of nanoparticles on sandstone were corroborated by thermogravimetric analysis (TGA) (TA Instruments, New Castle, USA). For this, the sample was burned under an air atmosphere at 10 °C min^{-1} up to 800 °C.

4.1.4.4. Rheological Analysis of CN.LYS Synthesis Solutions

The stability of the synthesis solutions was evaluated at different concentrations of CN.LYS (CN-LYS1, CN.LYS2, and CN.LYS3). For this purpose, a Kinexus Ultra+ rheometer (Malvern Panalytical, Malvern, UK) utilizing a concentric cylinder sensor equipped with a Peltier cell for temperature control was used. The tests were first carried out by varying the shear rate from 1 to 250 s^{-1} in order to define the adequate shear rate (50 s^{-1}). The test conditions were carried out to mimic the real synthesis conditions in terms of temperature and stirring. The process started at 60 °C for 1 h, after which the temperature was controlled to simulate the natural cooling process at 57, 45, 37, and 34 °C until the viscosity reached a constant value. Only 30 mL was needed for the test, while the current reaction was carried out at 1.8 L.

4.1.4.5. Dispersion of Nanoparticles in Solution

The electrophoretic light scattering (ELS) technique was used to evaluate the surface charge of the particles and their dispersion stability at 25 °C in a NanoPlus-3 zeta/nanoparticle analyzer (Micromeritics, Norcross, USA). In this test, several nanoparticle suspensions were prepared at 10 mg.L^{-1}, with a pH adjusted between 2 to 12 by adding solutions of 0.1 mol.L^{-1} HCl or 0.01 mol.L^{-1} NaOH, and then subjected to analysis. The zeta potential was calculated using the Smoluchowski equation, derived from the calculation of the Doppler effect.

$$\zeta = \eta U / \varepsilon \quad \textbf{(4.2)}$$

$$U = \frac{V}{E} \quad \textbf{(4.3)}$$

$$\Delta v = 2V\, n \sin\left(\frac{\theta}{2}\right) / \lambda \quad \textbf{(4.4)}$$

where ζ is the zeta potential, η is the viscosity of the fluid (water), U is the electrophoretic mobility, ε is the permittivity, V represents the speed of movement of the particles, E is the electric field, Δv is the Doppler effect, n is the index of refraction, θ is the angle of detection, and λ is the wavelength of the incident light.

4.1.5. Adsorption Tests at High Pressure

The adsorption tests carried out below atmospheric pressure were described in sub-Section 4.1.4.2. At high pressure, the CO_2 adsorption capacity was evaluated in two different conditions: (i) under pure CO_2 in a manometric device (up to 3.0 MPa) and (ii) under a CO_2/N_2 flow in a gravimetric device (up to 2.6 MPa). The details of each protocol are presented below.

4.1.5.1. Adsorption at High Pressure for Pure CO_2–Manometric Device

The carbon nanospheres (CN.LYS2), sandstone, and impregnated sandstone (at mass fractions of 10 and 20%) were investigated in High Pressure Volume Analyzer, HPVAII-200 (Micromeritics, Norcross, USA) at 0 °C, 25 °C, and 50 °C and at pressures from 3×10^{-3} up to 3.0 MPa. In order to have enough total surface area for adsorption and to minimize measurement errors, the amount of each material inside the sample holder was around 0.5 g for nanoparticles, 1.5 g for impregnated sandstone, and 14 g for sandstone. The

contribution of the empty sample holder was systematically measured and subtracted to all data to improve accuracy. The isosteric heat of adsorption, Q_{ST}, was calculated using the isosteric method with the Microactive software (from Micromeritics, Norcross, USA) from three adsorption isotherms at 0, 25, and 50 °C, based on the Clausius–Clapeyron equation [8]:

$$-\frac{Q_{ST}}{R} = \frac{\partial \ln(P)}{\partial(1/T)} \tag{3.5}$$

where R is the universal gas constant (8.314 J mol^{-1} K^{-1}), P is the absolute pressure, and T is the temperature.

The excess adsorbed CO_2 amount (N_{exc}, $g_{CO2}.g_{adsorbent}^{-1}$) was equal to the absolute adsorbed CO_2 amount ($N_{ads,}$ $g_{CO2}.g_{adsorbent}^{-1}$) minus the product of gas density in the bulk phase by the volume of the adsorbed phase. The values provided by the HPVA device were obtained on an excess basis, and therefore, the absolute amounts had to be determined as follows [9]:

$$N_{ads} = N_{exc}\left(1+\frac{P+M_{CO2}}{Z\,\rho_{liq}\,RT}\right) \tag{4.6}$$

where M_{CO2} is the molecular weight of CO_2 (44.013 g mol^{-1}), Z is the compressibility factor at the considered pressure and temperature, and ρ_{liq} is the density of liquid CO_2 (1032 × 10^3 g m^{-3}).

The isotherms were fitted with the Sips and Toth models, which take into account multilayer adsorption. Table 4. 1 presents the equations for each model [10-12]. K_S and K_T represent adsorption equilibrium constants for the Sips and Toth models, respectively, and the n and t parameters indicate the heterogeneity of the system for the Sips and Toth models, respectively. The heterogeneity may originate from the solid structure, from the solid energy properties, or the adsorbate [11]. The n or t parameters are usually greater than unity, and when they are the unit, the models assume the Langmuir equation [11].

Table 4. 1. Models for adsorption isotherms.

Model	Equations	Parameters
Sips	$N_{ads} = N_m \frac{(K_S P)^{1/n}}{1+(K_S P)^{1/n}}$ **(4.7)**	N_{ads} (mmol g^{-1}) is the adsorbed amount, N_m (mmol g^{-1}) is the adsorption capacity at equilibrium, P (kPa) is the equilibrium pressure, and K_S and n are the Sips adsorption equilibrium constants, related to the affinity and the heterogeneity of the system, respectively.
Toth	$N_{ads} = N_m \frac{K_T P}{(1+(K_T P)^t)^{1/t}}$ **(4.8)**	N_{ads}, N_m, and P have the same meaning as above, and K_T and t are the Toth adsorption equilibrium constants, related to the affinity and the heterogeneity of the system, respectively.

4.1.5.2. Adsorption at High Pressure for CO_2 and N_2–Gravimetric Device

The CN.LYS2, sandstone, and impregnated sandstone CO_2 isotherms (with a mass fraction of 20% of nanoparticles) were investigated using a HP TGA 750 thermogravimetric analyzer (TA Instruments, New Castle, USA) at 50 °C and high pressure from 0.03 to 3.0 MPa for CO_2 and N_2. This device was equipped with a magnetic levitation top-loading balance, which made it possible to achieve high accuracy and reduce the volume of the system. The amount of each material put inside the sample holder was around 15 mg for nanoparticles, 40 mg for sandstone, and 40 mg for impregnated sandstone, to have enough total surface area for adsorption.

The contribution of the buoyancy effect was manually subtracted from the data using blank tests carried out in the same conditions but with an empty sample holder. From the adsorption results of each N_2 and CO_2 isotherm, it was possible to predict the selectivity by applying the ideal adsorbed solution theory (IAST), which allows estimating the competitive adsorption of the compounds in a mixture of gases as the flue gas. Based on the literature, a model flue gas comprising 80% N_2 and 20% CO_2 was selected. The IAST was implemented in a Python routine (package-pyIAST from Simon et al. [13]).

4.2. Results and Discussion

The results are divided into two main sections: a) materials characteristics (nanoparticles and sandstone) and b) study of the interaction between CO_2/nanoparticles/sandstone by adsorption isotherms under different operation conditions (T, P).

4.2.1. Materials Characteristics

The morphology of the carbon materials obtained from melamine and carbon tetrachloride was very heterogeneous. Figure 4. 1-a,b presents SEM images of two different zones wherein more or less agglomerated nanospheres can be observed (Figure 4. 1-b). When the images are observed at lower magnification, it can be noticed that some areas have fiber and block morphologies (Figure 4. 1-c), while other areas have nanospheres/microspheres morphologies (Figure 4. 1-d).

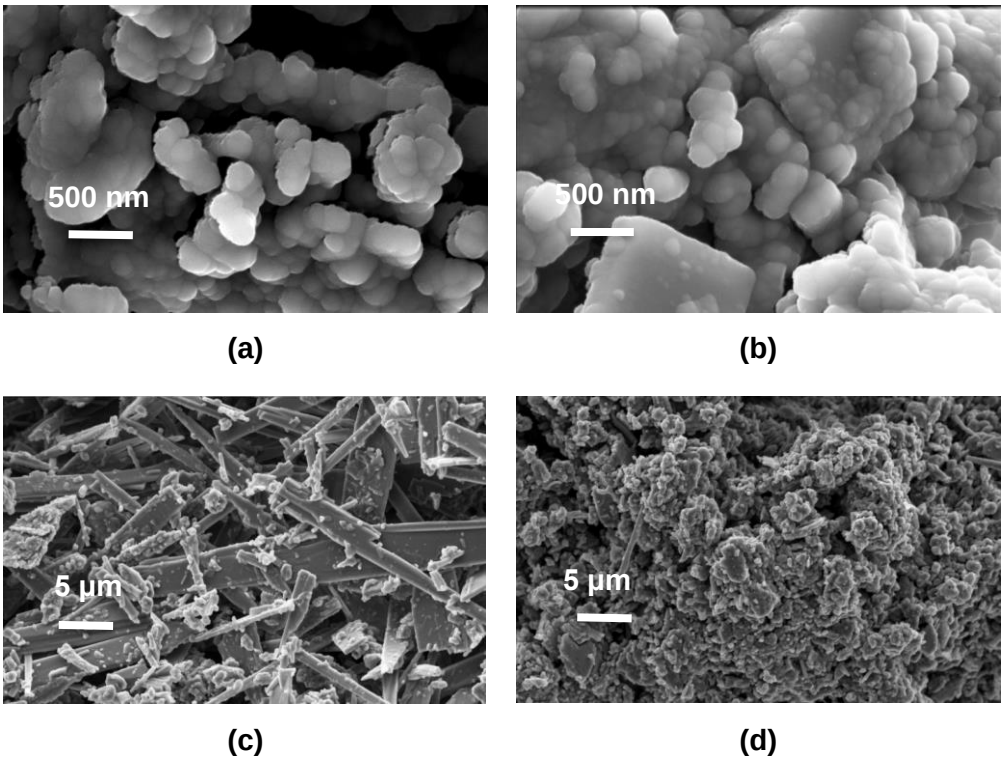

Figure 4. 1. SEM images at 5 kV of carbon nanospheres from melamine (CN.MEL) before resorcinol/formaldehyde coating and final pyrolysis: (**a**) and (**b**) nanospheres and build fibers and blocks; (**c**) area with structures in the form of fibers and blocks, and (**d**) distribution of nanospheres, fibers, and blocks.

After coating with resorcinol/formaldehyde, the hydrodynamic diameter of the CN.MEL particles were higher than the limit of detection of the equipment (10 μm). For the e-CCS process, this material might, thus, induce technical problems, due to the possible obstruction of the naturally porous structure of the rock.

The ultimate analysis (Table 4. 2) shows that this material had a nitrogen content close to 50% before coating and carbonization (Gel.MEL1), but of only 9.2% after coating with resorcinol/formaldehyde (Gel.MEL2) and 2.2% after carbonization (CN.MEL). Therefore, CN.LYS and CN.MEL materials exhibited similar nitrogen contents. Some N-rich carbon materials, reported in the literature, have nitrogen content close to those obtained in this work [1]. The oxygen content was measured independently from carbon, hydrogen and nitrogen content.

Table 4. 2. Ultimate analysis of nanoparticles synthesized with melamine (CN.MEL) and L-lysine (CN.LYS).

	C (mass fraction %)	**H (mass fraction %)**	**N (mass fraction %)**	**O (mass fraction %)**
Gel.MEL1	22.8	4.7	49.1	7.3
Gel.MEL2	55.9	5.0	9.2	31.0
CN.MEL	85.6	2.3	2.2	10.2
Gel.LYS1	59.5	6.7	5.1	31.9
Gel.LYS2	61.7	6.7	5.0	31.6
Gel.LYS3	62.7	6.4	5.0	28.3
CN.LYS1	88.6	1.7	1.7	9.9
CN.LYS2	91.1	1.7	1.9	12.0
CN.LYS3	91.9	2.1	2.2	12.8

The Gel.MEL1 (49.1% of nitrogen) was submitted to CO_2 and N_2 adsorption (at 0 °C and −196 °C, respectively), but it was impossible to obtain the corresponding isotherms, possibly because of its too low surface area. It is well known that the pyrolysis step induces a significant increase of narrow porosity by the elimination of volatile species. However, when the Gel.MEL1 is directly pyrolyzed, most of the material undergoes decompositions, and the yield is very low (< 5%).

The adsorption and desorption isotherms (N_2 at −196 °C and CO_2 at 0 °C) for nanomaterials synthesized with melamine (CN.MEL) and L-lysine (CN.LYS) are presented in Figure 4. 2, and the textural parameters obtained from adsorption isotherms are presented in Table 4. 3.

Table 4. 3. Parameters obtained from adsorption isotherms (N_2 at −196 °C and CO_2 at 0 °C) for nanomaterials synthesized with melamine (CN.MEL) and L-lysine (CN.LYS).

	A_{BET} ($m^2\,g^{-1}$)	$V_{0.95}$ ($cm^3\,g^{-1}$)	$V_{mic\text{-}N2}$ ($cm^3\,g^{-1}$)	$V_{mic\text{-}CO2}$ ($cm^3\,g^{-1}$)	V_{mes} ($cm^3\,g^{-1}$)	L_0 (nm)	$E_{ads.CO2}$ (kJ mol^{-1})
CN.MEL	713	0.42	0.28 (66.6%)	0.26	0.14	0.77	30.9
CN.LYS1	385	0.22	0.16 (72.7%)	0.18	0.06	0.84	32.4
CN.LYS2	612	0.36	0.23 (63.9%)	0.25	0.13	0.56	31.6
CN.LYS3	320	0.13	0.12 (92.3%)	-	0.01	0.62	-

The micropore and the mesopore fractions of the CN.MEL and CN.LYS2 materials were similar (67–64% and 33–36%, respectively), although their total pore volumes (at P/P_0 = 0.95) were rather different. Both CN.LYS1 and CN.LYS3 exhibited higher micropore fractions (72.7 and 92.3%, respectively), but had lower values of A_{BET} and total pore volumes than those of CN.MEL and CN.LYS2 materials (Figure 4. 2). The mesoporous

volume of CN.MEL is evidenced by the hysteresis loop in the range of relative pressures between 0.46 and 0.66. In the CN.LYS series, only CN.LYS2 was also mesoporous, but with a different structure as deduced from the different shape of the hysteresis loop, occurring at higher relative pressure. The CN.LYS1 texture was moderately mesoporous (28.6%) after the first dilution, the CN.LYS2 texture was a little more mesoporous (36.6%), but after the third dilution, CN.LYS3 had a predominantly microporous texture, as evidenced by the type Ia of its N_2 isotherm. The adsorption capacity of CO_2 at 0 °C was as expected according to the range reported in the literature, but the synthesis process reported in this study was easier than many others reported so far [1, 14, 15]. The experimental development considered important parameters for a possible industrial application, such as operation at atmospheric pressure, relatively low temperature (60 °C), and relatively low time (1 hour) before carbonization. The carbon nanospheres are usually synthesized by methods that demand greater energy and time [16].

In order to provide explanations of the aforementioned trends, Figure 4. 3 presents TEM pictures of Gel.LYS (materials before carbonization) and CN.LYS (materials after carbonization).

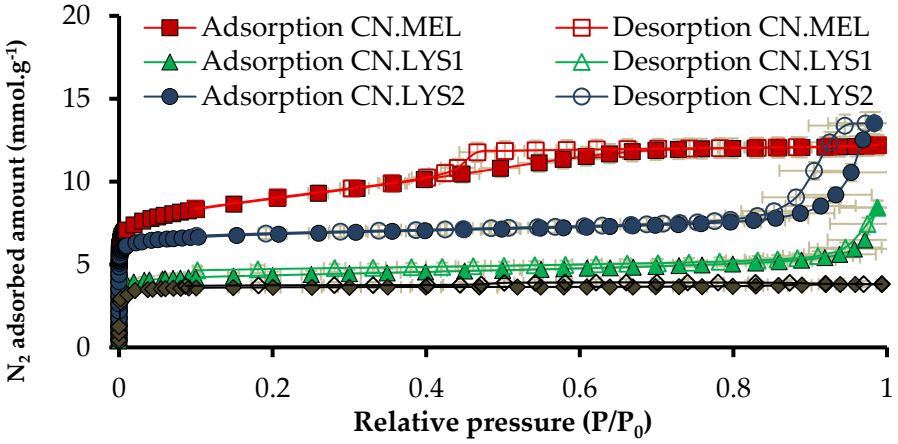

(a)

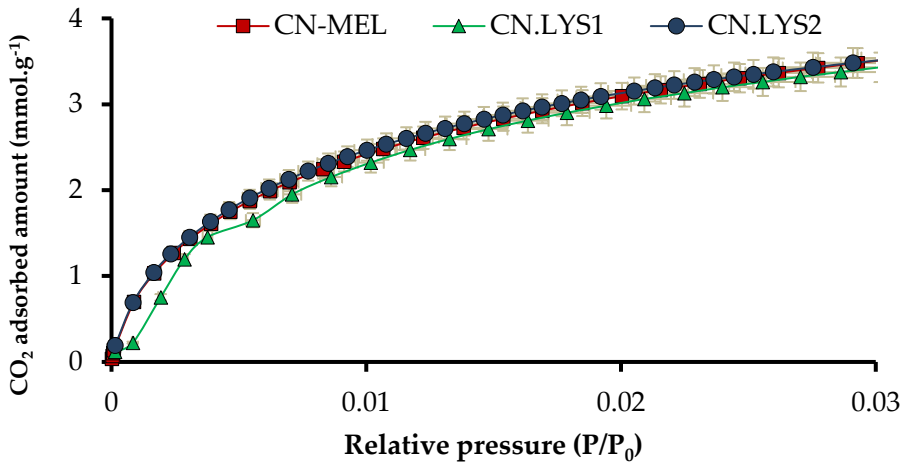

(b)

Figure 4. 2. Adsorption isotherms for nanoparticles synthesized with melamine (CN.MEL) and L-lysine (CN.LYS) (**a**) N_2 adsorption (full symbols) and desorption (empty symbols) at −196 °C and (**b**) CO_2 adsorption at 0 °C.

Figure 4. 3-a,b present CN.LYS1 before and after carbonization, respectively. Here a mixture of larger and smaller nanospheres can be seen. Figure 4. 3-c,d present smaller particles (approximately 50 nm) for CN.LYS2 before and after carbonization. These particles are more transparent than those of the CN.LYS1 and CN.LYS3 materials, due to the more mesoporous texture of the CN.LYS2 material. Figure 4. 3-e,f present CN.LYS3 before and after carbonization. It can be seen that a gel was formed around the spheres. The L-lysine acts as a catalyst in the reaction, and therefore, if its amount is limited for the third dilution process, it might be the reason for the formation of a gel coating the spheres instead of producing more nanospheres, which obstructs the porous structure of CN.LYS3. This would affect the results presented in Figure 4. 2 and Table 4. 3 for CN.LYS3. The reproducibility for CN.LYS is significant; the variation of size and CO_2 capacity is less than 1%.

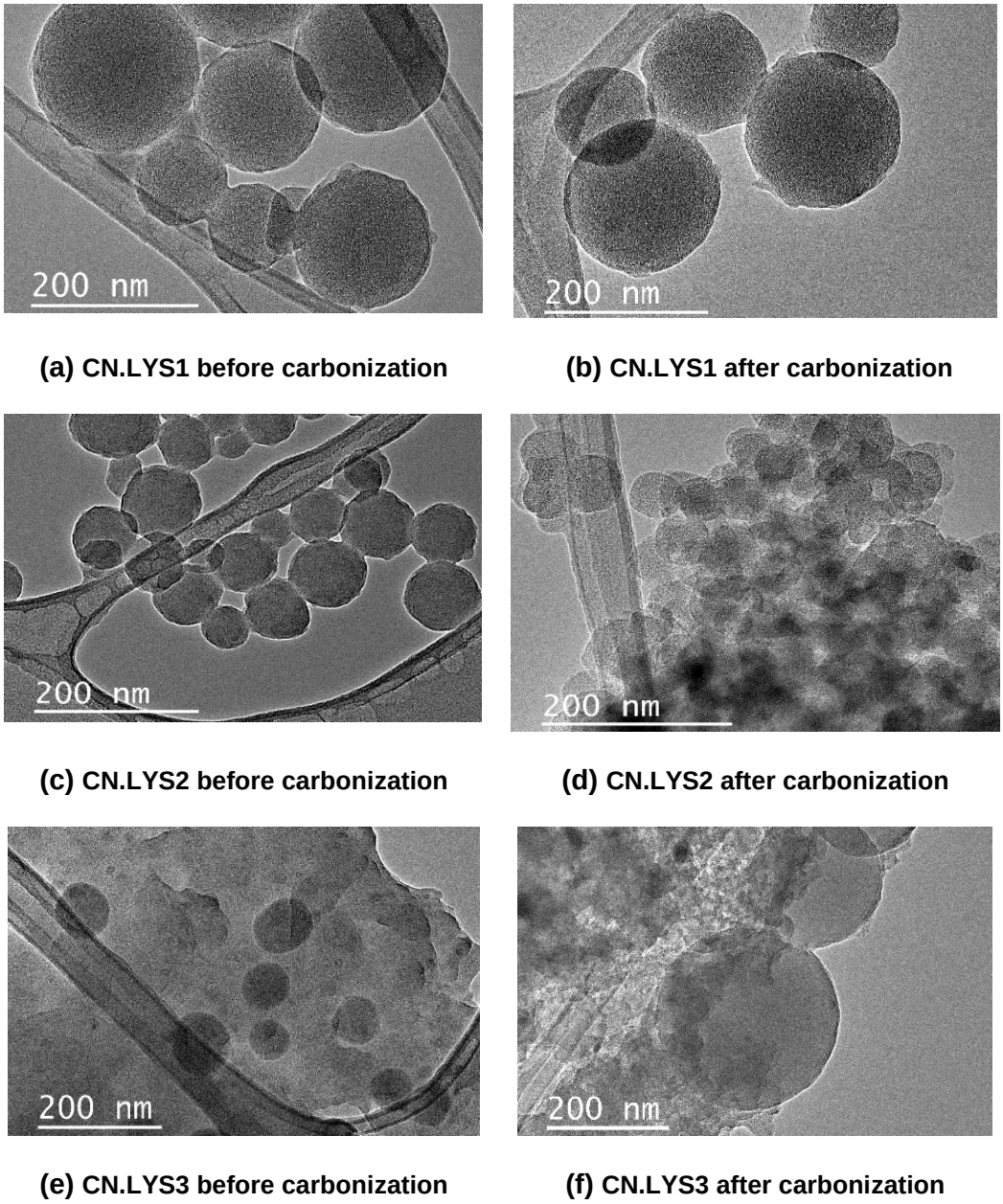

(a) CN.LYS1 before carbonization **(b) CN.LYS1 after carbonization**

(c) CN.LYS2 before carbonization **(d) CN.LYS2 after carbonization**

(e) CN.LYS3 before carbonization **(f) CN.LYS3 after carbonization**

Figure 4. 3. TEM images of carbon nanospheres synthesized with L-lysine. (**a**) Gel.LYS1, (**b**) CN.LYS1, (**c**) Gel.LYS2, (**d**) CN.LYS2, (**e**) Gel.LYS3, and (**f**) CN.LYS3.

Figure 4. 4 presents the rheological behavior of the synthesis solution/colloid/suspension (Sol.LYS1 without dilution, Sol.LYS2 for dilution 1, and Sol.LYS3 for dilution 2). The changes in temperature and the stirring were chosen to reproduce the conditions of synthesis (60 °C for 1 h and after cooling at room temperature). The cooling stage was controlled in the rheometer. The viscosity has changed during synthesis because the

reactive system underwent polymerization and condensation-related changes to form the nanospheres so that the system passed from the solution to the colloid and the suspension. The differences in viscosity were related to the concentration of reagents in the solutions: the third solution, Sol.LYS3, presented fewer changes during the synthesis process because the system had a lower concentration of reagents, as it is presented in Figure 4. 3.

Based on the particle size analysis, porous texture, nitrogen content, and adsorbed amount of CO_2 (at 0 °C and up to 1 bar), the CN.LYS material was selected to perform the adsorption tests in conditions closer to those of the reservoir. Despite the high CO_2 adsorption capacities exhibited by the CN.MEL material, its size, and shape would not allow its application in real reservoir conditions. Besides, its synthesis process was more complex, with a higher number of steps and higher consumption of energy and time, which were not compensated by significantly better physicochemical properties regarding the CN.LYS.

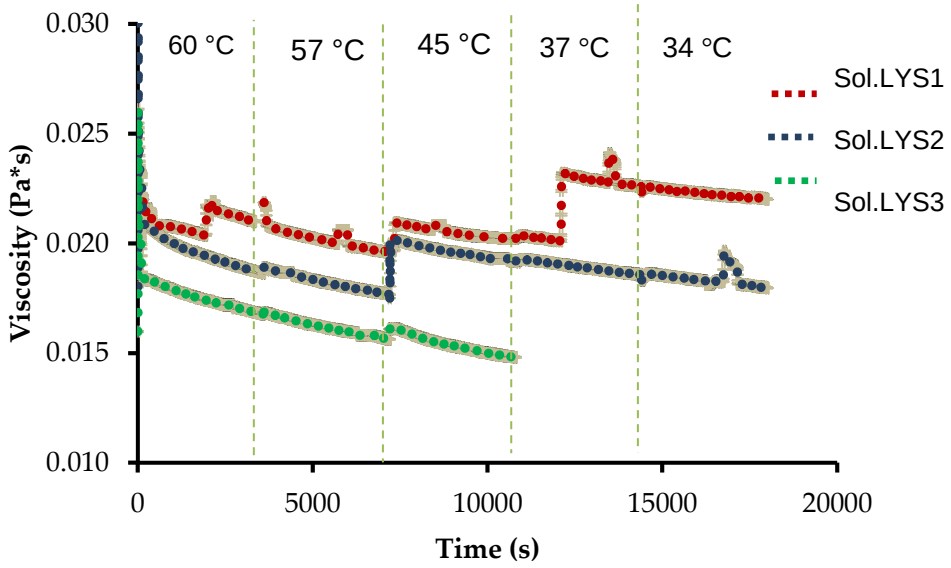

Figure 4. 4. Rheological analysis of synthesis solutions with L-Lysine (Sol.LYS) in the same thermal conditions but with different resorcinol/water molar ratios: 1:2778 (Sol.LYS1), 1:5556 (Sol.LYS2), and 1:11112 (Sol.LYS3).

To analyze the behavior of the nanoparticles in an aqueous medium, Table 4. 4 presents the mean particle size of nanomaterials (CN.LYS), and Figure 4. 5 presents their zeta potentials. According to the Stokes–Einstein equation, the diffusion coefficient is inversely proportional to particle size or hydrodynamic diameter; therefore, it is possible to analyze whether the nanoparticles could interact to form aggregates. Precipitation is only possible if the aggregates are big enough. Another important concept is zeta potential; if zeta potential is high (negative or positive), the particles are stable due to the high electrostatic repulsion between them. On the contrary, a low zeta potential (approaching zero) increases the probability of particles colliding, and thus forming aggregates. The hydrodynamic diameter was calculated for nanoparticles in water (at pH 5.8) and ethanol (at pH 7). The aggregate size was less in ethanol (Table 4. 4) because the pH affects the behavior in solution (Figure 4. 5). However, the results for nanoparticles suspended in water were close to those obtained for nanoparticles suspended in ethanol. For an industrial application and injection into the porous medium, the most economical way is a suspension in water.

Table 4. 4. Mean particle size of nanomaterials in suspension, synthesized with L-lysine.

Material	d_p 50 (nm) in water (pH 5.8)	d_p 50 (nm) in ethanol (pH 7)
Gel.LYS1	579.4	361.5
Gel.LYS2	314.2	274.2
Gel.LYS3	1083.4	1957.1
CN.LYS1	801.1	785.9
CN.LYS2	242.6	239.9
CN.LYS3	2828.7	2587.4

For CN.LYS1 and CN.LYS3, a pH higher than 7 was better for rocks impregnation because the zeta potential was farther from zero. For CN.LYS2, a pH higher than 7 or lower than 4.7 was better for rocks impregnation. Gel.LYS2 presented the highest values of zeta potential at pH below 4, increasing the natural precipitation time of nanoparticles after the synthesis process.

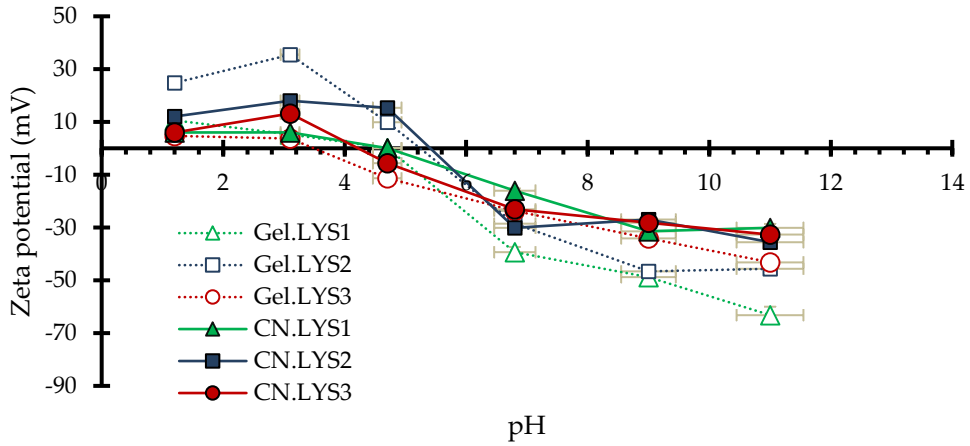

Figure 4. 5. Zeta potential for carbon nanoparticles synthesized with L-lysine.

Figure 4. 6 presents SEM images of the sandstone surface before (Figure 4. 6-a) and after (Figure 4. 6-b) the impregnation step. Impregnation was achieved in water because of its lower cost and non-hazardous nature, making it ideal for industrial applications. The distribution of CN.LYS2 particles on the surface was homogeneously distributed (Figure 4. 6-b). The size of the aggregates was between 100 and 200 nm. After one year, the sandstone continued to be impregnated, without showing any disintegration of nanoparticles from the sandstone surface. By thermogravimetric analysis, variations of less than 5% of the percentage of impregnation were obtained. This variation can also be related to the impregnation method without stirring, which might produce zones of lower nanoparticle concentration.

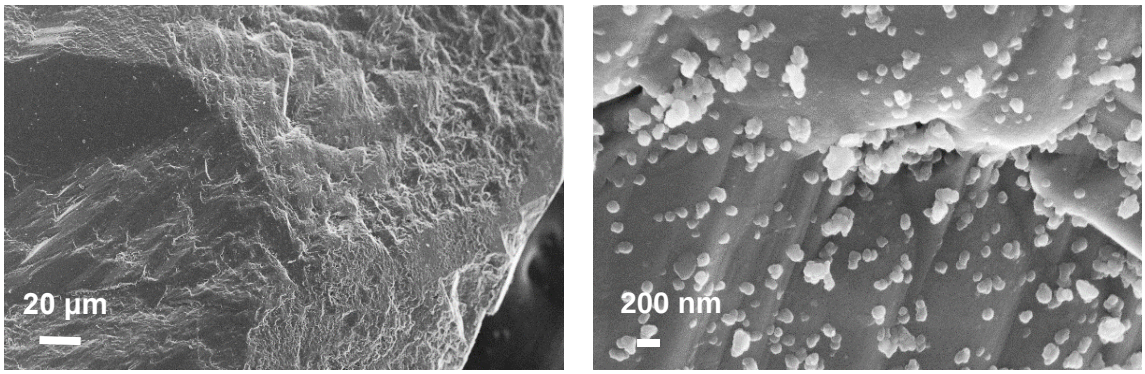

Figure 4. 6. SEM images of (**a**) sandstone and (**b**) sandstone impregnated with a mass fraction of 20% of CN.LYS2.

The sandstone presented an A_{BET} of 0.4 $m^2\ g^{-1}$, and its CO_2 adsorption capacity could not be measured using conventional methods (< 0.0013 mmol g^{-1} at 0 °C and atmospheric pressure). Sandstone is mainly composed of silica, which has an acidic character as the CO_2 molecule. Consequently, if the specific area of the sandstone is low, its CO_2 adsorption capacity is even lower than that which might be expected for this specific area.

The sandstone was impregnated at a low nanoparticle concentration to evaluate its economic feasibility at the industrial level. The sandstone impregnated with mass fractions of 0.01 and 0.1% did not show a significant increase in its surface properties, unlike samples with higher mass fractions, as shown in Table 4. 5. The textural parameters of the impregnated sandstones were indeed improved as the percentage of nanoparticles on their surface increased. At a mass fraction of 20%, A_{BET} and $V_{0,95}$ increased by factors as high as 225 and 670, respectively.

Table 4. 5. Parameters obtained from adsorption isotherms (N_2 at −196 °C and CO_2 at 0 °C) for sandstone impregnated with mass fractions of 1, 5, 10, and 20 % of CN.LYS2.

	A_{BET} ($m^2\ g^{-1}$)	$V_{0.95}$ ($cm^3\ g^{-1}$)	$V_{mic\text{-}N2}$ ($cm^3\ g^{-1}$)	$V_{mic\text{-}CO2}$ ($cm^3\ g^{-1}$)	V_{mes} ($cm^3\ g^{-1}$)	L_0 (nm)
SS-1	2	0.003	0.002	0.002	0.001	0.56
SS-5	20	0.016	0.01	0.012	0.006	0.53
SS-10	49	0.035	0.021	0.023	0.014	0.51
SS-20	99	0.067	0.042	0.044	0.025	0.52

Figure 4. 7 shows adsorption isotherms of CO_2 at atmospheric pressure and 0 °C, for raw sandstone and sandstone impregnated at mass fractions of 0.01, 0.1, 1, 5, 10, and 20% of CN.LYS2. In addition, it shows the slope changes related to the affinity between the adsorbent medium and the adsorbate. The materials did not have significant affinity with CO_2 at mass fractions of 0.01 and 0.1% and without CN.LYS2. The affinity and adsorption capacity increased with the percentage of nanoparticles in the system. The latter presented a different behavior above a mass fraction of 1%. Indeed, at a mass fraction of 1%, the adsorption capacity was increased by a factor 21 with respect to raw sandstone, although

the value was still low, 0.03 mmol g^{-1}. At a mass fraction of 20%, the value was far higher, 0.63 mmol g^{-1}, corresponding to an increment factor of 499. Different materials have been reported in the literature [1, 14] with specific surface modifications to increase the adsorption capacity of CO_2, but the value of adsorption capacity was similar to that of sandstone by adding a mass fraction of 10 or 20% of nanoparticles.

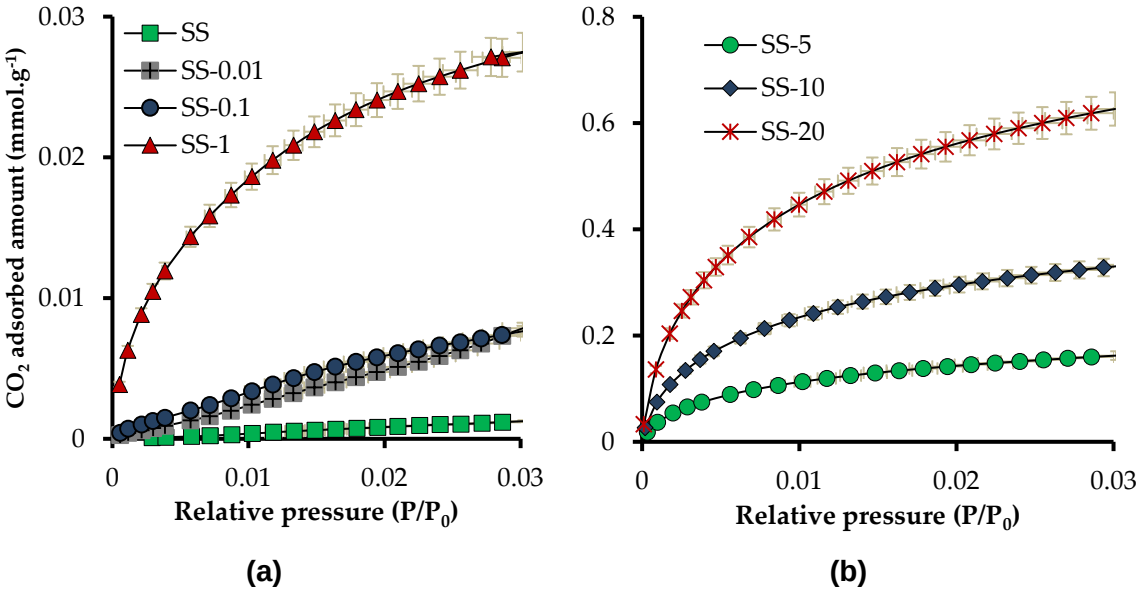

Figure 4. 7. Adsorption isotherms of CO_2 at atmospheric pressure and 0 °C. (**a**) Mass fractions ≤1% and (**b**) mass fractions ≥5%.

The effect of the impregnation method on the CO_2 adsorption capacity at atmospheric pressure and 0°C was then evaluated. As explained before, immersion and soaking were achieved using two different sets of conditions: (i) 6 h and 600 rpm and (ii) 24 h without stirring. Increasing the soaking time by 18 h improved the adsorption capacity by more than 25% (Table 4. 6). The values presented in Figure 4. 7, adsorption isotherms of CO_2 at atmospheric pressure and 0 °C, thus correspond to Conditions 2.

Table 4. 6. Relationship between soaking time and adsorption capacity of CO_2 at atmospheric pressure, 0 °C and mass fractions of 5, 10, and 20%. Conditions 1: 6 h and 600 rpm; Conditions 2: 24 h without stirring.

	5%	**10%**	**20%**
Conditions 1 (mmol g^{-1})	0.12	0.27	0.49
Conditions 2 (mmol g^{-1})	0.16	0.33	0.63
Increment (%) from conditions 1 to 2	40.5	25.4	27.2

To evaluate the possible synergistic behavior between NC.LYS2 and sandstone, the theoretical and experimental values of the CO_2 adsorption capacity, are presented in Table 4. 7. Theoretical values were calculated by assuming a linear relationship and taking into account the CO_2 adsorption capacities and the percentages of each solid. The difference between theoretical and experimental values ranged from 5 to 10%, which corresponds to the experimental error given the inaccuracy in the measurement of the very low CO_2 adsorption capacity of the sandstone. The differences could also be related to the segregation of nanoparticles during the impregnation process, the nanoparticles not being homogeneously distributed on the surface of the sandstone.

Table 4. 7. CO_2 adsorption capacity at atmospheric pressure, 0°C, and mass fractions of 1, 5, 10, and 20 %. Theoretical and experimental values.

	1%	**5%**	**10%**	**20%**
Theoretical N_{ads} (mmol g^{-1})	0.036	0.175	0.349	0.697
Experimental N_{ads} (mmol g^{-1})	0.027	0.162	0.333	0.627
Relative difference (%)	23.8	7.4	4.7	10.1

4.2.2. High-Pressure Adsorption Tests

4.2.2.1. Pure CO_2 Adsorption at High Pressure–Manometric Measurement Method

The e-CCS process requires evaluating the behavior of the materials at high pressure (up to 3 MPa) and the temperature of a hypothetical reservoir (50 °C). Figure 4. 8-a–c presents the absolute CO_2 adsorbed amount and the excess amount for CN.LYS2 at 0, 25, and 50 °C. The difference between excess and absolute amounts appeared above 1 MPa, and represented 8.3% at 0 °C, 6.7% at 25 °C, and 5.9% at 50 °C. This difference was lower when the temperature increased. Such a trend is consistent with the fact that, at similar pressure, the density of the bulk phase decreases when the temperature increases. The high-pressure intrinsic CO_2 adsorption capacity of sandstone without impregnation had a negligible effect on the measurement. Therefore, the evaluation was only carried out for sandstone impregnated at mass fractions of 10% (Figure 4. 8-d-f) and 20% (Figure 4. 8-g-i). The difference between excess and absolute adsorbed amounts of impregnated sandstone was similar to that of CN.LYS2, stranded out after 1 MPa, and represented less than 10%, on average.

To observe the pressure effect on the adsorption capacity of CN.LYS2, the N_{ads} at atmospheric pressure and 0 °C (3.48 mmol g^{-1}) was compared to N_{ads} at 3 MPa and 0 °C (5.80 mmol g^{-1}). The increase of pressure produced an increase of N_{ads} of 66.6%, indicating physisorption as the main adsorption mechanism. At 50 °C, as expected, the adsorption capacity decreased by 20% due to the exothermic character of adsorption. The obtained adsorption capacity is competitive compared to other results reported for nanomaterials under similar conditions [14, 17, 18]. The effect of pressure on the impregnated sandstone was also observed by comparing N_{ads} at atmospheric pressure and 0 °C (0.34 mmol g^{-1} for SS-10 and 0.63 mmol g^{-1} for SS-20) to N_{ads} at 3 MPa and 0 °C (0.47 mmol g^{-1} for SS-10 and 1.04 mmol g^{-1} for SS-20). The corresponding increases were 38.2% (SS-10) and 66.0% (SS-20), respectively. The maximum N_{ads} under reservoir conditions was 0.85 mmol g^{-1} at a mass fraction of 20% of CN.LYS2.

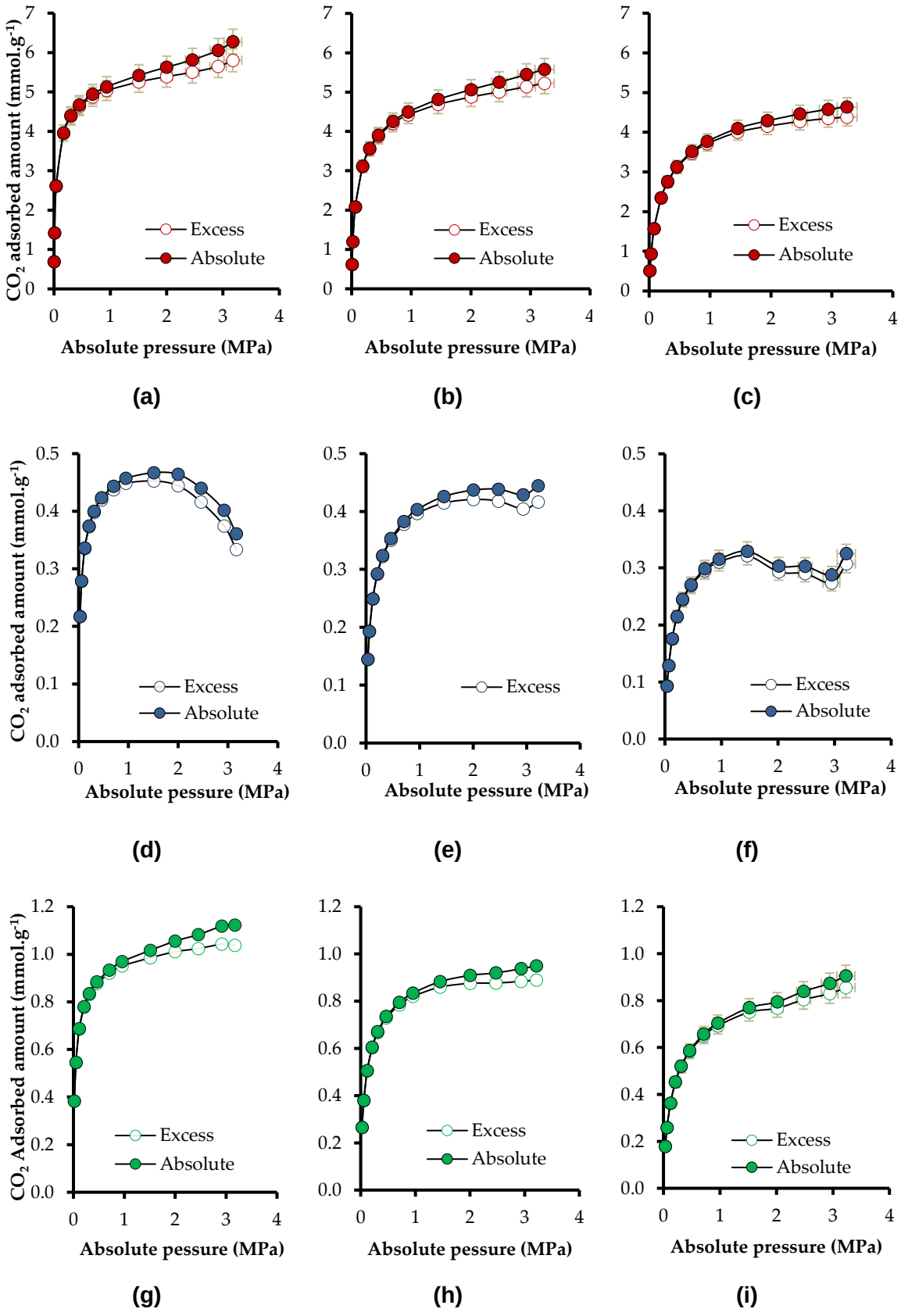
CO2 adsorbed amount (mmol.g-1)
Absolute pressure (MPa)
Excess
Absolute
(a)
(b)
(c)
Absolute pessure (MPa)
(d)
(e)
(f)
CO2 Adsorbed amount (mmol.g-1)
(g)
(h)
(i)

Figure 4. 8. Adsorption isotherms of CO_2 at high pressure (3×10^{-3} up to 3.0 MPa) of CN.LYS2 at (**a**) 0 °C, (**b**) 25 °C, and (**c**) 50 °C; SS-10 (sandstone impregnated with a mass fraction of 10%CN.LYS2) at (**d**) 0 °C, (**e**) 25 °C, and (**f**) 50 °C; SS-20 (sandstone impregnated with a mass fraction of 20%CN.LYS2) at (**g**) 0 °C, (**h**) 25 °C and (**i**) 50 °C.

Figure 4. 9 presents incremental factors comparing N_{ads} for sandstone without impregnation to N_{ads} after impregnation with mass fractions of 10 and 20% at 3 MPa and 0, 25, and 50 °C. In the conditions of a shallow reservoir (50 °C and 3.0 MPa), the incremental factor was 677 for SS-20. For the e-CCS process, the pressure could increase up 6.0 MPa so that CO_2 is still in the vapor phase, which allows a higher adsorbed amount.

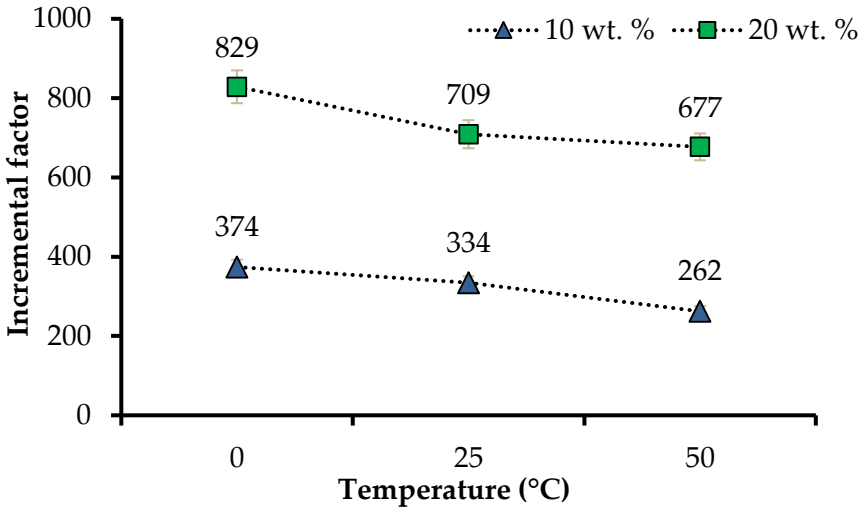

Figure 4. 9. Relationship between the impregnation percentages (mass fractions of 10 and 20%) and the adsorption capacity of CO_2 at 3 MPa and 0, 25, and 50 °C.

Figure 4. 10, Figure 4. 11 and Figure 4. 12 present the fit of the Sips and Toth models to the CO_2 adsorption isotherms at high pressure and 0, 25, and 50°C for CN.LYS2, SS-10, and SS-20. As expected, the Toth and Sips models led to very good fits: $R^2 > 0.99$ for CN.LYS2, SS-10, and SS-20, and $R^2 > 0.75$ for SS-10 at 0 °C. In the latter case, the concavity of the isotherm was mainly due to the very rapid increase of the bulk density as

a function of pressure with respect to the increase of the density of the adsorbed phase at a pressure higher than 1.5 MPa.

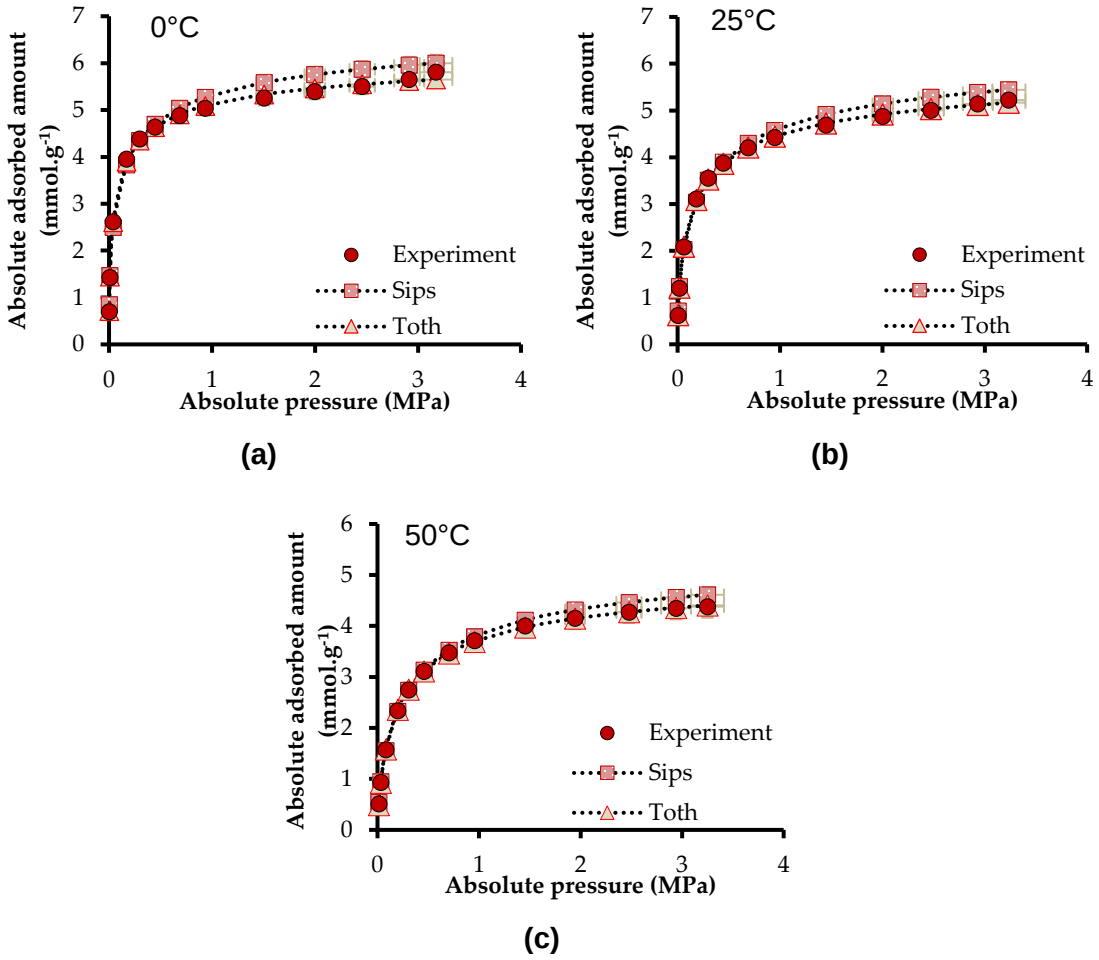

Figure 4. 10. Adsorption isotherms fitted by the Sips and Toth models for carbon nanospheres synthesized with L-lysine (CN.LYS2) at (**a**) 0 °C, (**b**) 25 °C, and (**c**) 50 °C.

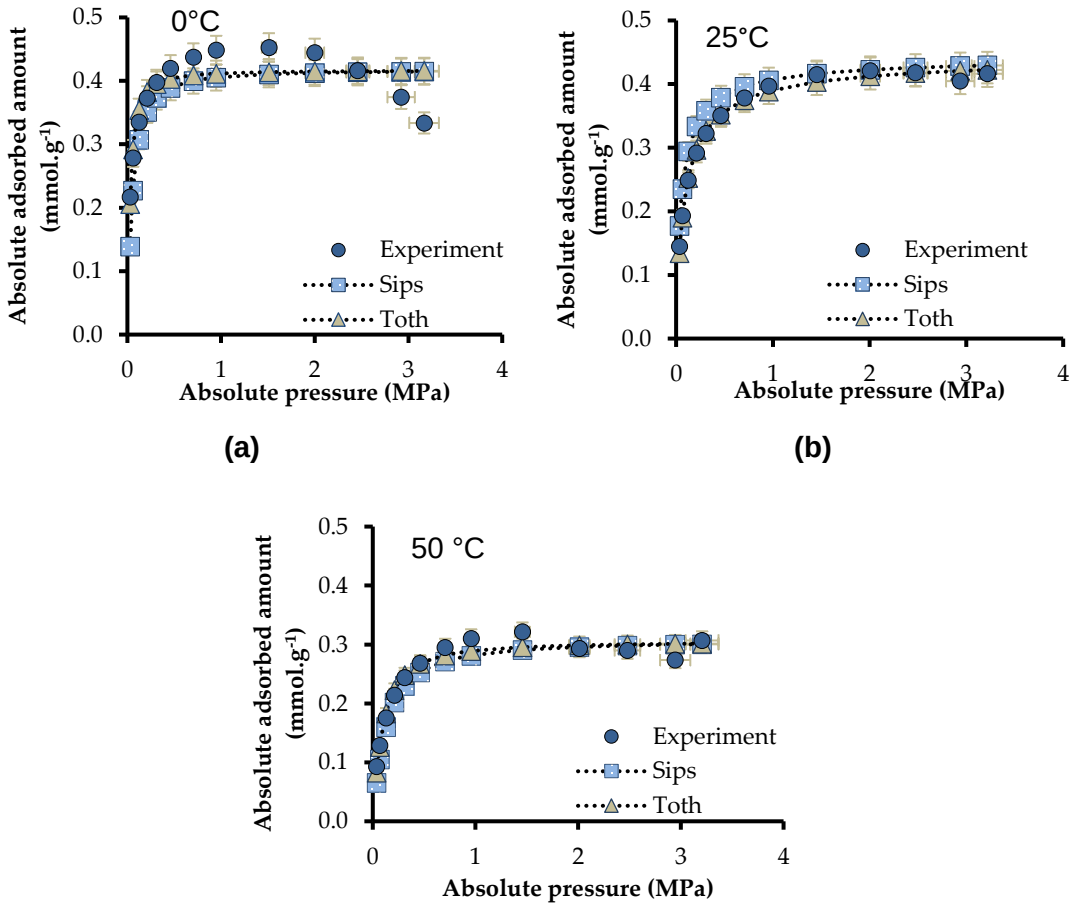

Figure 4. 11. Adsorption isotherms fitted by the Sips and Toth models for sandstone impregnated with a mass fraction of 10% of carbon nanospheres synthesized with L-Lysine (CN.LYS2) at (**a**) 0° C, (**b**) 25 °C, and (**c**) 50 °C.

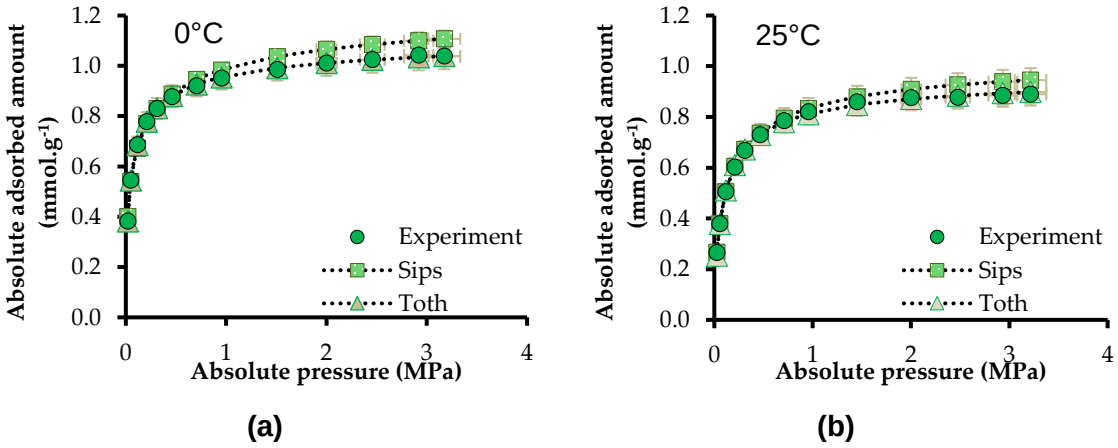

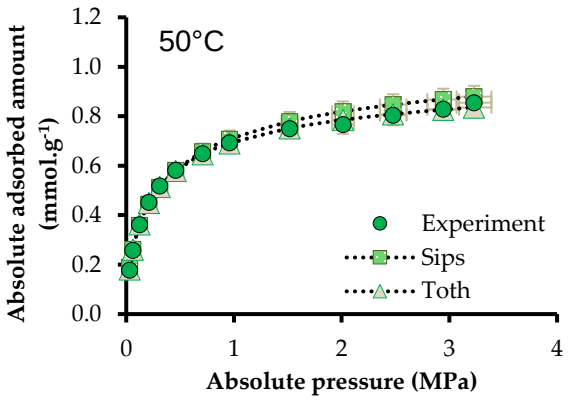

(c)

Figure 4. 12. Adsorption isotherms fitted the Sips and Toth models for sandstone impregnated with a mass fraction of 20% of carbon nanospheres synthesized with L-Lysine (CN.LYS2) at (**a**) 0 °C, (**b**) 25 °C, and (**c**) 50 °C.

Figure 4. 13-a presents the isosteric heat of adsorption (Q_{st}) of CN.LYS2 and of sandstone impregnated with mass fractions of 10 and 20%, as a function of N_{ads} expressed in mmol per gram of total adsorbent material. N_{ads} for SS-10 and SS-20 was small, and thus, Figure 4. 13-b presents Q_{st} as a function of N_{ads} in mmol per gram of carbon adsorbent material. The values of Q_{st} varied from 25 to 33 kJ mol^{-1}, which indicates a strong interaction in the adsorption system (high affinity). The interactions with the porous carbon structure could be increased by nitrogen-containing groups that are present onto the carbon surface. Nitrogen groups can indeed promote interactions between CO_2 and the substrate. The values of Q_{st} compare favorably with those reported in the literature for different materials doped or not with nitrogen (20–25 kJ mol^{-1}, on average) [18-21].

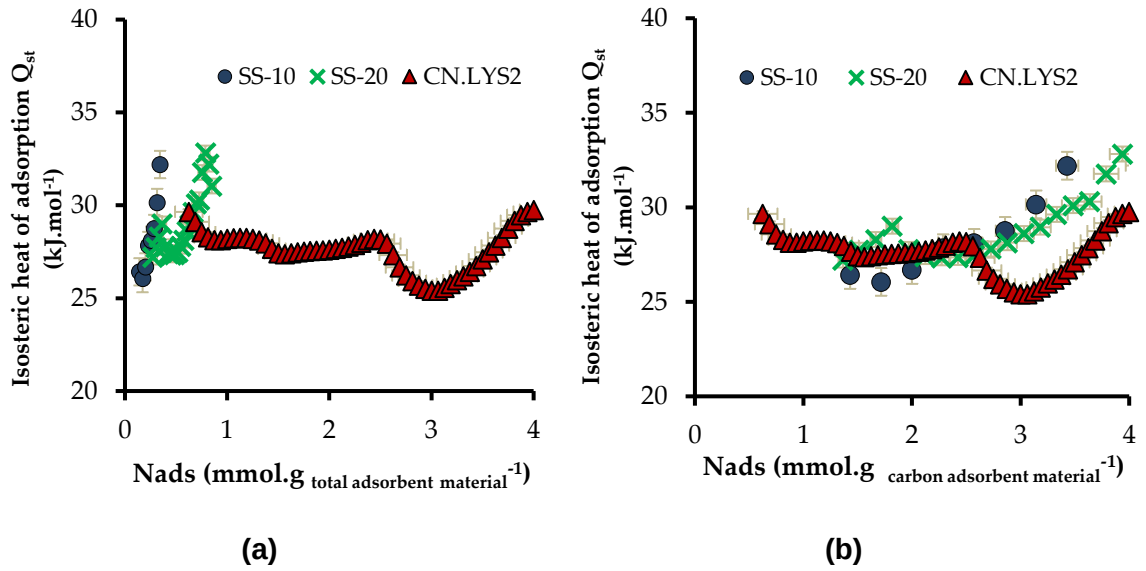

Figure 4. 13. Isosteric heat of adsorption of CN.LYS2 and sandstone impregnated with mass fractions of 10 and 20%, as a function of the adsorbed CO_2 amount expressed: (**a**) in mmol per total amount of adsorbent material (sandstone and CN.LYS2) and (**b**) in mmol per amount of carbon adsorbent material.

The isosteric heat of adsorption of CN.LYS2 presented two distinct behaviors, whether N_{ads} was either (i) lower or (ii) higher than 3 mmol $g_{carbonadsorbentmaterial}^{-1}$. For case (i), Q_{st} decreased with N_{ads} due to the increasing distance between the last adsorbed layer and the carbon surface, thus decreasing the molecular interactions (Figure 4. 13-b). For case (ii), i.e., when N_{ads} was higher than 3 mmol $g_{carbonadsorbentmaterial}^{-1}$, Q_{st} increased due to the increased interactions between adsorbate molecules [18]. For SS-10 and SS-20, the value of Q_{st} also increased with N_{ads}. Because the interactions between sandstone (silica) and CO_2 were weak and because the contribution of the surface area associated with the carbon material was lower than for CN.LYS2 alone, it can be assumed again that the interactions between the adsorbed gas layers prevailed [18].

4.2.2.2. CO_2 and N_2 Adsorption at High Pressure–Gravimetric Measurement Method

Using the PyIAST application and using the pure-components adsorption isotherms obtained by experimental tests, it is possible to characterize the behavior of each component and to predict the adsorbed amount of each component present in a mixture

[13]. It is, thus, possible to obtain the adsorbed amount at a constant temperature by varying the concentration of the components (at constant pressure) or the pressure (at constant concentrations). Initially, it is necessary to use the “isothermal interpolator” to generate data points that follow a given isothermal model, avoiding the search for an appropriate analytical model and examining the quality of its fit to the data (i.e., Langmuir, Freundlich or Toth, among others) [13]. An isothermal interpolator is a tool included in the PyIAST package. After that, PyIAST takes the interpolated data for its calculations. Calculations are done using a predesigned routine in Python [13].

In the present case, the experimental data of each pure component (CO_2 and N_2) were obtained by HP-TGA at 50 °C, between 0.1 and 2.5 MPa, and with a flow of CO_2 or N_2 (50 mL min^{-1} up to 1.0 MPa and 70 mL min^{-1} up to 2.5 MPa). The prediction was calculated at 50 °C by varying: 1) the system pressure from 0.1 to 2.5 MPa at a constant CO_2 concentration of 20% and 2) the concentration of CO_2, from 5 to 100% at a constant pressure of 2.5 MPa.

The evaluated materials were CN.LYS2 and sandstone from a real reservoir (RS) impregnated with a mass fraction of 20% of CN.LYS2. It is important to mention that it might be possible to obtain considerable adsorbed quantities for a cleaning and adsorption balance of more than 12–24 hours because the nanomaterials (main adsorbent) are micro/mesoporous. A longer cleaning time thus allows eliminating adsorbed gases and moisture. In the same way, an adequate equilibrium time allows for greater diffusion of the gas into the porous structure and greater interactions with the material, which would allow a higher adsorbed amount. Therefore, to analyze the selectivity, a shorter time was used (cleaning and adsorption equilibrium time of 2 hours at each pressure).

It was not possible to obtain the CO_2 isotherm for RS because the latter had a too low surface area, so the maximum value for RS at 50 °C and 2.5 MPa was 0.033 mmol g^{-1}. For RS, the adsorbed amount of N_2 was 3.19 mmol g^{-1} at 50 °C and 2.5 MPa. Figure 4. 14-a and Figure 4. 14-b present the CO_2 and N_2 adsorption isotherms under continuous gas flow for CN.LYS2 and RS-20. The increment factor of N_{ads} for RS-20 with respect to RS was 19 (0.66 mmol g^{-1} at 50 °C and 2.5 MPa). Also, the theoretical value of N_{ads} for RS with a mass fraction of 20% of CN.LYS2 was 0.78 mmol g^{-1}, but the experimental value was 0.66 mmol g^{-1} (i.e., 85% of the theoretical one).

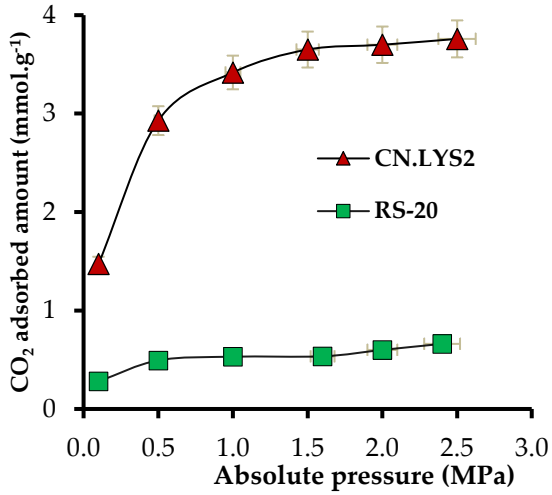
CO2 adsorbed amount (mmol.g-1)
CN.LYS2
RS-20
Absolute pressure (MPa)

(a)

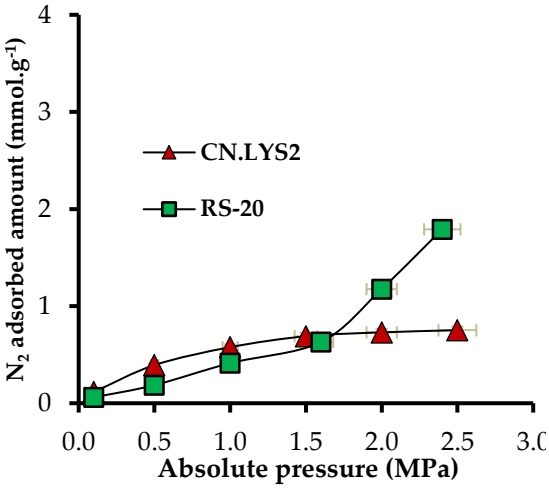
N2 adsorbed amount (mmol.g-1)
CN.LYS2
RS-20
Absolute pressure (MPa)

(b)

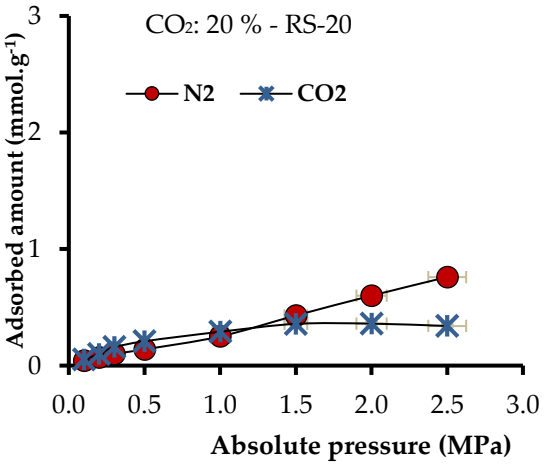
CO2: 20 % - RS-20
N2
CO2
Adsorbed amount (mmol.g-1)
Absolute pressure (MPa)

(c)

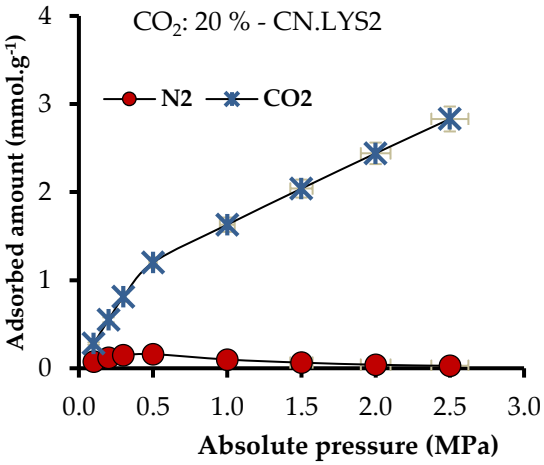
CO2: 20 % - CN.LYS2
N2
CO2
Adsorbed amount (mmol.g-1)
Absolute pressure (MPa)

(d)

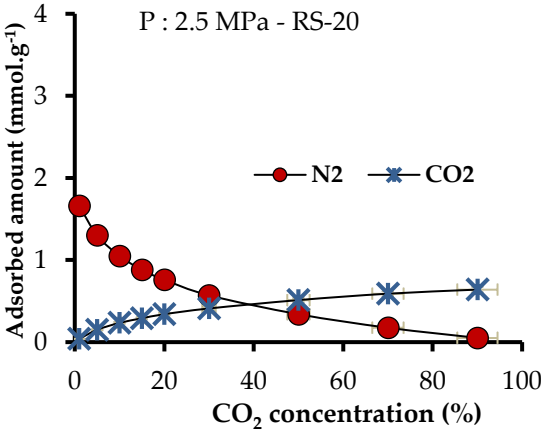
P : 2.5 MPa - RS-20
N2
CO2
Adsorbed amount (mmol.g-1)
CO2 concentration (%)

(e)

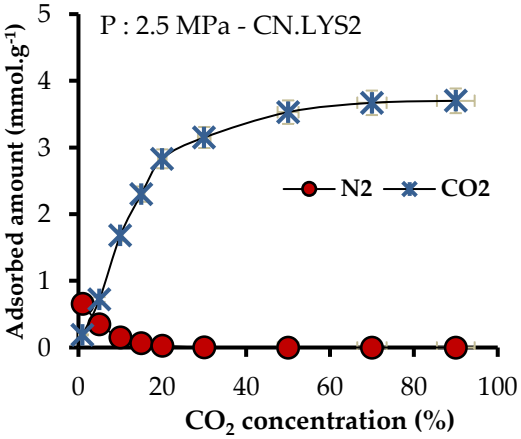
P : 2.5 MPa - CN.LYS2
N2
CO2
Adsorbed amount (mmol.g-1)
CO2 concentration (%)

(f)

Figure 4. 141. Adsorption isotherm of CN.LYS2 and RS-20 at 50 °C between 0.1 and 2.5 MPa for (**a**) pure CO_2 and (**b**) pure N_2. Adsorption isotherm simulating a N_2/CO_2 mixture at 50 °C, the constant CO_2 concentration of 20%, and varying the pressure for (**c**) RS-20 and (**d**) CN.LYS2; and varying the CO_2 concentration at a constant pressure of 2.5 MPa for (**e**) RS-20 and (**f**) CN.LYS2.

Figure 4. 14-c,d presents the simulated adsorbed amount for an N_2/CO_2 mixture at a constant CO_2 concentration of 20% and 50 °C by varying the pressure for RS-20 and CN.LYS2, respectively. For RS-20, the affinity for CO_2 was higher (P < 1 MPa) compared to RS without impregnation, but the N_{ads} for N_2 was superior (123.5%) to that for CO_2 (Figure 4. 14-c). For RS-20, the CO_2 isotherm obtained a form that would be impossible to obtain without impregnation due to the lack of surface area and molecular interactions. The isotherm for CN.LYS2 showed a higher affinity for CO_2 and a correspondingly higher N_{ads} than for N_2, which, above 0.5 MPa, decreased considerably (Figure 4. 14-d). Similar conditions occurred when the CO_2 concentration was varied at 2.5 MPa and 50 °C (Figure 4. 14-e,f), CN.LYS2 had more affinity for CO_2 than RS-20, and CN.LYS2 had a considerably higher N_{ads} for CO_2 than for N_2. Figure 4. 14-e shows the increment of N_{ads} only for CO_2 while the CO_2 concentration was increased in RS-20; at low concentrations of CO_2 (< 30%), the N_{ads} for N_2 was higher. For CN.LYS2 at low concentrations of CO_2 (1%), the slope increment was significant, indicating a higher affinity for CO_2 at low concentrations.

From Figure 4. 14, it can be concluded that pyIAST is a useful tool because it is possible to simulate the behavior of adsorption systems from some pure gas adsorption data.

4.3. Partial conclusions

Nitrogen-rich carbon nanospheres allowed increasing the adsorption capacity by a factor of 677 with a mass fraction of only 20% (CN.LYS2) under realistic reservoir conditions (50 °C and 3 MPa). This capacity was possible thanks to the higher surface area and to the favorable chemical composition, which promoted the capture and storage of CO_2.

These N-doped carbon nanospheres, synthesized by a simple process, had competitive CO_2 capture performances compared to other special materials reported in the literature. This process could reduce time and cost for possible future applications of e-CCS process.

4.4. References

[1] J. Wang, L. Huang, R. Yang, Z. Zhang, J. Wu, Y. Gao*, et al.*, "Recent advances in solid sorbents for CO 2 capture and new development trends," *Energy & Environmental Science,* vol. 7, pp. 3478-3518, 2014.

[2] M. Plaza, C. Pevida, A. Arenillas, F. Rubiera, and J. Pis, "CO2 capture by adsorption with nitrogen enriched carbons," *Fuel,* vol. 86, pp. 2204-2212, 2007.

[3] J. Wei, D. Zhou, Z. Sun, Y. Deng, Y. Xia, and D. Zhao, "A controllable synthesis of rich nitrogen-doped ordered mesoporous carbon for CO2 capture and supercapacitors," *Advanced Functional Materials,* vol. 23, pp. 2322-2328, 2013.

[4] W.-J. Son, J.-S. Choi, and W.-S. Ahn, "Adsorptive removal of carbon dioxide using polyethyleneimine-loaded mesoporous silica materials," *Microporous and Mesoporous Materials,* vol. 113, pp. 31-40, 2008.

[5] Y.-R. Dong, N. Nishiyama, Y. Egashira, and K. Ueyama, "Basic Amid Acid-Assisted Synthesis of Resorcinol− Formaldehyde Polymer and Carbon Nanospheres," *Industrial & engineering chemistry research,* vol. 47, pp. 4712-4716, 2008.

[6] X. Bai, J. Li, C. Cao, and S. Hussain, "Solvothermal synthesis of the special shape (deformable) hollow g-C3N4 nanospheres," *Materials Letters,* vol. 65, pp. 1101-1104, 2011.

[7] M. Franco-Aguirre, R. D. Zabala, S. H. Lopera, C. A. Franco, and F. B. Cortés, "Interaction of anionic surfactant-nanoparticles for gas-Wettability alteration of sandstone in tight gas-condensate reservoirs," *Journal of Natural Gas Science and Engineering,* vol. 51, pp. 53-64, 2018.

[8] S. Schaefer, V. Fierro, M. Izquierdo, and A. Celzard, "Assessment of hydrogen storage in activated carbons produced from hydrothermally treated organic materials," *international journal of hydrogen energy,* vol. 41, pp. 12146-12156, 2016.

[9] S. Schaefer, V. Fierro, A. Szczurek, M. Izquierdo, and A. Celzard, "Physisorption, chemisorption and spill-over contributions to hydrogen storage," *international journal of hydrogen energy,* vol. 41, pp. 17442-17452, 2016.

[10] N. Tzabar and H. ter Brake, "Adsorption isotherms and Sips models of nitrogen, methane, ethane, and propane on commercial activated carbons and polyvinylidene chloride," *Adsorption,* vol. 22, pp. 901-914, 2016.

[11] N. Álvarez-Gutiérrez, M. Gil, F. Rubiera, and C. Pevida, "Adsorption performance indicators for the CO2/CH4 separation: Application to biomass-based activated carbons," *Fuel Processing Technology,* vol. 142, pp. 361-369, 2016.

[12] A. Abdeljaoued, N. Querejeta, I. Durán, N. Álvarez-Gutiérrez, C. Pevida, and M. Chahbani, "Preparation and Evaluation of a Coconut Shell-Based Activated Carbon for CO2/CH4 Separation," *Energies,* vol. 11, p. 1748, 2018.

[13] C. M. Simon, B. Smit, and M. Haranczyk, "pyIAST: Ideal adsorbed solution theory (IAST) Python package," *Computer Physics Communications,* vol. 200, pp. 364-380, 2016.

[14] A. Alonso, J. Moral-Vico, A. A. Markeb, M. Busquets-Fité, D. Komilis, V. Puntes*, et al.*, "Critical review of existing nanomaterial adsorbents to capture carbon dioxide and methane," *Science of the total environment,* vol. 595, pp. 51-62, 2017.

[15] S. Cavenati, C. A. Grande, and A. E. Rodrigues, "Adsorption equilibrium of methane, carbon dioxide, and nitrogen on zeolite 13X at high pressures," *Journal of Chemical & Engineering Data,* vol. 49, pp. 1095-1101, 2004.

[16] E. P.-C. Bailon-García, Agustín F.; Rodriguez Acevedo, Elizabeth; Carrasco-Marín, Francisco, "Nanoparticle Fabrication Methods," in *Formation Damage in Oil and Gas Reservoirs. Nanotechnology Applications for its Inhibition/Remediation*, C. A. a. C. C. Franco, Farid B, Ed., 1 ed: Nova Science Publishers, 2018, pp. 69-150.

[17] Y. Ma, Z. Wang, X. Xu, and J. Wang, "Review on porous nanomaterials for adsorption and photocatalytic conversion of CO2," *Chinese Journal of Catalysis,* vol. 38, pp. 1956-1969, 2017.

[18] S. Himeno, T. Komatsu, and S. Fujita, "High-pressure adsorption equilibria of methane and carbon dioxide on several activated carbons," *Journal of Chemical & Engineering Data,* vol. 50, pp. 369-376, 2005.

[19] D. J. Babu, M. Bruns, R. Schneider, D. Gerthsen, and J. r. J. Schneider, "Understanding the influence of N-doping on the CO2 adsorption characteristics in

carbon nanomaterials," *The Journal of Physical Chemistry C,* vol. 121, pp. 616-626, 2017.

[20] J. Dunne, R. Mariwala, M. Rao, S. Sircar, R. Gorte, and A. Myers, "Calorimetric heats of adsorption and adsorption isotherms. 1. O2, N2, Ar, CO2, CH4, C2H6, and SF6 on silicalite," *Langmuir,* vol. 12, pp. 5888-5895, 1996.

[21] R. V. Siriwardane, M.-S. Shen, E. P. Fisher, and J. A. Poston, "Adsorption of CO2 on molecular sieves and activated carbon," *Energy & Fuels,* vol. 15, pp. 279-284, 2001.


LIBERTAD Y ORDEN
INTER · AULAS · ACADEMIÆ · QUÆRE · VERUM


UNIVERSITAS · GRANATENSIS
PLUS ULTRA
· 1531 ·

5. Carbonized-Mg/Ni MOF-74 applied to e-CCS process

The metal-organic frameworks-MOF are constructed through transition metal ions and organic ligands, which have been evaluated in CO_2 capture processes [1-3]. The investigations are focused on the development of new structures, a different configuration of metal ions and ligands, functionalization, hybrid materials, among others. The metal ion directly influences the molecular interactions with CO_2, and the organic ligand allows defining the magnitude of the porosity and the specific surface area, which generates more sites for interaction. A MOF disadvantage is the performance in aqueous media, due to the competition of H_2O for active adsorption sites [1], which also could affect the MOF structure.

MOFs have a high adsorption capacity in high-pressure adsorption processes. However, MOF some disadvantages such as obtainment from more complex reagents for scaling (compared with carbon materials), MOF shapes and size are not suitable for reservoir application, because can be affected the porosity, and could be unstable under wet conditions. Whence, conventional MOF could not be suitable for the e-CCS process, but their evaluation is important due to the high capacity of CO_2 capture, it would be worth carrying out studies on its stability and decrease in size.

The main objective of this chapter is obtaining stable metal-organic frameworks. For this purpose, MOF-74 with Ni and Mg as metal cores were synthesized and characterized. After that, the materials were carbonized, in order to conserve the original MOF porous structure and obtain the stability of carbon materials. After that, the best carbonized-MOF was used as modifying agents of sandstone rock. Smaller MOF particles were synthesized through conventional solvothermal conditions (24 h), and by heating in a microwave oven for shorter

periods (1.5 h). The CO_2 adsorption process, as well as its thermodynamic parameters, were evaluated under atmospheric and high-pressure conditions, mimic reservoir conditions.

5.1. Materials and Methods

Two different MOFs were synthesized using solvothermal method under different conditions, Ni-MOF74 and Mg-MOF74, which becomes eight different materials. The synthesized nanostructures were labeled and synthesized as follows:

-***Ni-MOF-24:*** MOF-74 with nickel as the metal ion. Solvothermal process for 24 h in a conventional oven.

-***Ni-MOF-1.5:*** MOF-74 with nickel as the metal ion. Solvothermal process for 1.5 h in microwaves oven.

- ***Mg-MOF-24:*** MOF-74 with magnesium as the metal ion. Solvothermal process for 24 h in a conventional oven.

- ***Mg-MOF-1.5:*** MOF-74 with magnesium as the metal ion. Solvothermal process for 1.5 h in microwaves oven.

- ***C-Ni-MOF-24, C-Ni-MOF-1.5, C-Mg-MOF-24, C-Mg-MOF-1.5:*** These materials are materials previously synthesized and carbonized.

MOFs were characterized in order to select the best material, considering the smallest size, adsorption capacity, and stability after carbonization. The material's performance was evaluated by CO_2 adsorption at atmospheric pressure and 0 °C, and best materials by varying pressure (up to 3.0 MPa) and temperature (0, 25 and 50 °C) conditions. The detailed procedures are presented below. Ottawa sandstone was used as a porous medium and was impregnated with the best MOF at 20 %.

5.1.1. Materials and Reagents

For the synthesis processes, the following reagents were used: Magnesium nitrate hydrate ($Mg(NO_3)_2$-$6H_2O$) (> 99%), nickel nitrate hydrate ($Ni(NO_3)_2$-$6H_2O$) (> 99%), 2,5-dihydroxyterephthalic acid (DOT) (98%), N.N-dimethylformamide (DMF) (>99.5%), ethanol (≥ 99%), methanol (99%) and deionized water.

For the carbonization process, Ar was used (high purity, grade 5.0). Clean Ottawa sandstone and sandstone from a real reservoir were used as porous media. The real sandstone was obtained from a Colombian oil field, which allows evaluating the real rock that might be used to implement the e-CCS process in depleted oil fields.

5.1.2. Synthesis of metal-organic frameworks (MOF)

5.1.2.1. Ni-MOF 74 Synthesis

The synthesis process was adapted from Bao and Wu [2]. A solution of $Ni(NO_3)_2$-$6H_2O$ (6.54 mmol), DOT (1.92 mmol), in a mixture of DMF, ethanol, and water (volume ratio 1:1:1) was stirring at 200 rpm for a 30 min. After that, the solution was heating in a solvothermal reactor at 100 °C for 24 h by mean of a conventional oven. The material was decanted and cleaned with methanol for 3 days. The final solid is dried at 120 °C and vacuum atmosphere. The microwave method uses the same solution but is heated in a Teflon autoclave by mean microwave oven for 1.5 h at 100 °C. After that, the material is cleaned and dried at the same conditions.

5.1.2.2. Mg-MOF 74 Synthesis

The synthesis process was adapted from Bao and Wu. [2, 4]. A solution of $Mg(NO_3)_2$-$6H_2O$ (5.62 mmol), DOT (1.7 mmol), in a mixture of DMF, ethanol, and water (volume ratio 15:1:1) was stirring at 200 rpm for a 30 min. After that, the solution was heating in a solvothermal reactor at 120 °C for 24 h by mean of a conventional oven. The material was decanted and cleaned with methanol for 3 days. The final solid is dried at 120 °C and vacuum atmosphere. The microwave method uses the same solution but is heated in a Teflon autoclave by mean microwave oven for 1.5 h at 120 °C. After that, the material is cleaned and dried at the same conditions.

5.1.2.3 Carbonization of MOF

The carbonization process was adapted from [5]. The materials were carbonized in a tube furnace with argon (Ar) flow rate of 20ml min^{-1} at 800°C for 3 h.

5.1.3. Impregnation of Sandstones

The sandstone was impregnated to decorate the rock surface with the C-Ni-MOF-24. Real sandstone (RS) was impregnated at mass fractions of 20% by immersion and soaking [6]. Initially, a fluid composed of particles and deionized water was sonicated at 40 °C for 4 h. Subsequently, the RS was introduced in the fluid at 60 °C for 24 h without stirring. Finally, the impregnated material was dried at 110 °C for 12 h. The impregnation method mimics the reservoir conditions in which the porous medium.

5.1.4. Characterization of the Nanomaterials

The following procedures allowed characterizing the physicochemical characteristics of the materials, essential for a good understanding of the results. For e-CCS applications, nanoparticles must have a balance between the smallest possible size, and high adsorption capacity.

5.1.4.1. Size and Structure of Nanomaterials

Scanning electron microscopy (SEM) was used to obtain the dry particle size, size distribution, and morphology. The observations were carried out using a JSM-7100 emission electron microscope (JEOL, Nieuw-Vennep, The Netherlands), a GEMINI-LEO1530 VP FE-SEM emission electron microscope (Carl Zeiss, Cambridge, UK).

In this case, the dynamic light scattering (DLS) study was not carried out, because the aggregate size of these materials exceeds the size limit allowed for equipment (10 µm).

5.1.4.2. Porous Structure of Nanomaterials and Sandstone

Materials were characterized by N_2 and CO_2 adsorption at −196 °C and 0 °C, respectively, using 3-Flex manometric adsorption equipment (Micromeritics, Norcross, USA). The total adsorbed volume ($V_{0.95}$) was taken as the physisorbed volume of N_2 at a relative pressure $P/P_0 = 0.95$. The Brunauer–Emmett–Teller (BET) model was applied to obtain the BET area (A_{BET}). Micropore volume (V_{mic}), average pore size (L_0), and CO_2 adsorption energy ($E_{ads–CO2}$) were obtained by application of the Dubinin–Radushkevich equation. The mesopore volume (V_{meso}) was obtained through the Barrett–Joyner–Halenda (BJH) model.

5.1.4.3. Chemical Composition of Materials and Sandstone

The chemical characterization was carried out by Energy dispersive spectroscopy (EDS) by SEM analyzer, JSM-7100 emission electron microscope (JEOL, Nieuw-Vennep, The Netherlands), a GEMINI-LEO1530 VP FE-SEM emission electron microscope (Carl Zeiss, Cambridge, UK).

Fourier transform infrared spectroscopy (FTIR) was used for sandstone characterization. An IRAffinity-1S FTIR spectrometer (Shimadzu, Columbia, USA) was operated at room temperature using potassium bromide in a KBr-to-material ratio of 30:1 (% w/w).
The impregnation percentages of MOF on surface sandstone were corroborated by thermogravimetric analysis (TGA) (TA Instruments, New Castle, USA). For this, the sample was burned under an air atmosphere at 10 °C min^{-1} up to 800 °C.

5.1.4.4. Dispersion of Nanoparticles in Solution

The electrophoretic light scattering (ELS) technique was used to evaluate the surface charge of the particles and their dispersion stability at 25 °C in a NanoPlus-3 zeta/nanoparticle analyzer (Micromeritics, Norcross, USA). In this test, several particle suspensions are prepared at 10 mg L^{-1}, with a pH adjusted between 2 to 12 by adding solutions of 0.1 mol L^{-1} HCl or 0.01 mol L^{-1} NaOH and then subjected to analysis. The zeta potential was calculated using the Smoluchowski equation, derived from the calculation of the Doppler effect.

$$\zeta = \eta U / \varepsilon \quad \textbf{(5.1)}$$

$$U = \frac{V}{E} \quad \textbf{(5.2)}$$

$$\Delta v = 2V\, n \sin\left(\frac{\theta}{2}\right) / \lambda \quad \textbf{(5.3)}$$

where ζ is the zeta potential, η is the viscosity of the fluid (water), U is the electrophoretic mobility, ε is the permittivity, V represents the speed of movement of the particles, E is the electric field, Δv is the Doppler effect, n is the index of refraction, θ is the angle of detection, and λ is the wavelength of the incident light.

5.1.5. Adsorption Tests at High Pressure

At high pressure, the CO_2 adsorption capacity was evaluated in two different conditions: (i) under pure CO_2 in a manometric device (up to 3.0 MPa) and (ii) under a CO_2 or N_2 flow in a gravimetric device (up to 2.6 MPa). The details of each protocol are presented below.

5.1.5.1. Adsorption at High Pressure for Pure CO_2–Manometric Device

The Ni-MOF-24 and C-Ni-MOF-24 were investigated in High-Pressure Volume Analyzer, HPVAII-200 (Micromeritics, Norcross, USA) at 0 °C, 25 °C, and 50 °C and at pressures from 3×10^{-3} up to 3.0 MPa. In order to have enough total surface area for adsorption and to minimize measurement errors, the amount of each material inside the sample holder was around 0.5 g for MOF and 14 g for sandstone. The contribution of the empty sample holder was systematically measured and subtracted to all data to improve accuracy. The isosteric heat of adsorption, Q_{ST}, was calculated using the isosteric method with the Microactive software (from Micromeritics, Norcross, USA) from three adsorption isotherms at 0, 25, and 50 °C, based on the Clausius–Clapeyron equation [51]:

$$-\frac{Q_{ST}}{R} = \frac{\partial \ln(P)}{\partial (1/T)} \quad \textbf{(5.4)}$$

where R is the universal gas constant (8.314 J mol^{-1} K^{-1}), P is the absolute pressure, and T is the temperature.

The excess adsorbed CO_2 amount (N_{exc}, $g_{CO2}.g_{adsorbent}^{-1}$) was equal to the absolute adsorbed CO_2 amount ($N_{ads,}$ $g_{CO2}.g_{adsorbent}^{-1}$) minus the product of gas density in the bulk phase by the volume of the adsorbed phase. The values provided by the HPVA device were

obtained on an excess basis, and therefore, the absolute amounts had to be determined as follows [52]:

$$N_{ads} = N_{exc}\left(1+\frac{P+M_{CO2}}{Z\,\rho_{liq}\,RT}\right) \quad \textbf{(5.5)}$$

where M_{CO2} is the molecular weight of CO_2 (44.013 g mol^{-1}), Z is the compressibility factor at the considered pressure and temperature, and ρ_{liq} is the density of liquid CO_2 (1032 × 10^3 g m^{-3}).

The isotherms were fitted with the Sips and Toth models, which take into account multilayer adsorption. Table 5. 1 presents the equations for each model [53–55]. K_S and K_T represent adsorption equilibrium constants for the Sips and Toth models, respectively, and the *n* and *t* parameters indicate the heterogeneity of the system for the Sips and Toth models, respectively. The heterogeneity may originate from the solid structure, from the solid energy properties, or the adsorbate [54]. The *n* or *t* parameters are usually higher than unity, and when they are the unit, the models assume the Langmuir equation [54].

Table 5. 1. Models for adsorption isotherms.

Model	Equations	Parameters
Sips	$N_{ads} = N_m \frac{(K_S\,P)^{1/n}}{1+(K_S\,P)^{1/n}}$ **(5.6)**	N_{ads} (mmol g^{-1}) is the adsorbed amount, N_m (mmol g^{-1}) is the adsorption capacity at equilibrium, P (kPa) is the equilibrium pressure, and K_S and n are the Sips adsorption equilibrium constants, related to the affinity and the heterogeneity of the system, respectively.
Toth	$N_{ads} = N_m \frac{K_T\,P}{(1+(K_T\,P)^t)^{1/t}}$ **(5.7)**	N_{ads}, N_m, and P have the same meaning as above, and K_T and t are the Toth adsorption equilibrium constants, related to the affinity and the heterogeneity of the system, respectively.

5.1.5.2. Adsorption at High Pressure for CO_2 and N_2–Gravimetric Device

CO_2 adsorption by C-Ni-MOF-24, sandstone, and impregnated sandstone (with a mass fraction of 20%) were investigated using an HP TGA 750 thermogravimetric analyzer (TA Instruments, New Castle, USA) at 50 °C and high pressure from 0.03 to 3.0 MPa for CO_2 and N_2. This device was equipped with a magnetic levitation top-loading balance, which made it possible to achieve high accuracy and reduce the volume of the system. The amount of each material put inside the sample holder was around 15 mg for MOF, 40 mg for sandstone, and 40 mg for impregnated sandstone, to have enough total surface area for adsorption.

The contribution of the buoyancy effect was manually subtracted from the data using blank tests carried out in the same conditions but with an empty sample holder. From the adsorption results of each N_2 and CO_2 isotherm, it was possible to predict the selectivity by applying the ideal adsorbed solution theory (IAST), which allows estimating the competitive adsorption of the compounds in a mixture of gases as the flue gas. Based on the literature, a model flue gas comprising 80% N_2 and 20% CO_2 was selected. The IAST was implemented in a Python routine (package-pyIAST from Simon et al. [56]).

5.2. Results and Discussion

The results are divided into two main sections: a) materials characteristics (MOF and sandstone) and b) study of the interaction between CO_2/MOF/sandstone by adsorption isotherms under different operation conditions (T, P).

5.2.1. Materials Characteristics

The synthesized MOF is presented in Figure 5. 1. Ni-MOF-24 and C-Ni-MOF-24 (Figure 5. 1-a,b) present a structure similar to flowers. The size is approximately 6 µm. After carbonization, the structure is preserved. On the other hand, the use of microwave heating theoretically allows generating a greater number of nucleation points, which have a reduced time to grow. On the contrary, in the conventional hydrothermal method, nucleation points are generated and grow during the long reaction time. The Ni-MOF-1.5 and C-Ni-MOF-1.5 present a smaller size but remain micrometric (Figure 5.1-c,d). Also, the structure is not

fully developed, so it may have less surface area available. In this case, the carbonized MOF still retains the structure.

In the Mg-MOF case, these materials are more sensitive to conditions of pressure and temperature. Also, Several synthesis processes were performed, and there was not reproducibility (conventional and microwave processes). For this reason, only Mg-MOF-24 was evaluated (Figure 5. 1-e).

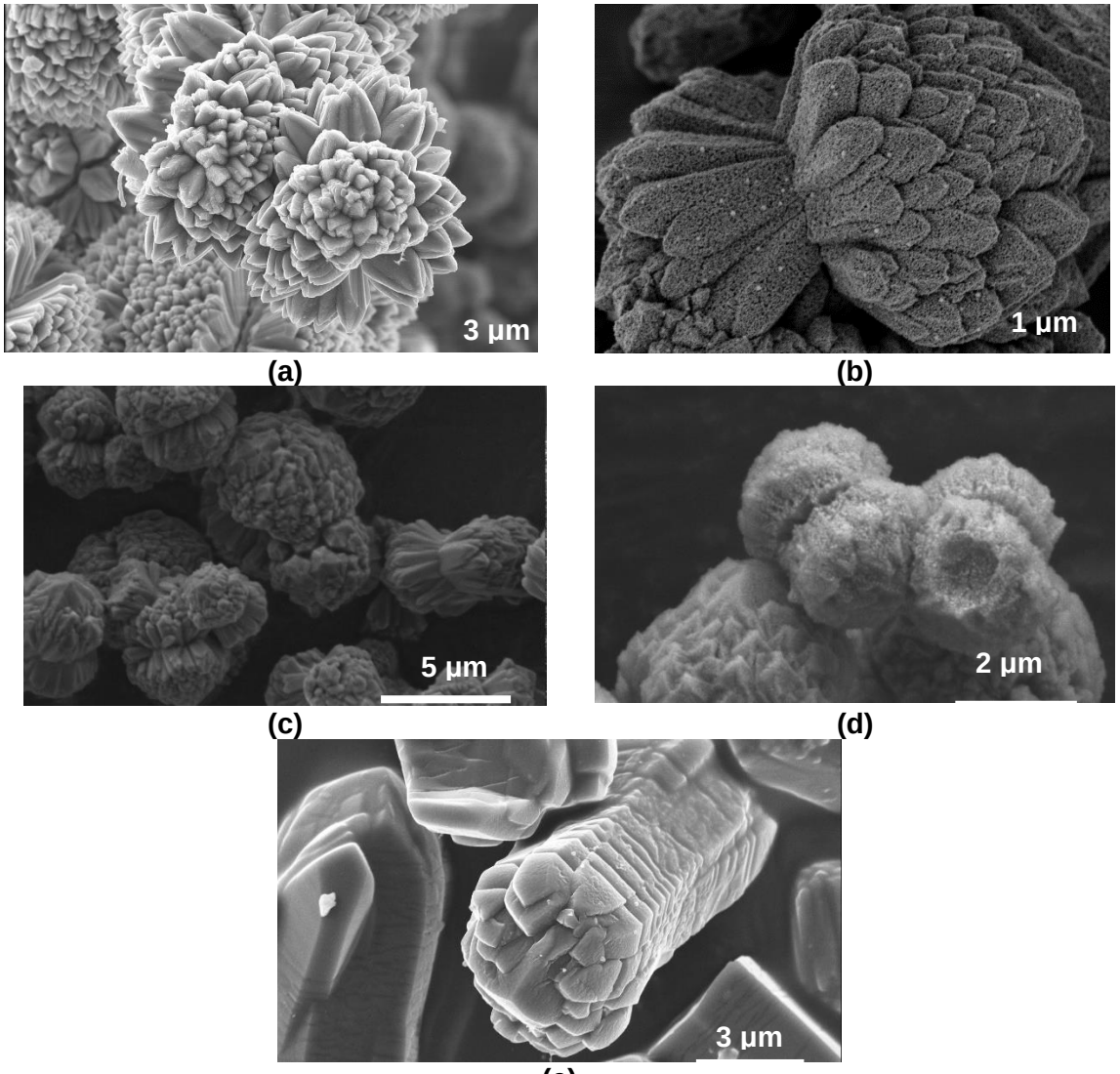

Figure 5. 1. SEM images of (**a**) Ni-MOF-24, (**b**) C-Ni-MOF-24, (**c)** Ni-MOF-1.5, (**d**) C-Ni-MOF-1.5, (**e**) Mg-MOF-24

The carbonized MOF compositions were evaluated by EDS (Figure 5. 2 and Figure 5. 3). The main components in Ni-MOF-24 are C (mass fraction of 53.3%) and Ni (mass fraction of 43.7%). This ratio is maintained by all of Ni-MOF samples. The main components in Mg-MOF-24 are C (mass fraction of 59%) and Mg (mass fraction of 41%). Also, present the distribution of a homogeneous component, as expected.

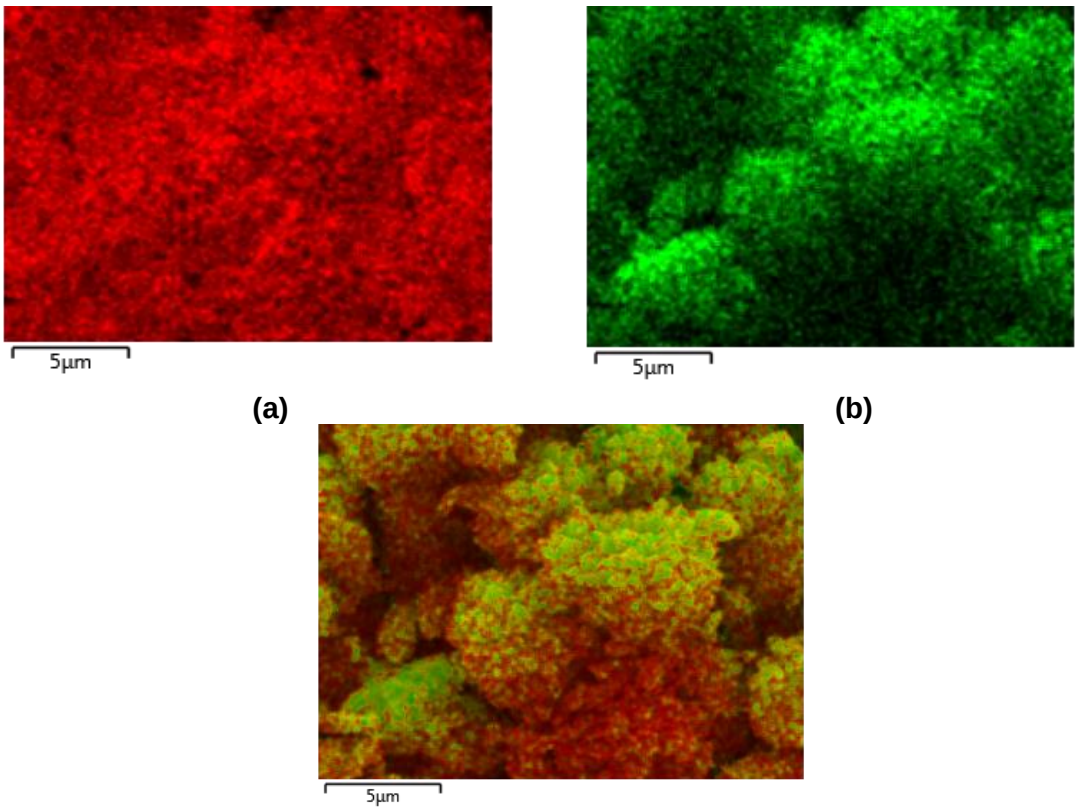

Figure 5. 2. EDS analysis for C-Ni-MOF-24 (**a**) Nickel distribution, (**b**) Carbon distribution, (**c**) Nickel and carbon distribution

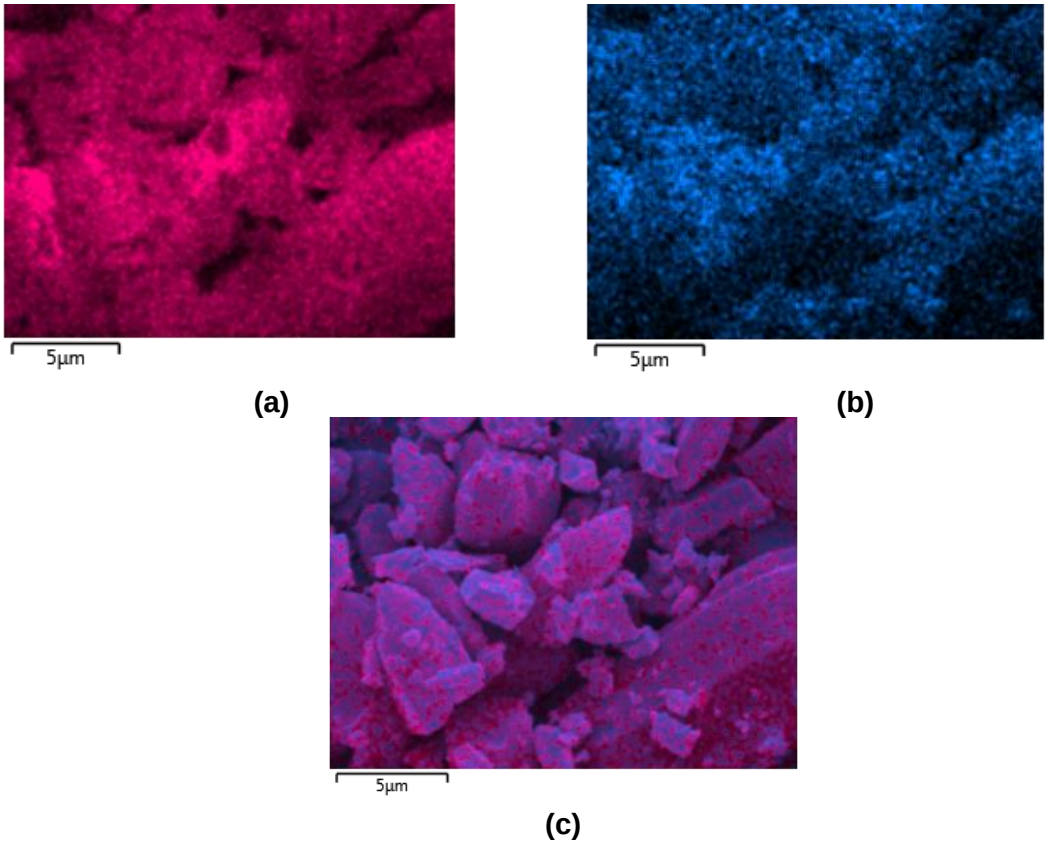

Figure 5. 3. EDS analysis for C-Mg-MOF-24 (**a**) Magnesium distribution, (**b**) Carbon distribution, (**c**) Magnesium and carbon distribution

Table 5. 2 presents the textural parameter for all materials synthesized. The Ni-MOF presents the largest surface areas (A_{BET}), which decrease considerably when the material is carbonized (77 % for Ni-MOF-24 and 92 % for Ni-MOF-1.5). Also, the porous structure change from micro to mesoporous (the increment is 84 % for C-Ni-MOF-24 and 90 % for C-Ni-MOF-1.5).

Comparing Mg-MOF-24 and Mg-MOF-1.5, the last one has a low porous volume. However, C-Mg-MOF-24 retains the same relationship between micro and mesoporosity.

Figure 5. 4 presents the CO_2 adsorption capacity at 0 °C and atmospheric pressure. The Mg-MOF-24 presents the best N_{ads} value (7.9 $mmol.g^{-1}$), which decreases 86 % for the same material obtains from the microwave process. Ni-MOF-24 presents the second-best N_{ads} value (6.44 mmol.g-1), and Ni-MOF-1.5 presents the third-best N_{ads} value (5.08

mmol.g-1). However, the N_{ads} decrease for Ni-MOF-24 and Ni-MOF-1.5 when these are carbonized (91 and 96 % respectively).

Table 5. 2. Parameters obtained from adsorption isotherms (N_2 at −196 °C and CO_2 at 0 °C) for MOF and C-MOF.

	A_{BET} ($m^2\,g^{-1}$)	$V_{0.95}$ ($cm^3\,g^{1}$)	$V_{mic\text{-}N2}$ ($cm^3\,g^{-1}$)	$V_{mic\text{-}CO2}$ ($cm^3\,g^{-1}$)	V_{mes} ($cm^3\,g^{-1}$)	L_0 (nm)	$E_{ads.CO2}$ (kJ mol^{-1})
Ni-MOF-24	831	0.33	0.30	0.32	0.01	0.1	41.0
Ni-MOF-1.5	847	0.34	0.32	0.33	0.02	0.7	27.9
C-Ni-MOF-24	232	0.35	0.10	0.34	0.25	1.5	15.7
C-Ni-MOF-1.5	66	0.23	0.03	0.01	0.2	0.9	23.0
Mg-MOF-24	923	0.34	0.12	0.5	0.12	0.4	40.4
Mg-MOF-1.5	135	0.09	0.05	0.07	0.04	0.6	30.6
C-Mg-MOF-24	275	0.32	0.16	0.33	0.15	1.5	16.0

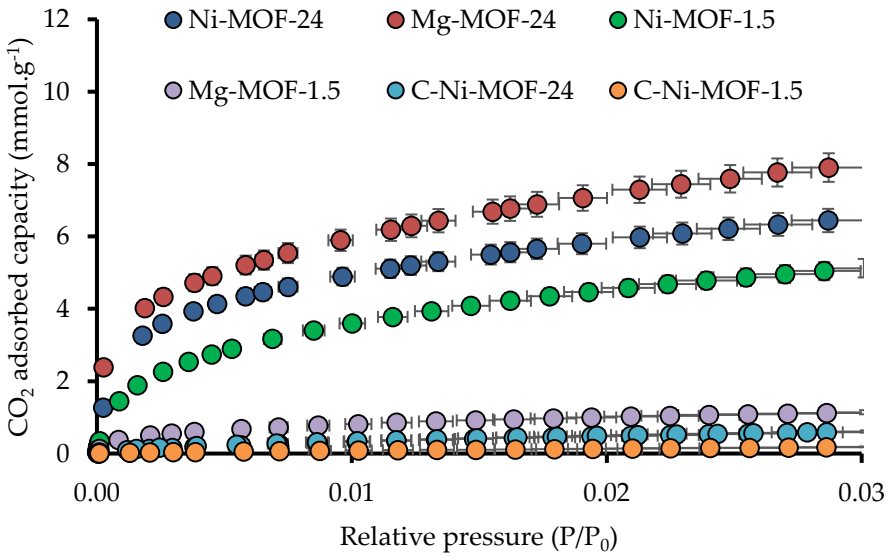

Figure 5. 4. CO_2 adsorption isotherms for MOF and C-MOF at 0 °C and atmospheric pressure.

The synthesis yield is 30 % to MOF from conventional or microwaves processes. For carbonized MOF is 34-36 %.

C-Ni-MOF-24 presents the best textural parameter, and particle size is similar to C-Ni-MOF-24, whereby it was impregnated in sandstone (Figure 4.4). After one year, the materials have the same stability, and no segregation is observed.

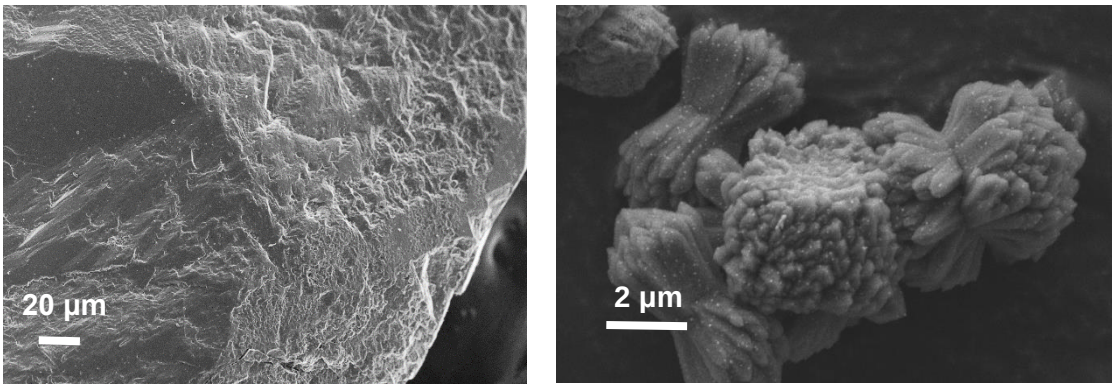

Figure 5. 5. SEM images of (**a**) sandstone and (**b**) sandstone impregnated with a mass fraction of 20% of C-Ni-MOF-24.

The sandstone presented an A_{BET} of 0.4 m^2 g^{-1}, and its CO_2 adsorption capacity could not be measured using conventional methods (< 0.0013 mmol g^{-1} at 0 °C and atmospheric pressure). From FTIR, sandstone is mainly composed of silica, which has an acidic character as the CO_2 molecule. Consequently, if the specific area of the sandstone is low, its CO_2 adsorption capacity is even lower than that which might be expected for this specific area.

After surface modification, the physical parameters are improved. This increase is mainly due to the contribution of the modifying material.

Table 5. 3. Parameters obtained from adsorption isotherms (N_2 at −196 °C and CO_2 at 0 °C) for sandstone impregnated with mass fractions of % of C-Ni-MOF-24

	A_{BET} ($m^2\ g^{-1}$)	$V_{0.95}$ ($cm^3\ g^1$)	$V_{mic\text{-}N2}$ ($cm^3\ g^{-1}$)	$V_{mic\text{-}CO2}$ ($cm^3\ g^{-1}$)	V_{mes} ($cm^3\ g^{-1}$)	L_0 (nm)	$E_{ads.CO2}$ (kJ mol^{-1})
SS-20	37.3	0.08	0.04	0.05	0.04	1.9	17.9
C-Ni-MOF-24	196	0.35	0.10	0.34	0.25	1.5	15.7

The possible synergistic behavior between C-Ni-MOF-24 and sandstone was evaluated employing the theoretical and experimental values of the CO_2 adsorption capacity are presented in Table 5. 4. Theoretical values were calculated by assuming a linear relationship and taking into account the CO_2 adsorption capacities and the percentages of each solid. From the thermogravimetric analysis, the real impregnation percentage is 22.3 %. The experimental N_{ads} value is higher than theoretical value (16.2 %), which could indicate a synergistic behavior or segregation of MOF during the impregnation process, and the nanoparticles may not be homogeneously distributed on the surface of the sandstone (the Nads difference is 0.043 $mmol.g^{-1}$).

Table 5. 4. The CO_2 adsorption capacity of sandstone at atmospheric pressure, 0°C, and a mass fraction of 20 % of C-Ni-MOF-24. Theoretical and experimental values.

	20%
Theoretical N_{ads} ($mmol.g^{-1}$)	0.119
Real Theoretical N_{ads} ($mmol.g^{-1}$)	0.133
Experimental N_{ads} ($mmol.g^{-1}$)	0.176
Relative difference (%)	32.2

Figure 5. 6 presents pH higher than 6 could be the best and feasible condition for impregnation at reservoir condition (water as aqueous media), due to the zeta potential was farther from zero, and there are fewer aggregates in the system, which benefits the greater distribution of the material in the porous medium.

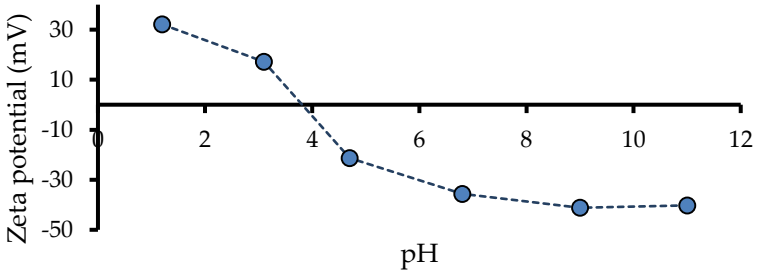

Figure 5. 6. Zeta potential for C-Ni-MOF-24

5.2.2. High-Pressure Adsorption Tests

5.2.2.1. Pure CO_2 Adsorption at High Pressure–Manometric Measurement Method

The e-CCS process requires evaluating the behavior of the materials at high pressure (up to 3 MPa) and the temperature of a hypothetical reservoir (50 °C). Figure 5.7 presents the absolute CO_2 adsorbed amount and the excess amount for Ni-MOF-24 and C-Ni-MOF-24 at 0, 25, and 50 °C. The difference between excess and absolute amounts appeared above 1 MPa and represented < 9 %. This difference was lower when the temperature increased. Such a trend is consistent with the fact that, at similar pressure, the density of the bulk phase decreases when the temperature increases. The high-pressure intrinsic CO_2 adsorption capacity of sandstone without impregnation had a negligible effect on the measurement.

At 50 °C, as expected, the adsorption capacity decreased by 26% due to the exothermic character of adsorption. The obtained adsorption capacity is competitive compared to other results reported for nanomaterials under similar conditions [1-3].

In this case, the carbonized MOF presents a higher CO_2 adsorption capacity at 0 and 25 °C (21 and 13 %, respectively). However, the CO_2 adsorption capacity at 50 °C is less (34 %). This behavior, may be related to the sensitivity of the conventional material, which may affect its structure (0 and 25 °C). At low pressure (< 1 MPa), there is more affinity in the Ni-MOF-24/CO_2 system (In this stage, adsorption for Ni-MOF-24 is higher than C-Ni-MOF-24).

After 1.5 and 2.0 MPa, the system shows the possible multilayer adsorption that occurs in high-pressure processes (adsorption for C-Ni-MOF-24 is higher than Ni-MOF-24).

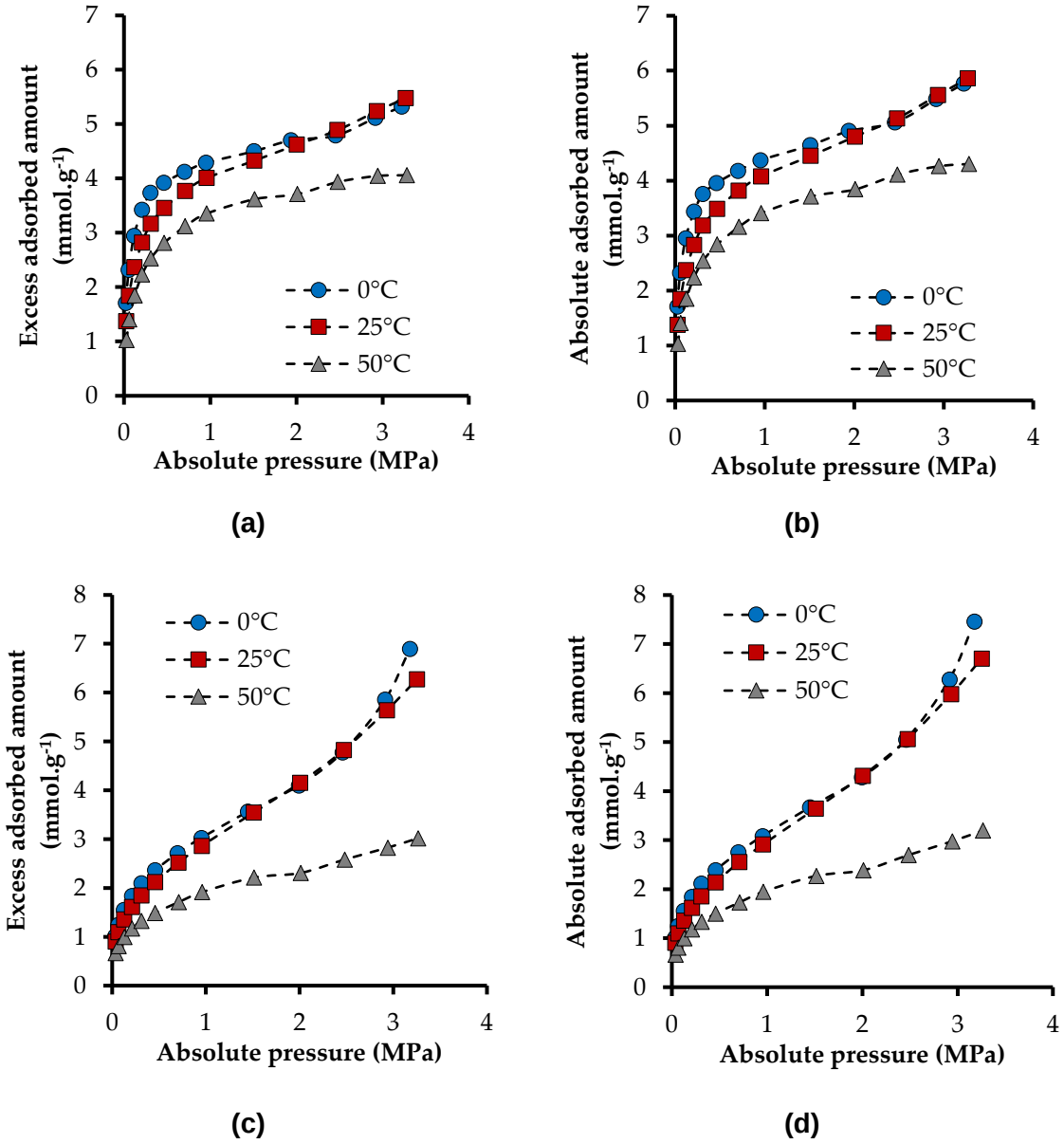

Figure 5. 7. Adsorption isotherms of CO_2 at high pressure (3×10^{-3} up to 3.0 MPa) of Ni-MOF-24 at (**a**) Excess N_{ads}, (**b**) Absolute N_{ads}; and C-Ni-MOF-24 at (**c**) Excess N_{ads} and (**d**) Absolute N_{ads}

As expected, the Toth and Sips models led to very good fits: $R^2 > 0.95$. The fit is better at the beginning of the isotherm for both materials (Figure 5. 8).

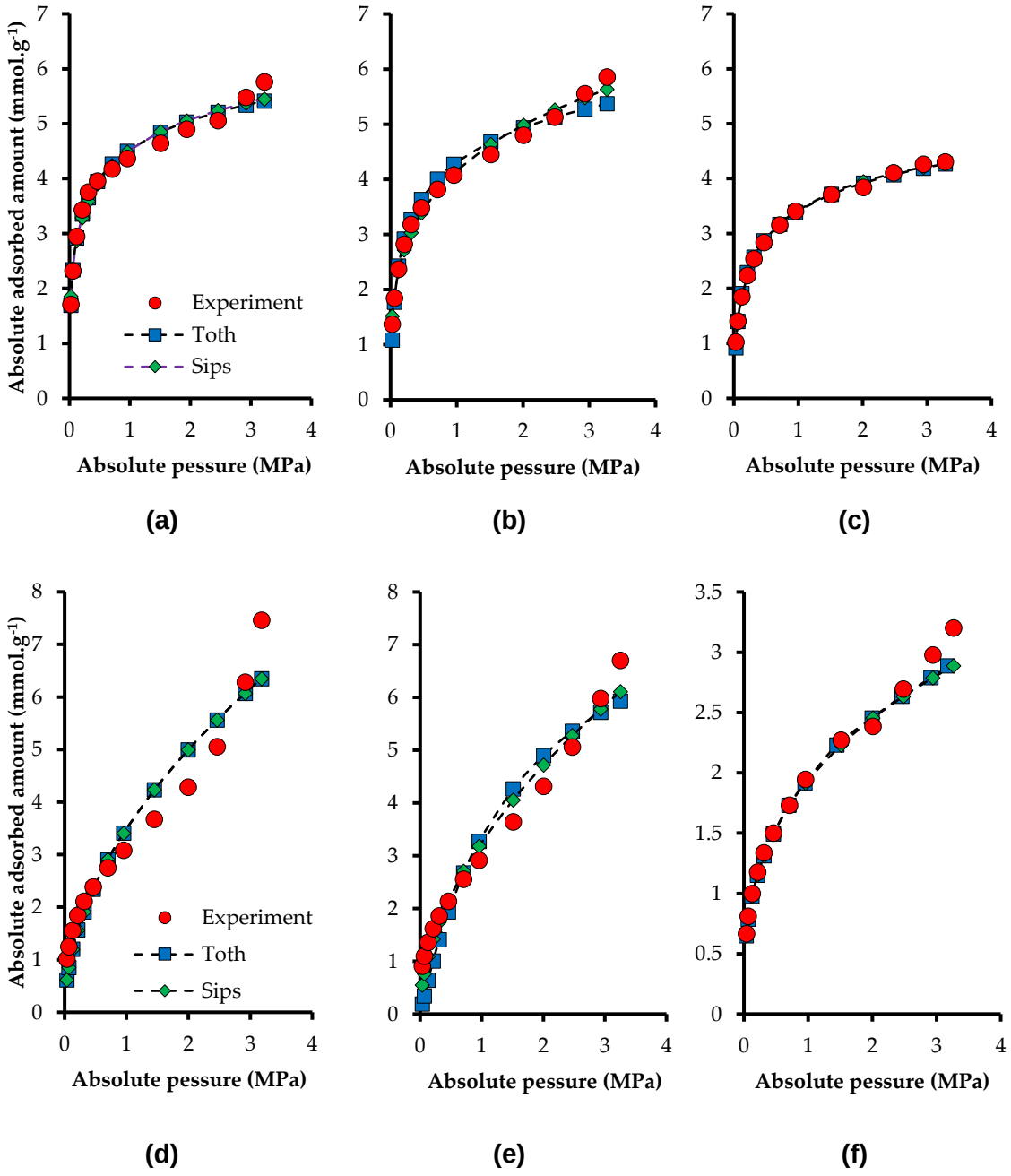

Figure 5. 8. Adsorption isotherms fitted by the Sips and Toth models for Ni-MOF-24 at (**a**) 0 °C, (**b**) 25 °C, and (**c**) 50 °C and C-NI-MOF-24 at (**a**) 0 °C, (**b**) 25 °C, and (**c**) 50 °C

Figure 5. 9 presents the isosteric heat of adsorption (Q_{st}) of Ni-MOF-24 and C-Ni-MOF-24. Ni-MOF-24 presents a Q_{st} slightly higher than C-Ni-MOF-24. This increase corresponds to

the first reaction stage, where Ni-MOF-24 presents a greater affinity in the adsorption isotherms. When there is a greater N_{ads} value, CO_2 interactions with the surface decrease. C-Ni-MOF-24 presents a greater decreasing, due to the greater N_{ads} value in that last stage (greater multilayer formation).

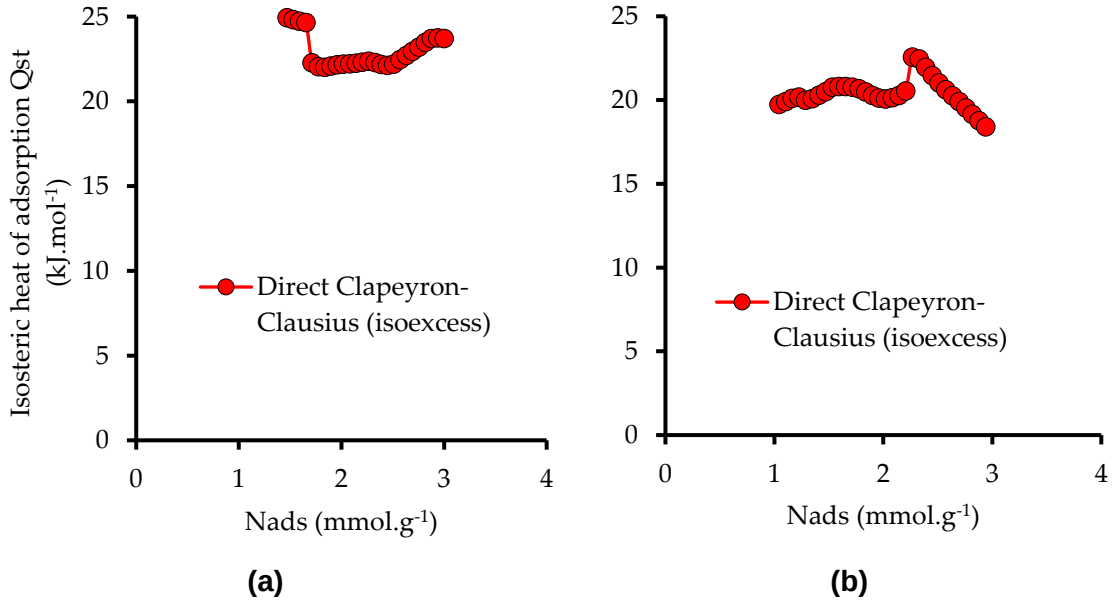

Figure 5. 9. Isosteric heat of adsorption of C-Ni-MOF-24 and sandstone impregnated with mass fractions of 10 and 20%, as a function of the adsorbed CO_2 amount expressed: (**a**) in mmol per total amount of adsorbent material (sandstone and CN.LYS2) and (**b**) in mmol per amount of carbon adsorbent material.

5.2.2.2. CO_2 and N_2 Adsorption at High Pressure–Gravimetric Measurement Method

Using the PyIAST application and using the pure-components adsorption isotherms obtained by experimental tests, it is possible to characterize the behavior of each component and to predict the adsorbed amount of each component present in a mixture [56]. It is, thus, possible to obtain the adsorbed amount at a constant temperature by varying the concentration of the components (at constant pressure) or the pressure (at constant concentrations). Initially, it is necessary to use the "isothermal interpolator" to generate data points that follow a given isothermal model, avoiding the search for an appropriate analytical model and examining the quality of its fit to the data (i.e., Langmuir, Freundlich or Toth,

among others) [7]. An isothermal interpolator is a tool included in the PyIAST package. After that, PyIAST takes the interpolated data for its calculations. Calculations are done using a predesigned routine [7].

In the present case, the experimental data of each pure component (CO_2 and N_2) were obtained by HP-TGA at 50 °C, between 0.1 and 2.5 MPa, and with a flow of CO_2 or N_2 (50 mL min^{-1} up to 1.0 MPa and 70 mL min^{-1} up to 2.5 MPa). The prediction was calculated at 50 °C by varying: 1) the system pressure from 0.1 to 2.5 MPa at a constant CO_2 concentration of 20%, and 2) the concentration of CO_2, from 5 to 100% at a constant pressure of 2.5 MPa.

The evaluated materials were sandstone from a real Colombian reservoir (RS) impregnated with a mass fraction of 20% of C-Ni-MOF-24. It is important to mention that it might be possible to obtain considerable adsorbed quantities for a cleaning and adsorption balance of more than 12–24 hours because the nanomaterials (main adsorbent) are microporous. A longer cleaning time thus allows eliminating adsorbed gases and moisture. In the same way, an adequate equilibrium time allows for greater diffusion of the gas into the porous structure and greater interactions with the material, which would allow a higher adsorbed amount. Therefore, to analyze the selectivity, a shorter time was used (cleaning and adsorption equilibrium time of 2 hours at each pressure).

It was not possible to obtain the CO_2 isotherm for RS because the latter had a too low surface area, so the maximum value for RS at 50 °C and 2.5 MPa was 0.033 mmol g^{-1}. For RS, the adsorbed amount of N_2 was 3.19 mmol g^{-1} at 50 °C and 2.5 MPa. Figure 5.10-a,b presents the CO_2 and N_2 adsorption isotherms under continuous gas flow for RS-20. The increment factor of N_{ads} for RS-20 with respect to RS was 16 (0.57 mmol g^{-1} at 50 °C and 2.5 MPa). Also, the theoretical value of N_{ads} for RS with a mass fraction of 20% of C-Ni-MOF-24 was 0.63 mmol g^{-1}, but the experimental value was 0.57 mmol g^{-1} (i.e., 90% of the theoretical one).

Figure 5. 10-c presents the simulated adsorbed amount for an N_2/CO_2 mixture at a constant CO_2 concentration of 20% and 50 °C by varying the pressure for RS-20. The affinity for CO_2 was considerable (P < 1 MPa), but the N_{ads} for N_2 is superior (54 %) to that for CO_2. When

the system operates at CO2 concentration > 40 %, the N_{ads} for CO_2 is superior (Figure 5. 10-d).

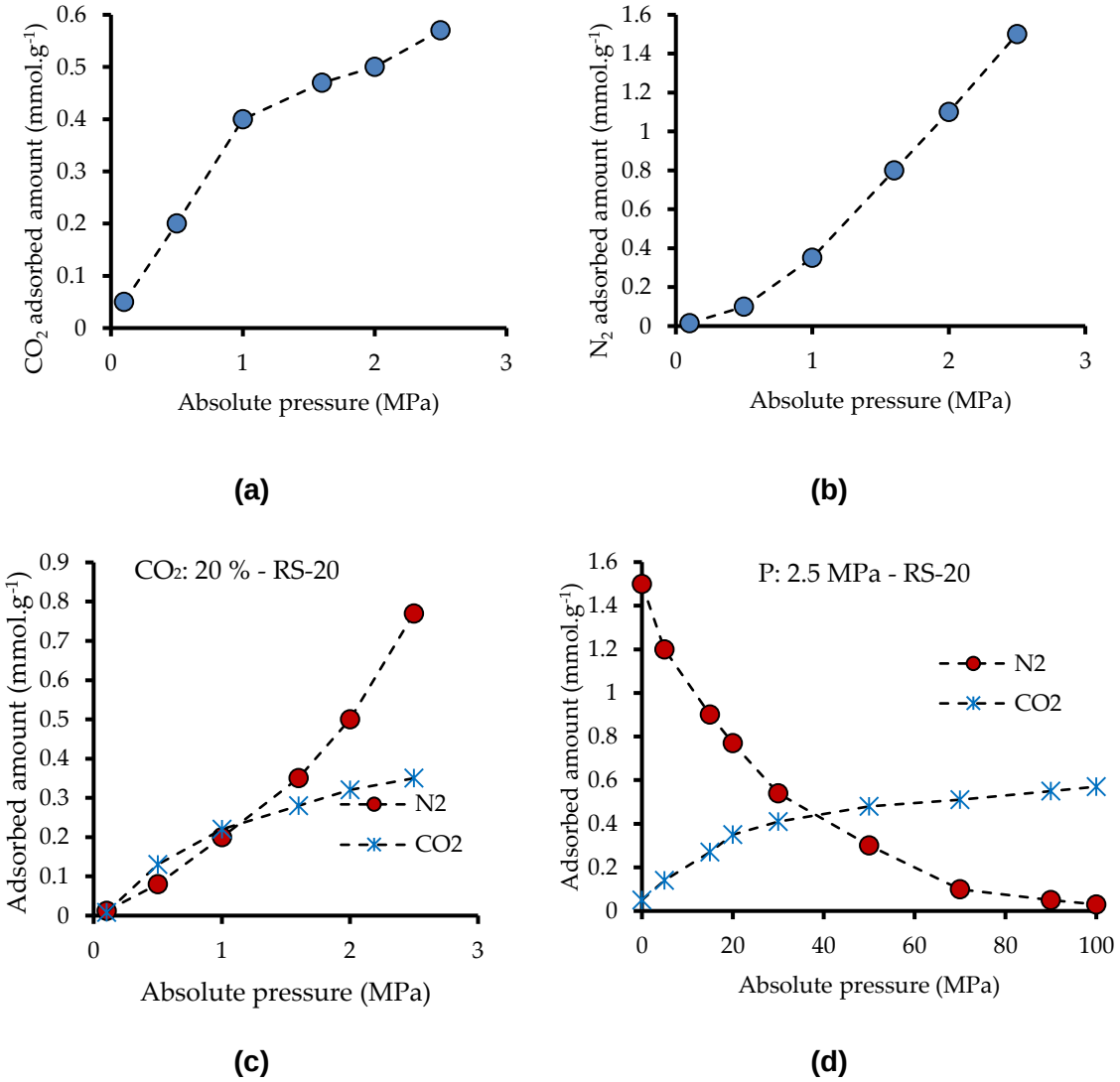

Figure 5. 10. Adsorption isotherm of SS-20 (surface modification at a mass fraction of 20% of C-Ni-MOF-24) at 50 °C between 0.1 and 2.5 MPa for (**a**) pure CO_2 and (**b**) pure N_2. Adsorption isotherm simulating an N_2/CO_2 mixture at 50 °C (**c**) constant CO_2 concentration (20%) and varying the pressure and (**d**) varying the CO_2 concentration at a constant pressure of 2.5 MPa

From Figure 14, it can be concluded that PyIAST is a useful tool because it is possible to simulate the behavior of adsorption systems from some pure gas adsorption data.

At reservoir conditions, it is possible to increase N_{ads} in 43746% (Ottawa sandstone) and 1627 % for Colombian sandstone from the oilfield.

5.3. Partial conclusions

Metal-organic frameworks-MOFs allowed increasing the adsorption capacity under realistic reservoir conditions (50 °C and 3 MPa). This increase was possible thanks to the higher surface area and to the favorable chemical composition, which promoted the capture and storage of CO_2. These materials had competitive CO_2 capture performances compared to other special materials reported in the literature, but their stability must be evaluated. Therefore, this research opens an interesting line of research that would expand knowledge in the field of specific materials for geological applications.

5.4. References

[1] J. Wang, L. Huang, R. Yang, Z. Zhang, J. Wu, Y. Gao*, et al.*, "Recent advances in solid sorbents for CO 2 capture and new development trends," *Energy & Environmental Science,* vol. 7, pp. 3478-3518, 2014.

[2] X. Wu, Z. Bao, B. Yuan, J. Wang, Y. Sun, H. Luo*, et al.*, "Microwave synthesis and characterization of MOF-74 (M= Ni, Mg) for gas separation," *Microporous and Mesoporous Materials,* vol. 180, pp. 114-122, 2013.

[3] J. An and N. L. Rosi, "Tuning MOF CO2 adsorption properties via cation exchange," *Journal of the American Chemical Society,* vol. 132, pp. 5578-5579, 2010.

[4] Z. Bao, S. Alnemrat, L. Yu, I. Vasiliev, Q. Ren, X. Lu*, et al.*, "Adsorption of ethane, ethylene, propane, and propylene on a magnesium-based metal–organic framework," *Langmuir,* vol. 27, pp. 13554-13562, 2011.

[5] B. Chen, Z. Yang, G. Ma, D. Kong, W. Xiong, J. Wang*, et al.*, "Heteroatom-doped porous carbons with enhanced carbon dioxide uptake and excellent methylene blue adsorption capacities," *Microporous and Mesoporous Materials,* vol. 257, pp. 1-8, 2018.

[6] M. Franco-Aguirre, R. D. Zabala, S. H. Lopera, C. A. Franco, and F. B. Cortés, "Interaction of anionic surfactant-nanoparticles for gas-Wettability alteration of

sandstone in tight gas-condensate reservoirs," *Journal of Natural Gas Science and Engineering,* vol. 51, pp. 53-64, 2018.

[7] C. M. Simon, B. Smit, and M. Haranczyk, "pyIAST: Ideal adsorbed solution theory (IAST) Python package," *Computer Physics Communications,* vol. 200, pp. 364-380, 2016.


LIBERTAD
Y
ORDEN
INTER · AULAS · ACADEMIÆ · QUÆRE · VERUM


UNIVERSITAS · GRANATENSIS
PLUS
ULTRA
1531

6. Carbon molecular nanosieves from biomass residues applied to e-CCS process

This chapter presents the evaluation of commercial sugar and cane molasses as carbon precursors in the synthesis of carbon nano/micromaterials. The objective of using these resources comes from their availability, low cost, and high carbohydrate content [1, 2]. Also, cane molasse is a byproduct of the sugar refinery industry [3].

Colombia has a history of violence and is related to significant social problems, as more than a million and a half people displaced, more than a thousand massacres, among others. Agriculture is an integral part of the Colombian economy, and it is developed in rural areas that have been vulnerable to violent conflict. There are large producers of cane, rice, corn, fruits, among other products, but several production chains have problems, some of them related to waste management. Organic waster or biomass, in some cases, represents social, health, and environmental problems. Nevertheless, these organic residues have the potential to be used for carbon micro/nanomaterials production, especially those that have high carbohydrates content [1, 2, 4], which could become an important economic line that promotes the economic development of the vulnerable regions and solve socio-environmental problems related to by-products.

International Sugar Organization estimates about 110 countries produce sugar, world sugar consumption is 172.441 Mt, and worldwide sugar production from cane is nearly 80% of global sugar production. In general, 100 tonnes of sugar cane will yield 10-11 tonnes of sugar and 3-4 tonnes of molasses [3].

Both precursors were used directly in the synthesis by hydrothermal route, subsequently characterized and evaluated in the CO_2 adsorption process at standard and high-pressure conditions. As the main novelty, carbon nano/microspheres obtained from cane molasses

behave like molecular sieves. This behavior allows a natural selectivity to CO_2 in mixtures of CO_2/N_2, under different pressure and temperature conditions.

6.1. Materials and Methods

Two different carbon nanostructures were synthesized using the hydrothermal method and latex template to obtain “hollow” spheres, initially in order to fill the interior space with amines and improve CO_2 selectivity. The nanostructures were labeled and synthesized as follows:

-***CN.SUG:*** Carbon micro/nanospheres obtained from a hydrothermal method, using commercial sugar as a carbon precursor.

-***CN.RON:*** Carbon micro/nanostructures obtained from a hydrothermal method, using cane molasses as a carbon precursor.

The latex template was synthesized in house. This material was selected as the template due latex is composed of carbon molecules, which are not completely removed from the nucleus after carbonization at 500°C, obtaining a different internal structure.

Both CN.SUG and CN.RON were characterized in order to select the best material, considering the smallest size, adsorption capacity, lower technical and economic cost.

5.1.1. Materials and Reagents

The used sugar is a typical white commercial sugar, Spanish trademark “Azucarera”. The composition sugar is mainly sucrose, which is a disaccharide formed by a glucose molecule and one of fructose. Cane molasses consist mainly of water, carbohydrates, protein, and fiber. Molasses is an agricultural product, whence it is hard to establish its exact composition. Climatic factors, soil structure, and processing conditions in the cane mill influence the final quality. Molasse was obtained from "El granjero integral" Spanish company. The molasse composition is presented in Table 6. 1.

Table 6. 1. Composition cane molasses (Dry base). “El granjero integral” Spanish company.

Component	Mass percentage (%)
Carbohydrates	71.1 (sugar 56.1%)
Protein	4
Fiber	7
Na	0.5
Ca	0.6
Mg	0.3
F	0.1

For synthesis, cleaning, drying, and carbonization, the following chemicals were used: Styrene (97%), acetoacetoxyethyl methacrylate (97%), sodium peroxydisulfate (97%), acetone (99.9%), ethanol (99.5%), and N_2 (high purity, grade 5.0).

Ottawa sandstone was used as a porous medium and was impregnated with the best nanomaterial at a mass fraction of 10 and 20%. The performance of the materials was evaluated by CO_2 adsorption at two different situations: 1) Atmospheric pressure and 25 and 50 °C, and 2) Varying pressure (up to 2.5 MPa) and 25 and 50°C. The detailed procedures are presented below.

6.1.2. Synthesis of Nanomaterials

6.1.2.1. Synthesis of carbon nanospheres

The process was adapted from White et al. [1], using a latex template (Synthesized "in house") and defining particular concentrations of reagents. The mass ratio H_2O/carbon precursor is 1800:1, and the mass ratio latex/carbon precursor is 1:10. The latex nanoparticles are put in water with a 0.05 ml of Span 60 in order to disperse hydrophobic particles in the aqueous medium, at 25 °C for 4 h and 200 rpm. After that, the carbon precursor is added to the system for 30 min. This solution was put in a stainless-steel

autoclave (Techinstro, Nagpur, India) with a capacity of 200 mL and introduced into an oven (Thermo Fisher Scientific, Massachusetts, USA) at 180 °C for 24 h. After the reaction, the carbon gels are filtered and washed with excess deionized H_2O. Later, gels are washed with acetone for 3 days, in order to exchange water molecules and preserve the porous structure during carbonization. Finally, the obtained polymer was dried at 120 °C for 12 h and carbonized under N_2 flowing at 60 mL min^{-1} and 500 °C for 6 hours, using a tubular furnace (Thermo Fisher Scientific, Massachusetts, USA). CN.SUG1 and CN.RON1 are obtained. After that, the concentrations are diluted at mass ratio (H_2O/carbon precursor) of 3600:1 in order to obtained smaller particle sizes. Following the same synthesis procedure, CN.SUG2 and CN.RON2 are obtained.

6.1.2.2. Synthesis of latex nanotemplates

The process was carried out following the Agrawal et al. method [5]. For this, 85 g of water, 9.5 g of styrene, and 0.5 g of acetoacetoxyethyl methacrylate were charged into a double-wall glass reactor equipped with a reflux condenser, mechanical stirrer, temperature controller, and nitrogen inlet. After bubbling the nitrogen gas through the reaction media for 30 min, the reaction temperature was increased to 70 °C, and aqueous sodium peroxydisulfate solution (0.15 g in 5 g of water) was added to start the polymerization process. The reaction was carried out at 70 °C for 24 h, and polystyrene spheres were collected and dried at a dynamic vacuum.

6.1.3. Impregnation of Sandstones

The sandstone was impregnated to decorate the rock surface with CN.RON2 and improve the surface area and molecular interactions. Ottawa sandstone (SS) was impregnated with CN.RON2 at mass fractions of 10 and 20% by immersion and soaking [50]. Initially, a fluid composed of carbon material and deionized water was sonicated at 40 °C for 4 h. Subsequently, the SS was introduced in the nanofluid at 60 °C for 24 h without stirring. Finally, the impregnated material was dried at 110 °C for 12 h. The impregnation method mimics the reservoir conditions in which the porous medium might be impregnated

6.1.4. Characterization of the Nanomaterials

The following procedures allowed characterizing the physicochemical characteristics of the materials, essential for a good understanding of the results. For the e-CCS application, nanoparticles must have a possible smallest size, a spherical shape, a high surface area.

6.1.4.1. Size and Structure of Nanomaterials

Different techniques were used to evaluate the particle size distribution: scanning electron microscopy (SEM) was used to obtain the dry particle size, size distribution, and morphology of CN.SUG and CN.RON. The observations were carried out by means of a JSM-7100 emission electron microscope (JEOL, Nieuw-Vennep, The Netherlands), a GEMINI-LEO1530 VP FE-SEM emission electron microscope (Carl Zeiss, Cambridge, UK).

Dynamic light scattering (DLS) was carried out by means of a NanoPlus-3 zeta/nanoparticle analyzer (Micromeritics, Norcross, USA) at 25 °C in a glass cell (capacity of 0.9 mL), which was used to obtain the mean particle size of nanoparticles dispersed in a fluid, which hydrate and interact with each other. The mean particle size was calculated from the diffusional properties of the particle, indicating the size of the hydrated and solvated particle. For this purpose, a nanoparticle solution, 10 mg L^{-1}, was dispersed in water or ethanol and sonicated for 6 h before analysis. Particles suspended in a liquid have a Brownian motion due to the random collisions with solvent molecules. This motion causes the particles to diffuse through the medium. The diffusion coefficient, D, is inversely proportional to the particle size or hydrodynamic diameter, d, according to the Stokes-Einstein equation:

$$D = \frac{k_B T}{3 \pi \eta d} \quad \textbf{(6.1)}$$

where k_B is Boltzmann's constant, T is the absolute temperature, and η is the viscosity.

6.1.4.2. Porous Structure of Nanomaterials and Sandstone

Materials were characterized by N_2 and CO_2 adsorption at −196 °C and 0 °C, respectively, using 3-Flex manometric adsorption equipment (Micromeritics, Norcross, USA). The total adsorbed volume ($V_{0.95}$) was taken as the physisorbed volume of N_2 at a relative pressure $P/P_0 = 0.95$. The Brunauer–Emmett–Teller (BET) model was applied to obtain the BET area

(A_{BET}). Micropore volume (V_{mic}), average pore size (L_0), and CO_2 adsorption energy ($E_{ads-CO2}$) were obtained by application of the Dubinin–Radushkevich equation. The mesopore volume (V_{meso}) was obtained through the Barrett–Joyner–Halenda (BJH) model.

6.1.4.3. Chemical Composition of Nanomaterials and Sandstone

The chemical characterization was carried out by carbon, hydrogen, oxygen, and nitrogen (CHON) analysis for nano/micromaterials, and by Fourier transform infrared spectroscopy (FTIR) for sandstone. An IRAffinity-1S FTIR spectrometer (Shimadzu, Columbia, USA) was operated at room temperature using potassium bromide in a KBr-to-material ratio of 30:1 (% w/w). The impregnation percentages of nanoparticles on sandstone were corroborated by thermogravimetric analysis (TGA) (TA Instruments, New Castle, USA). For this, the sample was burned under an air atmosphere at 10 °C min^{-1} up to 800 °C.

6.1.4.4. Dispersion of Nanoparticles in Solution

The electrophoretic light scattering (ELS) technique was used to evaluate the surface charge of the particles and their dispersion stability at 25 °C in a NanoPlus-3 zeta/nanoparticle analyzer (Micromeritics, Norcross, USA). In this test, several nanoparticle suspensions were prepared at 10 mg L^{-1}, with a pH adjusted between 2 to 12 by adding solutions of 0.1 mol L^{-1} HCl or 0.01 mol L^{-1} NaOH and then subjected to analysis. The zeta potential was calculated using the Smoluchowski equation, derived from the calculation of the Doppler effect.

$$\zeta = \eta U / \varepsilon \quad \textbf{(6.2)}$$

$$U = \frac{V}{E} \quad \textbf{(6.3)}$$

$$\Delta\nu = 2V\, n \sin\left(\frac{\theta}{2}\right) / \lambda \quad \textbf{(6.4)}$$

where ζ is the zeta potential, η is the viscosity of the fluid (water), U is the electrophoretic mobility, ε is the permittivity, V represents the speed of movement of the particles, E is the electric field, $\Delta\nu$ is the Doppler effect, n is the index of refraction, θ is the angle of detection, and λ is the wavelength of the incident light.

6.1.5. Adsorption Tests

The CN.RON2, sandstone, and impregnated sandstone (with a mass fraction of 10 and 20% of CN.RON2) were evaluated at 25 and 50 °C and high pressure from 0.03 to 2.5 MPa for CO_2 and N_2.

The adsorption tests were carried out using a HP TGA 750 thermogravimetric analyzer (TA Instruments, New Castle, USA). This device was equipped with a magnetic levitation top-loading balance, which made it possible to achieve high accuracy and reduce the volume of the system. The amount of each material put inside the sample holder was around 15 mg for nanoparticles, 40 mg for sandstone, and impregnated sandstone, to have enough total surface area for adsorption. The contribution of the buoyancy effect was manually subtracted from the data using blank tests carried out in the same conditions but with an empty sample holder.

The isotherms were fitted with the Sips and Toth models, which take into account multilayer adsorption. Table 6. 2 presents the equations for each model [53–55]. K_S and K_T represent adsorption equilibrium constants for the Sips and Toth models, respectively, and the *n* and *t* parameters indicate the heterogeneity of the system for the Sips and Toth models, respectively. The heterogeneity may originate from the solid structure, from the solid energy properties, or the adsorbate [54]. The *n* or *t* parameters are usually higher than unity, and when they are the unit, the models assume the Langmuir equation [54].

Table 6. 2. Models for adsorption isotherms.

Model	Equations	Parameters
Sips	$N_{ads} = N_m \frac{(K_S P)^{1/n}}{1+(K_S P)^{1/n}}$ **(6.5)**	N_{ads} (mmol g^{-1}) is the adsorbed amount, N_m (mmol g^{-1}) is the adsorption capacity at equilibrium, *P* (kPa) is the equilibrium pressure, and K_S and *n* are the Sips adsorption equilibrium constants, related to the affinity and the heterogeneity of the system, respectively.

Toth	$N_{ads} = N_m \frac{K_T P}{(1+(K_T P)^t)^{1/t}}$	**(6.6)**	N_{ads}, N_m, and P have the same meaning as above, and K_T and t are the Toth adsorption equilibrium constants, related to the affinity and the heterogeneity of the system, respectively.

6.2. Results and Discussion

The results are divided into two main sections: a) materials characteristics and b) study of the interaction between CO_2/nanomaterials/sandstone by adsorption isotherms under different operation conditions (T, P).

6.2.1. Materials Characteristics

The morphology and size distribution of the carbon materials obtained from sugar and molasses at a mass ratio of H_2O/carbon precursor of 1800:1, is presented in Figure 6. 1. CN.SUG1 is composed of broken spheres (Figure 6.1-a,c). It is possibly due to the low release rate of vapors present within the structure during the carbonation process. These vapors reach internal pressures higher than the material can withstand, breaking the structure. Also, the initial formation of hollow nanoparticles can be observed. CN.RON1 is composed of nanospheres, but other carbon structures may be related to the other original components of molasses (Figure 6.1-b,d). Due to the growth of the CN.RON1 particles, a hollow structure is not observed. The latex template is presented in Figure 6.1-e. It can be observed nanospheres of size homogeneously distributed, but with a bit of aggregation between particles. For this reason and taking into account its hydrophobic character, the use of surfactant was necessary.

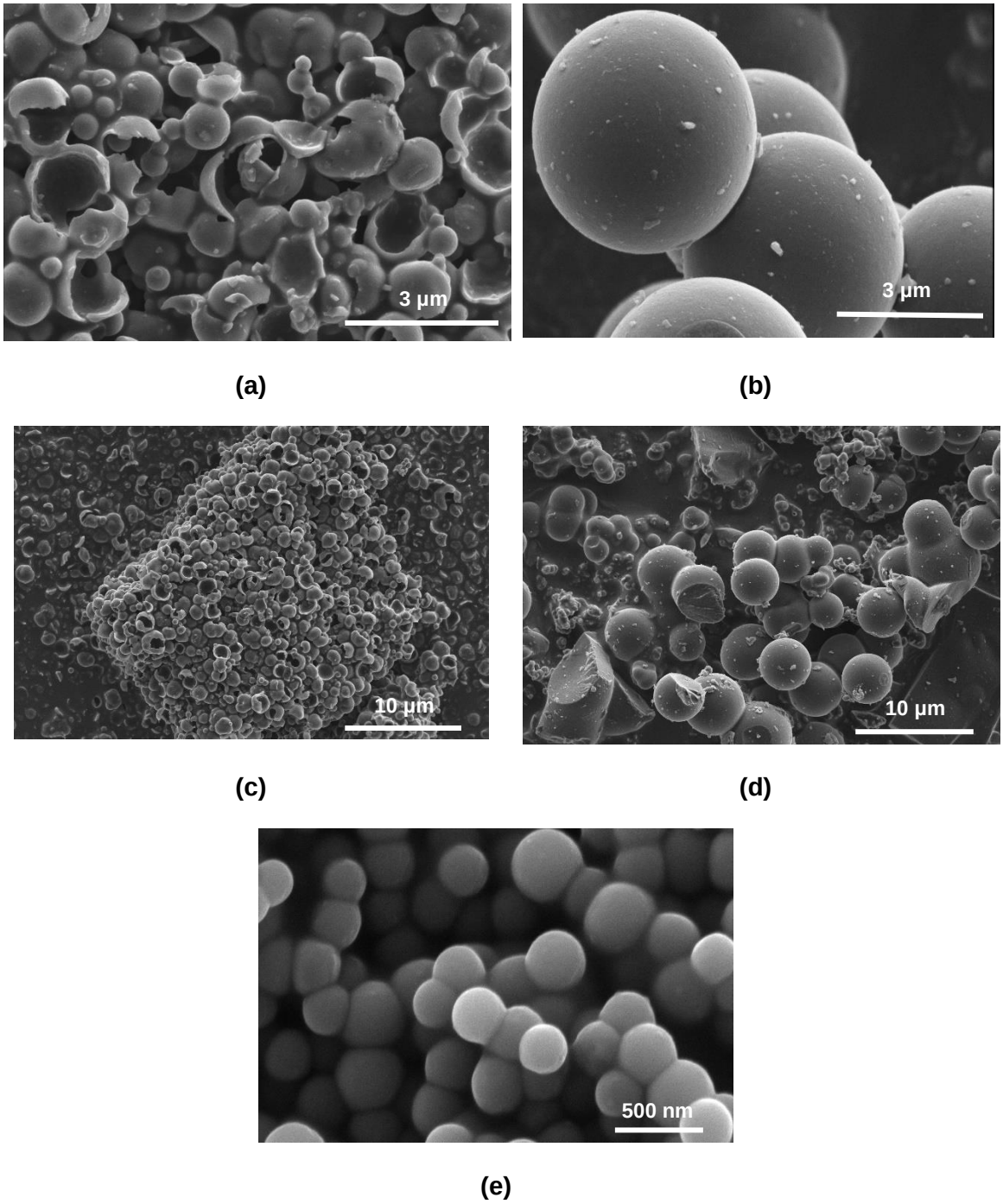

Figure 6. 1. SEM images at 5 kV of carbon nanospheres at mass relation of water/carbon precursor 1800:1: (**a**) and (**c**) CN.SUG1 and (**b**) and (**d**) CN.RON1. (**e**) Latex nanoparticles (Template).

In order to reduce the particle size, a second synthesis process was performed with a mass ratio of H_2O/carbon precursor of 3600:1. The size was analyzed using dynamic light scattering (DLS) to analyze the behavior of the nanoparticles in an aqueous medium. Table 6. 3 presents the mean particle size of materials, and Figure 6. 2 presents their zeta potentials. According to the Stokes-Einstein equation, the diffusion coefficient is inversely proportional to particle size or hydrodynamic diameter; therefore, it is possible to analyze whether the nanoparticles could interact to form aggregates.

The hydrodynamic diameter was calculated for nanoparticles in water (at pH 5.8) and ethanol (at pH 7). The aggregate size was less in ethanol (Table 6. 3) because the pH affects the behavior in solution (Figure 6. 2), and there is less interfacial tension in the system with ethanol. For an industrial application and injection into the porous medium, the most economical way is a suspension in water.

Precipitation is only possible if the aggregates are big enough, which happens for CN.SUG1 and CN.RON1, which have a considerable particle size (Figure 6. 1) and in an aqueous medium (at pH between 5 and 7) tend to add. Hence, the hydrodynamic diameter of CN.SUG1 was higher than the limit of detection of the equipment (10 µm). For CN.RON1 the measurement was unstable, possibly due mixing of dispersed particles and aggregates that exceed the size limit for the detection. The hydrodynamic diameter was less for CN.SUG2 and CN.RON2. In the case of CN.RON2, the particle size could be less than 100 nm because the aqueous system is, and here it hydrates and interacts with other particles, which is shown in Figure 6. 3-b.

Table 6. 3. Mean particle size of nanomaterials in suspension

Material	d_p 50 (nm) in water (pH 5.8)	d_p 50 (nm) in ethanol (pH 7)
CN.SUG1	-	-
CN.SUG2	967.3	789.5
CN.RON1	-	3650-8750
CN.RON2	256.2	143.2

On the other hand, if zeta potential is high (negative or positive), the particles are stable due to the high electrostatic repulsion between them. On the contrary, a low zeta potential (approaching zero) increases the probability of particles colliding, and thus forming aggregates. For CN.RON2, a pH higher or lower than 6 could be better for rocks impregnation because the zeta potential was farther from zero.

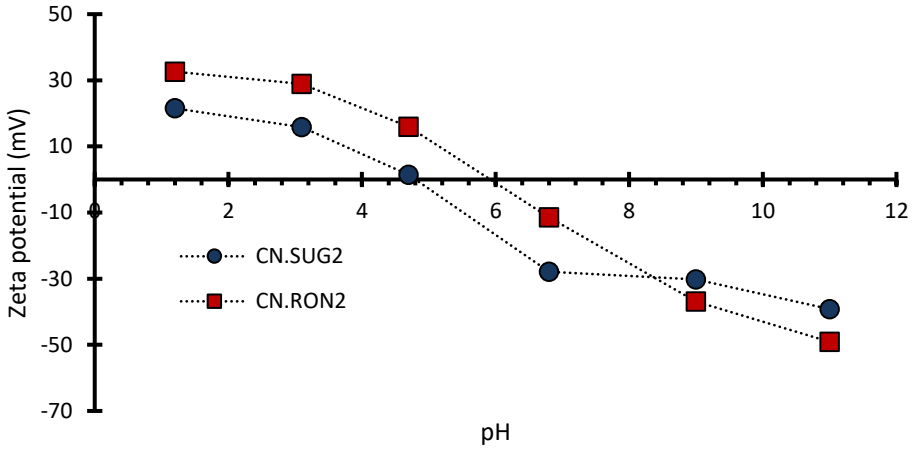

Figure 6. 2. Zeta potential for carbon nanoparticles synthesized with sugar and molasses at mass ratio H_2O/carbon precursor of 3600:1.

The impregnation process allowed to obtain a surface with a homogeneous nanoparticle distribution (Figure 6. 3).

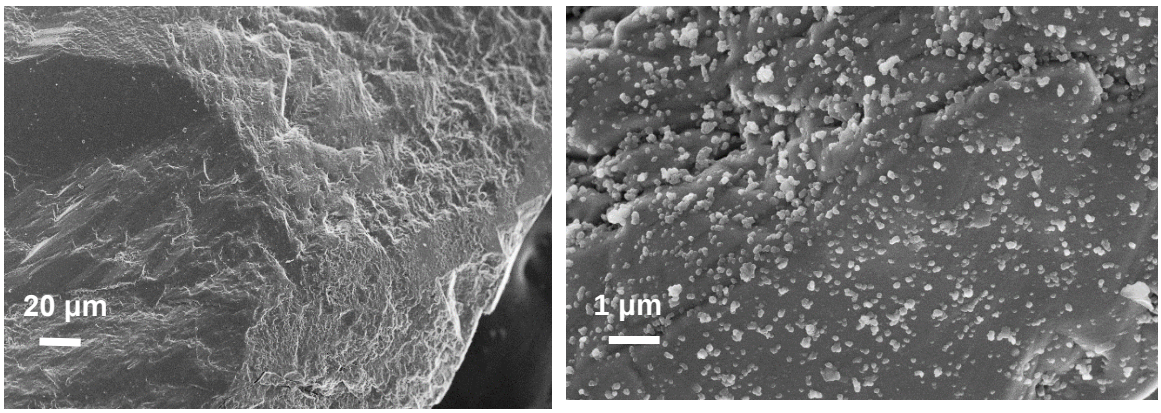

(a) **(b)**

Figure 6. 3. SEM images of (**a**) sandstone and (**b**) sandstone impregnated with a mass fraction of 20% (CN.RON2).

The adsorption and desorption isotherms (N_2 at −196 °C and CO_2 at 0 °C) for nanomaterials synthesized at a mass ratio of 3600:1 are presented in Figure 6. 4, and the textural parameters obtained from adsorption isotherms are presented in Table 6. 4.

Table 6. 4. Parameters obtained from adsorption isotherms (N_2 at −196 °C and CO_2 at 0 °C) for nanomaterials synthesized at a mass ratio of 3600:1 (CN.SUG2 and CN.RON2).

	A_{BET} ($m^2\ g^{-1}$)	$V_{0.95}$ ($cm^3\ g^{-1}$)	$V_{mic\text{-}N2}$ ($cm^3\ g^{-1}$)	$V_{mic\text{-}CO2}$ ($cm^3\ g^{-1}$)	V_{mes} ($cm^3\ g^{-1}$)	L_0 (nm)	$E_{ads.CO2}$ (kJ mol^{-1})
CN.SUG2	378	0.20	0.141 (70.5%)	0.18	0.05	0.78	25.3
CN.RON2	2	0.03	0.001 (3.3%)	0.22	0.03	2.46	9.7

CN.SUG2 presents a micropore fraction of 70.5%, which is desirable in a CO_2 capture process, but its total surface area (A_{BET}) is not considerable compared to other carbon materials [2]. This can be due to the aggregation presented in this material (Figure 6. 1). But comparing CN.SUG2 and CN.RON2 from N_2 adsorption, CN.SUG2 has better textural parameters (Figure 6. 4-a and Table 6. 4), which could benefit the CO_2 adsorption, because of CN.RON2 seems to be non-porous, and $V_{0,95}$ and $V_{mic\text{-}N2}$ are considerably low. However, the results of CO_2 adsorption present a point view different for CN.RON2,$V_{mic\text{-}N2}$ compares with $V_{mic\text{-}CO2}$ are considerably differents (a difference of 667%). Also, CO_2 adsorption capacity for CN.RON2 is competitive (Figure 6. 4-b), compare with CN.SUG2 (3.0 and 2.3 $mmol.g^{-1}$, respectively) and values reported in the literature.

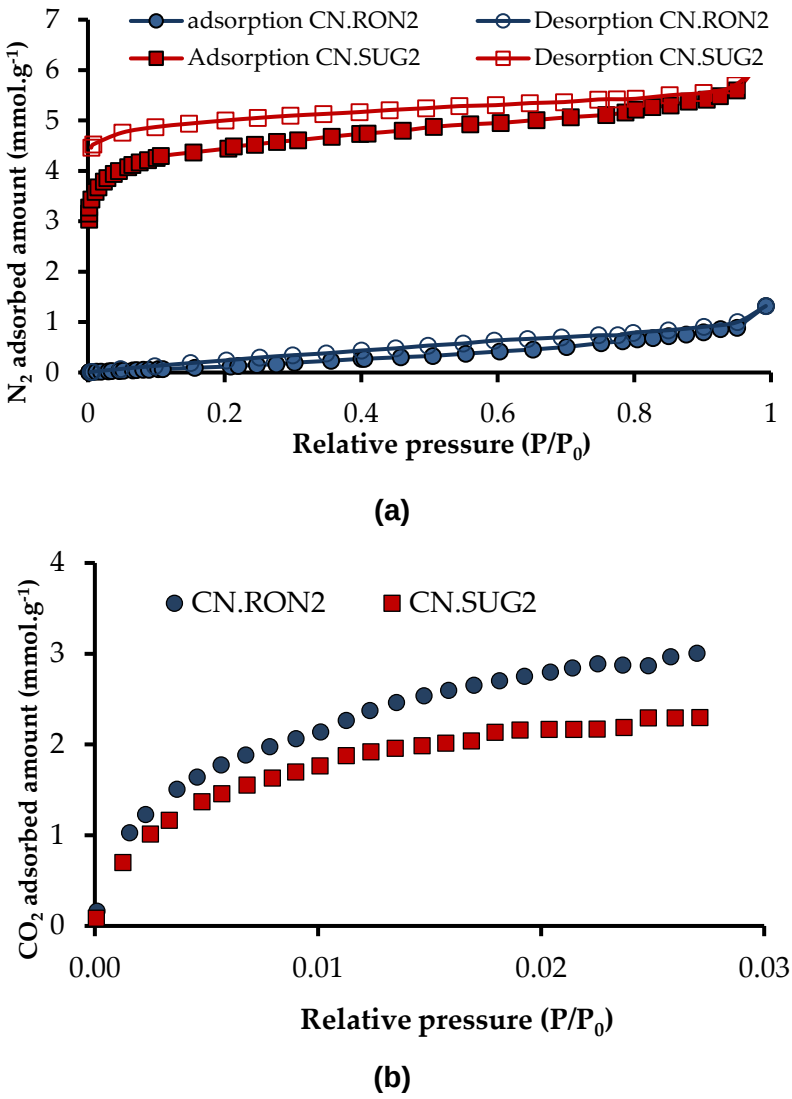

Figure 6. 4. Adsorption isotherms for nanoparticles synthesized with sugar and molasses at a mass ratio of H_2O/carbon precursor of 3600:1 (CN.SUG2 and CN.RON2) (**a**) N_2 adsorption at −196 °C, adsorption is full symbols, and desorption is empty symbols and (**b**) CO_2 adsorption at 0 °C.

The elemental analysis (CHON) was carried out for CN.SUG2 and CN.RON2 (Table 6. 5). Oxigen was analyzed independently. CN.RON2 presents an N_2 content considerable (compared with CN.SUG2), taking account, the material comes biomass and has not undergone additional processes.

Table 6. 5. Ultimate analysis of nanoparticles synthesized with sugar (CN.SUG2) and Molasses (CN.RON2).

	%N	%C	%H	%O
CN.SUG2	0.03	93.2	1.9	6.7
CN.RON2	1.07	87.6	1.8	8.3

Based on the above, CN.RON2 could have molecular sieve characteristics. Therefore, in the following section, adsorption tests were performed at different operating conditions in order to rule out the textural effect.

6.2.2. Adsorption analysis

The N_2 and CO_2 adsorbed capacity were evaluated for CN.RON2 in order to broaden the knowledge of this material, and determine if CN.RON2 could be considered a molecular sieve. Figure 6. 5 presents the adsorption isotherms for CN.RON2 at different conditions: 25 and 50 °C for CO_2 and N_2, and the fit with Sips and Toth models. Concerning the adsorption of CO_2 at 25 and 50 °C, as expected, the desorbed amount is higher for the lower temperature, with a difference of 1.32 $mmol.g^{-1}$ (at 2.5 MPa), due to the exothermic character of adsorption. Also, the Sips and Toth models led to very good fits: $R^2 > 0.99$.

On the other hand, N_2 adsorption capacity is negligible even at high-pressure conditions (<0.5 $mmol.g^{-1}$). Whereby this material could be a carbon molecular nanosieve. An additional experiment of N_2 adsorption was carried out at 25 °C for 0.1 and 2.5 MPa and 96 hours, but the system did not have much variation concerning values reported in Figure 6. 5.

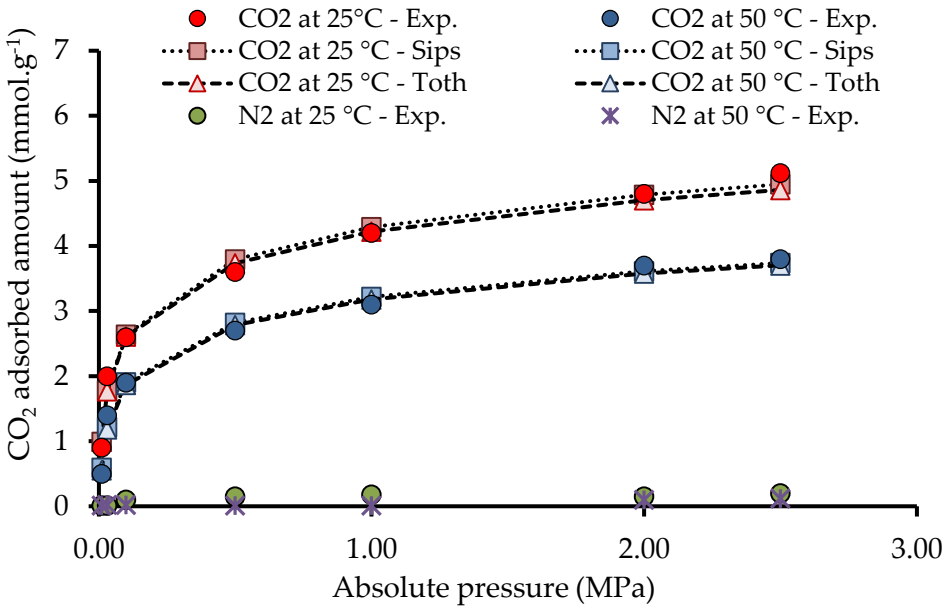

Figure 6. 5. Adsorption isotherms for CN.RON2 at different conditions: 25 and 50 °C for CO_2 and N_2, and the fit with Sips and Toth models

In chapter 4, sandstone was evaluated at low nanoparticle concentration to evaluate its economic feasibility at the industrial level (0.01, 0.1, 1, 5, 10, 20%), where 10 and 20 % were the best options. In this case, the CN.RON2 was evaluated at these mass fractions, and 25 and 50 °C (Figure 6. 6). The sandstone presented an A_{BET} of 0.4 $m^2\ g^{-1}$, and its CO_2 adsorption capacity could not be measured using conventional methods (< 0.0013 mmol g^{-1} at 0 °C and atmospheric pressure). Sandstone is mainly composed of silica, which has an acidic character as the CO_2 molecule. Consequently, if the specific area of the sandstone is low, its CO_2 adsorption capacity is even lower than that which might be expected for this specific area.

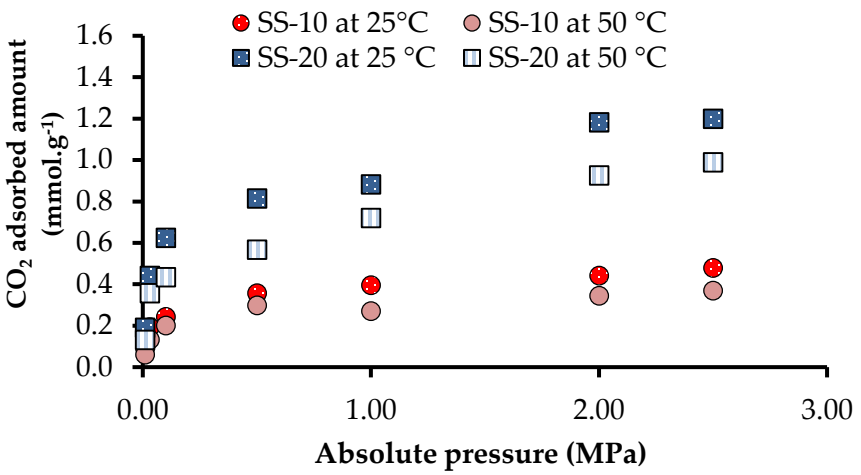

Figure 6. 6. Adsorption isotherms of CO_2 at high pressure (up to 2.5 MPa) of SS-10 (sandstone impregnated with a mass fraction of 10% CN.RON2) at 25 and 50 °C, and SS-20 (sandstone impregnated with a mass fraction of 20%CN.RON2) at 25 and 50 °C

Figure 6. 7 present the increments after sandstone impregnation with a mass fractions of 10 and 20 % (CN.RON2). The increment with 20% at reservoir conditions (50 °C and 2.5 MPa) is the best compared to other synthesized materials in this thesis. The microporous volume (from CO_2 adsorption at 0 °C) is not better than other materials so that the best performance could be associated with a higher affinity.

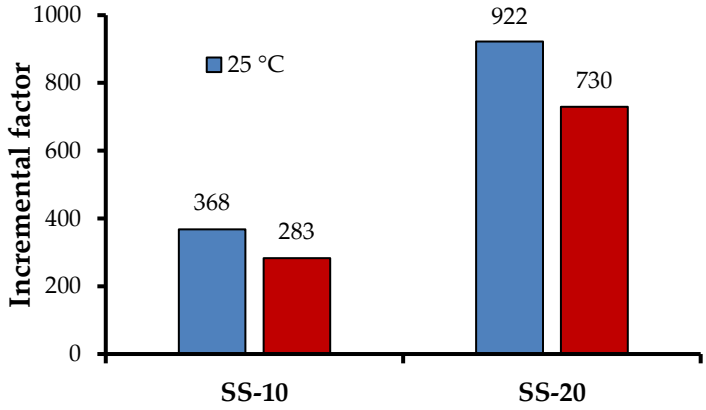

Figure 6. 7. The Incremental factor for CO_2 adsorption at 2.5 MPa and 25-50 °C. Sandstone impregnated with CN.RON2 at mass fractions of 10 and 20%.

The TGA analysis for SS-10 and SS-20 presents a variation of impregnation percentage. The real impregnation percentages are 8.6 and 20.8 %, respectively. It is observed that there is no correspondence between the experimental value and theoretical value, where experimental values for SS-8.6 and SS-20.8, present an increase (Table 6. 6). Therefore, in this system, there could be synergistic effects that enhance the adsorption capacity of CO_2. The nanoparticle comes from a biological precursor in which other components may be interacting at higher nanosieves percentages.

Table 6. 6. Theoretical and experimental values of CO_2 adsorption capacity at 2.5 MPa, 25 and 50°C, and mass fractions of 10 and 20 %.

	SS-8.6		**SS-20.8**	
	25 °C	**50 °C**	**25 °C**	**50 °C**
Theoretical N_{ads} (mmol g^{-1})	0.44	0.33	1.07	0.79
Experimental N_{ads} (mmol g^{-1})	0.48	0.37	1.20	0.99
Relative difference (%)	8.0	11.2	11.1	20.0

Based on the above, it is not necessary to surface modifying of nanomaterial to increase the CO_2 selectivity, nor to perform mixture evaluation (CO_2/N_2), due to the nanomaterial itself has high CO_2 selectivity.

In order to evaluate the effect of the polystyrene template on molecular sieve behavior, a hollow carbon nanoparticle was synthesized using resorcinol/formaldehyde and the same polystyrene template. The synthesis procedure is presented in Chapter 3, with a water/resorcinol ratio of 5556:1.

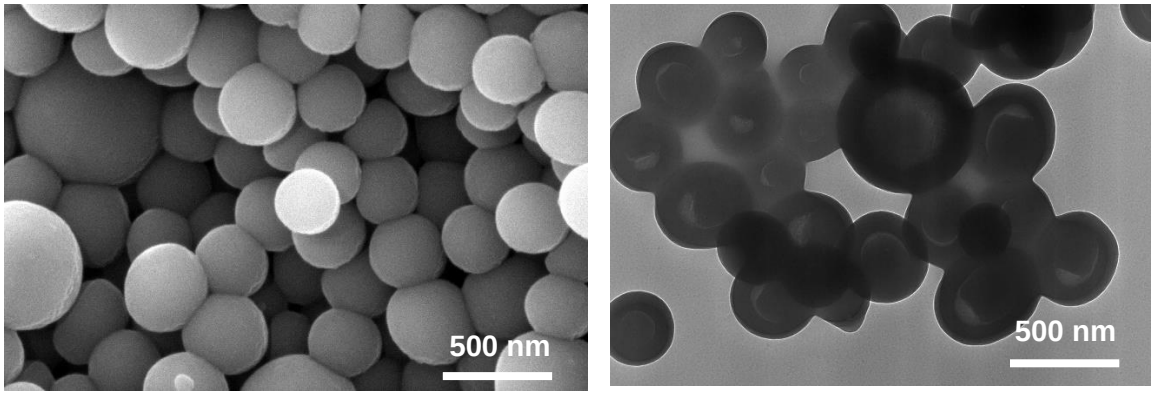

(a) **(b)**

Figure 6. 8. SEM and TEM images of carbon hollow nanospheres-CN.POL (water/resorcinol ratio of 5556:1; synthesized with latex template) (**a**) SEM (**b**) TEM

The A_{BET} for this materials (CN.POL) is 585 $m^2.g^{-1}$, $V_{0.95}$ is 0.30 $cm^3.g^{-1}$, $V_{mic\text{-}N2}$ is 0.23 $cm^3.g^{-1}$, $V_{mic\text{-}CO2}$ is 0.29 $cm^3.g^{-1}$ and V_{meso} is 0.06 $cm^3.g^{-1}$.

The obtained particles spherical with a relatively homogeneous size distribution (Figure 6. 8-a). Also, CN.POL does not present aggregation, such as latex nanoparticles, which indicates the excellent dispersion of latex nanoparticles before the reaction. As expected, the particles do not have a completely hollow-core due to the total non-carbonization of the latex nanoparticle (Figure 6. 8-b). The adsorption isotherms of N_2 and CO_2 are presented in Figure 6. 9. For CN.POL and CN.SUG is possible to obtain N_2 adsorption, but for CN.RON is impossible, regardless of the operating conditions used, but it has a considerable CO_2 adsorption capacity (similar value for three materials, CN.SUG, CN.RON, and CN.POL). CN.POL has a CO_2 adsorption capacity of 4.1 $mmol.g^{-1}$ at 3 MPa and 50 °C.

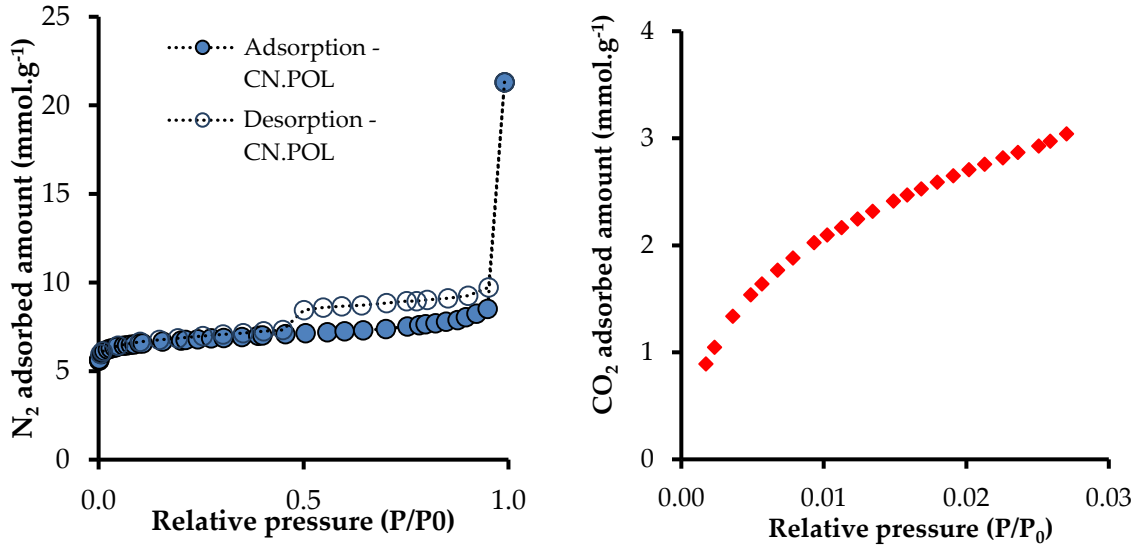

(a) **(b)**

Figure 6. 9. Adsorption isotherms for carbon hollow nanospheres-CN.POL (water/resorcinol ratio of 2250:1; synthesized with latex template) (**a**) N_2 adsorption at −196 °C, adsorption is full symbols and desorption is empty symbols and (**b**) CO_2 adsorption at 0 °C.

The carbonization of polymer precursors usually prepares carbon molecular sieves membranes at high temperatures, which is a rather complicated process involving multiple reactions [6]. Although research on carbon molecular sieves membranes dates back to as early as the 1990s [6, 7], the underlying mechanism of the formation of carbon molecular sieves membranes and their chemical and porous structures are still not fully understood [6]. The resultant carbon molecular sieves membranes commonly feature a bimodal structure for the pore size distribution: ultramicropores (<7 Å) for the size-sieving function, and micropores (7~20 Å) for the adsorption-diffusion function [6].

Therefore, the latex template could be interacting with specific cane molasses components such as fibers, carbohydrates, and proteins. The reported structures are diverse, but there are no reports of nanospheres that have molecular sieve behavior. Also, the CO_2 adsorption capacities reported in this chapter are competitive, and in some cases, superior to those

found in the literature, including materials with more complex syntheses or more stages [8, 9].

6.3. Partial Conclusions

Carbon molecular nanosieves synthesized from cane molasses allowed an increase factor of adsorption capacity by 730 with a mass fraction of only 20% (CN.RON2) under realistic reservoir conditions (50 °C and 3 MPa). This increase was possible thanks to the favorable chemical composition and physical structure, which promoted the natural selective capture and storage of CO_2. Although the synthesis process is carried out at a considerable temperature (180 °C), compared with other synthesized materials (N-rich carbon nanospheres by sol-gel method at 60 °C – Chapter 4), its high selectivity, adsorption capacity and cheap carbon precursor (biomass residue) make interesting material for the e-CCS process. For which it is required more characterization of the structure in order to have more clarity about the molecular sieve effect. Also, the molasses composition from other origins is important to ensure the reproducibility of carbon molecular nanosieve.

On the other hand, there are no reports on nanospheres that behave like molecular sieves; It is the first time worldwide. This development could represent a research line for various applications in which the spherical shape and nanometric size is an advantage, as in the e-CCS.

6.4. References

[1] R. J. White, K. Tauer, M. Antonietti, and M.-M. Titirici, "Functional hollow carbon nanospheres by latex templating," *Journal of the American Chemical Society,* vol. 132, pp. 17360-17363, 2010.

[2] J. Wang, L. Huang, R. Yang, Z. Zhang, J. Wu, Y. Gao*, et al.*, "Recent advances in solid sorbents for CO 2 capture and new development trends," *Energy & Environmental Science,* vol. 7, pp. 3478-3518, 2014.

[3] I. S. Organization. (2019, 10 July, 2019). *About Sugar*. Available: https://www.isosugar.org/sugarsector/sugar

[4] E. P.-C. Bailon-García, Agustín F.; Rodriguez Acevedo, Elizabeth; Carrasco-Marín, Francisco, "Nanoparticle Fabrication Methods," in *Formation Damage in Oil and Gas Reservoirs. Nanotechnology Applications for its Inhibition/Remediation*, C. A. a. C. C. Franco, Farid B, Ed., 1 ed: Nova Science Publishers, 2018, pp. 69-150.

[5] M. Agrawal, S. Gupta, A. Pich, N. E. Zafeiropoulos, and M. Stamm, "A facile approach to fabrication of ZnO− TiO2 hollow spheres," *Chemistry of Materials,* vol. 21, pp. 5343-5348, 2009.

[6] K. Huang and S. Dai, "Carbon Membranes for CO2 Separation," *Materials for Carbon Capture,* pp. 215-236.

[7] C. W. Jones and W. J. Koros, "Carbon molecular sieve gas separation membranes-I. Preparation and characterization based on polyimide precursors," *Carbon,* vol. 32, pp. 1419-1425, 1994.

[8] !!! INVALID CITATION !!! [41, 50-54].

[9] A. Wahby, J. M. Ramos-Fernández, M. Martínez-Escandell, A. Sepúlveda-Escribano, J. Silvestre-Albero, and F. Rodríguez-Reinoso, "High-surface-area carbon molecular sieves for selective CO2 adsorption," *ChemSusChem,* vol. 3, pp. 974-981, 2010.


LIBERTAD Y ORDEN
INTER · AULAS · ACADEMIÆ · QUÆRE · VERUM


UNIVERSITAS · GRANATENSIS
PLUS ULTRA
1531

7. Conclusions and recommendations

7.1. Conclusions

To the best of our knowledge, this is the first study using micro/nanoparticles to modify the CO_2 adsorption capacities of a shallow reservoir for a carbon capture and storage (CCS) process. Moreover, this is the first research proposing a possible new configuration of the CCS process in which the storage is performed in shallow reservoirs (less than 300 m). We called it enhanced CCS (e-CCS), for which the main advantage is that the CO_2 capture/separation step is removed, and the flue gas is injected directly into shallow deposits, where the CO_2 is gaseous, and the adsorption phenomena control the capture and storage.

The developed micro/nanomaterials are as competitive in the CO_2 adsorption process as those reported in the literature. The best obtained nanomaterial is the N-rich carbon nanospheres, allowing to increase the adsorption capacity of the sandstone in more than 677 times (from 0.00125 to 0.9 mmol g^{-1}), at shallow reservoir conditions 50 °C and 3.0 MPa). On the other hand, this material has been obtained by means of a simple synthesis method, in a single stage at 60 ° C (before carbonization). Which could allow its scalability at industrial level.

Molecular nanosieves obtained from cane molasses are a new nanomaterial with high potential for CO_2 adsorption, not only for application at the geological reservoir level. In addition, this material has the advantage, it is coming from agroindustry waste. Agriculture is an integral part of the Colombian economy, and its developed in some rural areas has been vulnerable to the country's armed conflict. Using a waste also avoids the competition when food can have a higher economic rather than social value. These organic residues, however, have potential in micro/nanomaterials production, especially those with a high

carbohydrate content. The micro/nanomaterials could become an important economic line to promote the future rural economic development. The production of advanced materials from low-cost carbon sources could also significantly reduce the operating costs of CCS/e-CCS.

The MOF presents high CO_2 capacity, but its stability and reproducibility can be complex. The microwave method to decrease the material's size, does not present significant changes. However, the carbonization method to obtain more stable structures allows to obtain materials with good performance at high pressure conditions. However, its scaling for a possible application in the e-CCS process could be complex and more expensive than the N-rich carbon materials obtained.

This research opens an interesting line of research that would expand knowledge in the field of carbon nanospheres for application in the adsorption and geological storage of CO_2.

7.2. Recommendations and future works

According to the results obtained, the following recommendations are proposed:

- To explore other carbon structures such as mesoporous nanospheres, ordered porous nanospheres modified with amines or nanocapsules filled with amines. In order to benefit the synergistic effect of adsorption and absorption phenomena for the e-CSS process.

- To explore other nitrogen compounds (amino acids, amines, among others) in sol-gel synthesis. In order to obtain nitrogen-rich carbon nanospheres in a single synthesis step.

- To corroborate the selective adsorption of CO_2/N_2 at the experimental level using mass spectrometry or gas analyzer, in order to verify the results obtained by PyIAST simulation.

- To evaluate the influence of molasses composition from different origins in obtaining carbon materials with molecular sieve characteristics.

- To evaluate the effect of steam water and other combustion gases such as NO_X, SO_X, O_2, among others, in CO_2 selectivity in the e-CCS process. Also, it would be important to evaluate the stability of carbon materials under corrosive gases at shallow reservoir conditions.

- To evaluate the effect of other components of a geological deposit, such as salts, organic material, minerals, among others, in the molecular interactions involved in the CCS process.

- To evaluate the effect of bicarbonate formation and its adsorption in systems combustion gases / nanoparticle / reservoir.

- To evaluate the methods for desorption of CO_2 and its effects in the systems.


LIBERTAD Y ORDEN
INTER · AULAS · ACADEMIÆ · QUÆRE · VERUM


UNIVERSITAS · GRANATENSIS
PLUS ULTRA
1531

8. Publications and scientific diffusion

As scientific contributions of this Ph.D. thesis, the following documents have been published:

8.1. Scientific papers and book chapters

- **Book Chapter:** “Chapter 3: Nanoparticle Fabrication Methods”. Formation Damage in Oil and Gas Reservoirs: Nanotechnology Applications for its Inhibition/Remediation. ***NOVA Science Publisher***. 2018. Esther Bailon-García, Agustín Perez-Cadenas, Elizabeth Rodríguez Acevedo, Francisco Carrasco-Marín. ISBN: 978-1-53613-902-0.

- **Paper:** An Enhanced Carbon Capture and Storage Process (e-CCS) Applied to Shallow Reservoirs using Nanofluids based on Nitrogen-Rich Carbon Nanospheres. ***Materials***, as part of the Special Issue Element-Doped Functional Carbon-based Materials. June, 2019; 12 (13) 2088. Elizabeth Rodriguez Acevedo, Farid B. Cortés, Camilo A. Franco, Francisco Carrasco-Marín, Agustín F. Pérez-Cadenas, Vanessa Fierro, Alain Celzard, Sébastien Schaefer and Agustin Cardona Molina. https://doi.org/10.3390/ma12132088

- **Paper:** High Pressure Effect on the n-C7 Asphaltenes Oxidation: Kinetic Analysis. ***Energy & Fuels.*** Oscar E. Medina, Jaime Gallego, Elizabeth Rodriguez Acevedo, Farid B. Cortés and Camilo A. Franco. https://doi.org/10.1021/acs.energyfuels.9b02611

- **Paper (In process):** Carbonized-Mg/Ni MOF 74 Applied to Enhanced Carbon Capture and Storage Process in Shallow Reservoirs (e-CCS). ***Materials***, as part of the Special Issue as part of the Special Issue Porous Materials for Energy and Environment. Elizabeth Rodriguez Acevedo, Farid B. Cortés, Camilo A. Franco, Francisco Carrasco-Marín, Agustín

F. Pérez-Cadenas, Antonio Rodríguez-Diéguez, Vanessa Fierro and Alain Celzard. January, 2020.

- **Paper (In process):** Carbon molecular nanospherical-sieves applied to Enhanced Carbon Capture and Storage Process in Shallow Reservoirs (e-CCS). Elizabeth Rodriguez Acevedo, Farid B. Cortés, Camilo A. Franco, Francisco Carrasco-Marín, Agustín F. Pérez-Cadenas.

8.2. Oral presentations

- **II Congreso/IVJornadas de Investigadores en Formación-JIFFI 2018.** "Nanoesferas de Carbono como Agentes Modificadores de Superficie en el Proceso de Captura y Almacenamiento de Carbono en Yacimientos Superficiales". June 20-22, 2018, Granada-España.

- **The World Conference on Carbon-CARBON 2018.** "Carbon Nanospheres as Modifying agent of Shallow Reservoir for Enhanced Carbon and Capture and Storage Process-CCS". July 1-6, 2018, Madrid-España.

- **Encuentro Internacional de Educación en Ingeniería-EIEI/ 2° Congreso Latinoamericano de Ingeniería-CLADI-ACOFI 2019.** "Desarrollo de Nanomateriales que permitan el Geo-almacenamiento de CO_2 Gaseoso en Yacimientos Someros". September 10-13, 2019. Cartagena, Colombia.

- **40th Workshop: Enhanced Oil Recovery and Technology Collaboration Programme-EOR-TCP 2019.** "A new configuration of Carbon Capture and Storage Process applied to Shallow Reservoirs (e-CCS) using Nanotechnology". September 16-20, 2019. Cartagena, Colombia.

- **IV Foro Regional, Retos y Oportunidades del Cambio Climático y Biodiversidad para Antioquia 2019.** "Nanotecnología aplicada a novedoso proceso de captura y almacenamiento de CO_2 (e-CCS). Octubre 29, 2019. Medellín, Colombia.

- **3 Minute thesis (Finalist).** Universidad Nacional de Colombia. December 02, 2019. Bogota, Colombia.

8.3. Poster presentations

- **I Simposio de la Unidad de Excelencia de Química Aplicada a Biomedicina y Medioambiente 2018.** "Nanoesferas de carbono como agente modificante de superficie en yacimientos someros para el mejoramiento del proceso de captura y almacenamiento de CO_2 - eCCS". January, 2018. Granada, Spain.

- **VII Escuela de Verano: Nuevas Tecnologías en Productividad y Recobro Mejorado de Petróleo y Gas 2019.** "Nitrogen-Rich Carbon Nanomaterials Applied to New Configuration of Carbon Capture and Storage Process-CCS in Shallow Reservoirs". May 29-31, 2019. Medellín, Colombia.

- **IV Foro Regional, Retos y Oportunidades del Cambio Climático y Biodiversidad para Antioquia 2019.** "Nanotecnología aplicada a novedoso proceso de captura y almacenamiento de CO_2 (e-CCS). Octubre 29, 2019. Medellín, Colombia.

8.4. Other broadcasts

- **Universidad Nacional de Colombia. "Unimedios" news agency**. **Science & Technology section.** "Nanoparticulas almacenarían CO_2 en yacimientos poco profundos". December 17, 2019. Bogotá, Colombia. (https://agenciadenoticias.unal.edu.co/detalle/article/nanoparticulas-almacenarian-co2-en-yacimientos-poco-profundos.html)